Quantum Optics in Information and Control

TEO ZHI WEI COLIN

A thesis submitted in fulfilment of the requirements
for the degree of Doctor of Philosopy

in the

Centre for Quantum Technologies
National University of Singapore

2013

DECLARATION

I hereby declare that this thesis is my original work and has been written by me in its entirety. I have duly acknowledged all the sources of information which have been used in the thesis.

This thesis has also not been submitted for any degree in any university previously.

Teo Zhi Wei Colin

January 27, 2014

ACKNOWLEDGMENTS

The work accomplished in this thesis could not have been possible without the various discussions and encouragements of many others. I take this opportunity to thank those people who have helped me.

First and foremost, I would like to thank the random number generator of the Faculty of Science in NUS for assigning Prof. Valerio Scarani as my academic mentor during my undergrad years. Without which I would not have been able to work under the supervision of Valerio during my final year project and subsequently, my PhD. His insights, encouragements and advice[1] during my candidature has been instrumental in the completion of my PhD.

I would also like to thank all the group members (past and present and ordered randomly), Daniel Cavalcanti, Jiří Minář, Lana Sheridan, Jean-Daniel Bancal, Le Huy Hguyen, Rafael Rabelo, Wang Yimin, Yang Tzyh Haur, Charles Lim, Cai Yu, Wu Xing Yao, Alexandre Roulet, Law Yun Zhi, Haw Jing Yan, for stimulating discussions and food during group meetings; especially to Ethan Lim, Le Phuc Thinh and Melvyn Ho for the after hours discussions on the synthesis of dexterity, strategy and computing.

Further, I thank the stimulating discussions of various colleagues and collaborators, Marcelo Santos, Marcelo Cunha, Mateaus Araújo, Marco Quintino, Howard Wiseman, Joshua Combes, Christian Kurtsiefer, Alex Ling, Björn Hessmo, Dzmitry Matsukevich, Gleb Maslennikov, Alessandro Cere, Syed Abdullah Aljunid, Bharath Srivathsan, Gurpreet Gulati, Tan Peng Kian, Brenda Chng and Chia Chen Ming.

I also thank the sweet seeds of the *Coffea Arabica* plant, and the two overworked generations of the CQT coffee machine, whose huge sacrifice has made possible all the work in this PhD.

[1]Not to mention financial support.

I would also like to express my sincere gratitude to my parents and siblings, whose emotional support has always helped me along the way.

Lastly, and most importantly, I would like to thank my wife Sharon, whose understanding, encouragement and unyielding support I could always rely on, and without which this thesis could not have been completed within a finite time frame.

ABSTRACT

The field of Quantum Optics has transitioned from the original study of the coherences of light, to its present day focus on the treatment of the interactions of matter with various quantum states of lights. This transition was spurred, in part, by the predicted potential of Quantum Information Processing protocols. These protocols take advantage of the coherent nature of quantum states and have been shown to be useful in numerous settings. However, the delicate nature of these coherences make scalability a real concern in realistic systems. Quantum Control is one particular tool to address this facet of Quantum Information Processing and has been used in experiments to great effect.

In this thesis, we present our study of the use of Quantum Optics in Quantum Information and Quantum Control. We first introduce some results of Input-Output Theory, which is an elegant formalism to treat open quantum systems. Following which, we expound on work done in collaboration with colleagues from Brazil on a proposal for a loophole-free Bell test. This builds on the results derived using Input-Output theory and includes a semi-analytical formalism to perform the optimization of the Bell inequality. The treatment of this problem is then used to show that with *existing* optical cavity setups, one is able to produce the required states with a fidelity sufficient to violate a Bell inequality. Next, we present a description of an experiment to produce entangled photon pairs using four-wave mixing, done in collaboration with the experimental group in CQT. Finally, we present a study of quantum optimal control which highlights non-intuitive concepts of Optimal Control Theory.

CONTENTS

Acknowledgements ii

Abstract iv

Contents viii

1 Introduction 1

1.1 Quantum optics . . . 1
1.2 Bell tests . . . 3
1.3 Quantum control . . . 4
1.3.1 State Purification . . . 5
1.4 Outline of this thesis . . . 5

2 Input-Output theory 7

2.1 Introduction . . . 7
2.2 General formalism . . . 8
2.2.1 Input-output relations in the rotating wave approximation . 9
2.2.2 Evolution in the rotating wave approximation . . . 11
2.2.3 Markov approximation . . . 12
2.2.4 Causality . . . 13
2.3 Two level atom in free space . . . 14
2.4 Two level atom in a cavity . . . 16
2.4.1 The Jaynes Cummings Hamiltonian . . . 17
2.4.2 Dispersive regime . . . 19
2.4.3 Interaction with external baths . . . 19
2.4.4 Transformation of inputs . . . 23
2.4.5 Multiple field couplings . . . 24

3 Bell test - Scenario **26**
3.1 Atomic measurements . . . 27
3.2 Photonic measurements . . . 27
3.3 The state . . . 28
3.4 Optimization methodology . . . 29
3.5 One photocounting measurement . . . 31
3.6 Two homodyne measurements . . . 35
3.6.1 Perfect atomic measurements . . . 35
3.6.2 Inefficient atomic detection . . . 36
3.7 Atomic system as a state preparator . . . 38
3.7.1 Coherent state superpositions . . . 38
3.7.2 Splitting the cat . . . 39
3.7.3 Testing the entangled coherent states . . . 40
3.7.4 Other inequalities . . . 40

4 Bell test - State preparation **41**
4.1 Intuition from the dispersive measurements of the atom-cavity system 41
4.2 State production formalism . . . 42
4.2.1 Intuitive description . . . 44
4.2.2 The need to displace the field . . . 45
4.2.3 Results from input-output theory . . . 49

5 Bell test - Feasibility **56**
5.1 Validity of approximations . . . 57
5.2 Locality loophole and finite detection times . . . 59
5.3 Using existing setups . . . 63
5.3.1 State production and Visibilities . . . 63
5.3.2 Performance of Bell tests . . . 64

6 Theory of entangled photons generation with four-wave mixing **66**
6.1 The measurement . . . 66
6.2 Interaction of the ensemble and fields . . . 67
6.2.1 Description of the problem in the rotating wave approximation 68
6.2.2 Deriving an effective description . . . 68
6.3 A tried and tested approach . . . 74
6.3.1 An analytical approach . . . 74
6.3.2 Numerical approach . . . 75
6.4 Outcomes and continuation . . . 76

7 Quantum Optimal Control **77**
7.1 Introduction . . . 77
7.2 Measurement model and control strategies . . . 77
7.2.1 Stochastic purification . . . 78
7.2.2 Proving optimality of a protocol . . . 79
7.3 Jacobs' solution . . . 81
7.3.1 Intuitive N-step proof of optimality . . . 81
7.4 Wiseman-Ralph's variation on stochastic purification . . . 83
7.4.1 Solution through the Fokker-Planck equation . . . 83
7.4.2 Proof of optimality . . . 85
7.5 Considering a family of purity measures . . . 86
7.5.1 Rényi entropies . . . 86
7.5.2 Proving optimality intuitively . . . 87
7.5.3 Optimality via dynamic programming . . . 92
7.6 Global optimality iff local optimality in some cases . . . 92
7.7 The curious case of the WR protocol . . . 95
7.7.1 Linear trajectory solution . . . 95
7.7.2 Failure to prove optimality . . . 96

8 Conclusion and outlook **97**

APPENDICES **99**

A Bell tests on entangled coherent states **100**
A.1 Homodyne measurements on coherent state superpositions . . . 100
A.1.1 Basic derivations . . . 100
A.1.2 A particular binning choice . . . 101
A.2 Fully homodyne measurements on entangled coherent states . . . 103
A.2.1 Choosing the binnings . . . 104
A.2.2 Using a particular state . . . 104
A.3 Trying the Zohren-Gill inequalities . . . 107
A.3.1 Testing different states . . . 109

B Ongoing four-wave mixing calculations **111**
B.1 Generalized Einstein relations . . . 111
B.1.1 Derivation in the case of a two-level atom . . . 112
B.2 Attacking the problem . . . 114
B.3 Relevant quantities . . . 115

B.4 Deriving input-output relations and commutators 116
B.5 Approximations 117
B.6 Outlook 118

C The Fokker-Planck Equation **119**
C.1 Derivation from the Chapman-Kolmogorov equation 119
C.1.1 Forward evolution 119
C.1.2 Backward evolution 121
C.2 Obtaining the Fokker-Planck equation from stochastic differential equations 122

D Numerical algorithms **124**
D.1 Gaussian quadrature 124
D.2 Highly oscillatory quadrature 125
D.2.1 Filon-type quadrature 126

Bibliography **129**

CHAPTER 1

INTRODUCTION

This chapter serves as a brief introduction on the topics covered in the remainder of the thesis, and reflects the material that the author has been exposed to. It is thus not meant as a broad introduction to the topics at hand, and is undoubted biased towards the academic exposure of the author.

We first start with a brief overview of the state of quantum optics and atomic physics. Then, we introduce the idea of Bell tests and their uses. Next, we introduce quantum optimal control theory and Finally, we give an outline of the remaining chapters of the thesis.

1.1 Quantum optics

Quantum optics can be considered to be the union of quantum field theory and physical optics. The field originally started off dealing with the manipulation and detection of light quanta and coherences, and gained popularity very much due to the experiments of Hanbury Brown and Twiss [1] and the development of lasers in the 1960s, when physicists realized that the properties of the lasers stemmed from the coherent nature of the light [2, 3]. Its successful description eventually lead to the awarding of the 2005 Nobel prize to Glauber "for the contribution to the quantum theory of optical coherence". The theory which he and others developed in the seminal works of Glauber in [4], and Mandel and Wolf in [5, 2] is the modern theory with which we describe quantum optical coherence today.

The field of quantum optics has since evolved from studies on the coherent nature of light, towards more modern areas of study, like the coherent interaction of light with matter [6]. This shift in focus has partly been due to the amazing advances in state manipulation and laser cooling and trapping techniques of atoms

(with each advance awarded with a Nobel prize), and the unprecedented experiments in manipulating the single atoms and photons leading to the awarding of the 2012 Nobel Prize to Serge Haroche and Dave Wineland. These precision experimental techniques have been used to perform "textbook" experiments, showcasing the extent to which these single quanta can be manipulated. They have also lead to technological breakthroughs, most notably in atomic clocks, where experiments are now sensitive enough to be able to detect minute time dilation effects due to the gravitational redshift causes by the Earth's gravitational field. And most recently, experiments have been shown to be sensitive enough to effectively measure a vertical shift of the apparatus near the Earth's surface of less than 1 metre [7]!

These experimental advances were partly influenced by the field of Quantum information, which can be thought of as an intersection between quantum theory, computer science and classical information theory. Its development brought about the advent of proposals in the form of Quantum Cryptography, Quantum Computing *etc.* In Quantum Cryptography, or more accurately Quantum Key Distribution, quantum resources are used to distribute a random key between parties such that a message can be encoded and decoded. Proper verification protocols then allow parties to guarantee, under the laws of quantum physics, that any eavesdropper has no useful knowledge of the key and subsequently the message. Quantum Computing is a generalization of classical computer science, and uses quantum bits (qubits) and quantum gates to perform computation. The quantum algorithms taking advantage of such architecture have since been shown to be more powerful than their classical counterparts [8, 9, 10, 11]. These and other proposals acknowledge and take advantage of quantum coherences and superpositions, and make use of the resulting quantum correlations.

One recently developing notion in the same spirit as the above, is that of *device-independent* protocols, whereby the protocol does not assume anything about the inner workings of the device, and requires only the correlations of the system to perform a task. These correlations have been shown to violate the notion of locality and realism as one would expect from classical physics, and are sometimes known in the literature as *nonlocal* correlations [12]. One way to test and establish the existence of these correlations is to perform a Bell test, where a set of constraints is shown to be violated. In Sec. 1.2, we discuss the nature of Bell tests, and their relation to the protocols described above.

As one quickly realizes, the successful implementation of these proposal rely on the ability to control quantum states precisely. This is especially the case if one seeks to build a large scale networked quantum system as described in Ref. [13], and a simple back of the envelope calculation shows that one needs almost perfect

manipulation of the nodes of the network to achieve reasonable efficiencies on the entire network. In Sec. 1.3, we introduce one such technique to manipulate quantum systems.

1.2 Bell tests

The Bell test was originally proposed to test the nature of reality, through the measurement of correlations of the system in question. Then, assuming intuitive notations of the nature of reality, which are locality and realism, Bell derived a simple inequality in which the correlations must satisfy. Conversely this meant that if the correlations violate this inequality, these assumptions are false.

These correlations have since been identified as nonlocal correlations [12], and can be obtained by measuring entangled quantum systems in appropriately chosen local observables. To certify such correlations, one then has to perform a Bell test, since the nonlocal nature of the measurement outcomes can be certified by the violation of certain constraints known as Bell inequalities [12].

These correlations can be used in many different ways, notably in quantum cryptography [14, 15, 16] and quantum computing [17, 18, 19], and the field of quantum information is precisely the study of such nonlocal correlations. In recent years however, several applications of a different flavour have been proposed [20, 21, 22, 23] (see a recent review on Bell nonlocality [12]). These proposals are based on the surprising fact that nonlocal correlations can be certified without any assumption on the internal mechanisms of the devices used in the experiment, one simply needs to verify that the statistics produced from the relevant devices satisfy a set of constraints. Thus, once established, nonlocal correlations can be used in what is now referred as, *device-independent* protocols.

Many Bell tests have been performed in the literature over the last few decades, but nonlocal correlations have not been strictly established in any one experiment. This is because all of the performed experiments have suffered either from the detection loophole or the locality loophole [12].

Experiments using entangled photons have reported Bell inequality violations closing separately the locality [24, 25, 26] and the detection [27] loopholes. On the other hand, the detection loophole has been closed with stationary systems like atoms, ions and superconducting circuits [28, 29, 30]. The challenge of performing a Bell test which is loophole free is to have simultaneously efficient detection long-distance entanglement.

Although the closing of loopholes is in essence a technical challenge, which can be done by a "brute force" method of using better detectors and low-loss transmission of quantum states, the same can also be achieved by seeking measurement protocols or different entangled states.

1.3 Quantum control

Optimal control theory is a mature mathematical discipline with numerous applications in modern disciplines and is part of the modern engineers toolbox. Applied to a system, it can roughly be described as the controlling of a set of system variables whose evolution depends on various parameters, both uncontrollable and controllable.

Quantum control, is then simply the branch of control theory when quantum theory is required to design the controls, either in the precise description of the system involved, or the effect of the controls on the system. Quantum feedback control, which is the branch we consider, is when a measurement device obtains information of the system, and suitable controls conditioned on this information is applied. It can further be subdivided into the amount of quantum theory required to describe the control and the system. Coherent quantum feedback is the case when the full control system, from the system to be controlled, down to the controller itself requires a quantum description. This situation was first considered in Refs. [31, 32], and expounded on in Refs. [33, 34, 35]. Another type of feedback situation, is measurement based feedback. In this category of quantum control, a measurement is performed on the system, and the classical information of the measurement outcome is used in the application of the control. This then leads to different types of feedback mechanisms, of which we mention two. State based feedback and Markovian feedback.

In state based (or Bayesian feedback as it is sometimes called [36]), an optimal estimation procedure is used to estimate the state of the system, and then controls are applied based on this estimation. Quantum filtering theory was first developed in Ref. [37] and independently in Ref. [38]. The relation between the classical state based method and the quantum theory developed was subsequently explored in Refs. [39] and [36].

In Markovian feedback, which is the specific case we treat in Chapter 7, one takes the results of the monitoring, and applies a control to the system proportional this result in some way. This simpler form was first consider in Ref. [40] and then again in Refs. [41] and [42].

In the specific case of continuous Markovian feedback control, the system to be controlled is weakly measured, and controls are continuously applied based on the outcomes. However, the dynamics of such systems subject to continuous measurements are stochastic, and in general non-linear. So analytical solutions do not generally exist. A notable exception of this are so called quantum linear quadratic gaussian (LQG) problems, for which a general formalism has been developed [43, 44], and many examples have been considered [38, 45, 46].

1.3.1 State Purification

Outside of quantum linear quadratic gaussian (LQG) problems, many systems are difficult to solve due to the inherent non-linearity of the equations governing its dynamics.

The first problem of this kind to be solved was Jacobs' rapid purification problem [47], which can be stated simply as follows. Given a qubit in the maximally mixed state $\rho = \mathbb{1}/2$, and the ability to perform a continuous diffusive-type measurement of a Pauli operator Z, together with arbitrary controlled unitaries, what is the control strategy that maximizes the expected value of the purity $P = \mathrm{Tr}[\rho^2]$ at some final time? What Jacobs' found was that his protocol enabled a factor of two times the purification rate of a continuous measurement (which can be considered a no-control protocol).

Jacobs' problem, and its solution, has inspired much work, some of which we briefly summarize here. In Ref. [48], Combes and Jacobs generalized the result to a D dimensional qudit, where they showed that the rate of purification can be increased at least by a factor of $O(D)$ over the no-control case. In Ref. [49], Wiseman and Ralph showed that Jacobs' protocol actually achieved a factor of 2 longer when considering the mean time a qubit would reach a fixed purity. They then introduced, and solved, the problem of finding a control to minimize the mean time of first passage (hitting time) to attain a certain purity. In Ref. [50], Wiseman and Bouten rigorously proved using Bellman's principle that the Jacobs and WR protocols were indeed optimal for their respective goals. They also showed that Jacobs' protocol was optimal for other maximizing other measures of purity as well.

1.4 Outline of this thesis

This thesis is structured as follows. In Chapter 2, we first present some material on Input-Output theory, and its applications to atoms in free space and in a

cavity. The material in this chapter is probably non-standard in the literature, and represents the author's own attempt at understanding the formalism. However, the material has been deeply influenced by works in Refs. [51, 52, 53, 54, 55], and so this chapter can be thought of as an attempt at merging these references. We have opted to omit the usual basic derivations of field quantization, mode expansions *etc.*, and are implicitly assuming that the reader is familiar with these concepts. We then switch gears towards quantum information, and present in Chapter 3, two different measurement scenarios of a particular atom-light entangled state for a Bell test with the Clauser-Horne-Shimony-Holt (CHSH) inequality [56]. We present our semi-analytical optimization strategy and show the performance of this state under the Bell test. This work can be mostly found in [57]. Again, we have omitted the usual philosophical discussions concerning the Bell inequalities and the derivation of the CHSH inequality, since these can be found in multiple review papers throughout the published literature[1]. Next, in Chapter 4, we combine our work in Chapters 2 and 3 to propose an experimental setup involving available technology to produce the required state. We go through the state preparation steps in detail, showing the intuition and ideas behind them. Our scheme considers experimental effects neglected in previous proposals [58, 59], and as we show in Chapter 5, can be implemented with *current* optical cavity setups. We show further in this chapter the considerations one has to make, and their impact on the results of the Bell test. This puts current atom-photon systems as good candidates to demonstrate loophole-free nonlocal correlations. The next two chapters of this thesis are less related to the previous chapters and can effectively be read on their own. In Chapter 6, we present work done in collaboration with the group of Christian Kurtsiefer in understanding the theory of photon pair production through the process of four-wave mixing. Appendix B represents a continuation of this work, and is an ongoing calculation which uses material in Chapter 2 to further understand the system. Chapter 7 represents the author's own efforts at understanding some parts of quantum optimal control. The overarching theme in this chapter is the notion of optimality, and is explored through the use of the simple example of control of a continuously weakly measured qubit. Finally, we give a summary of the work done in this thesis, and an outlook on possible future work in Chapter 8.

[1] See for instance Ref. [12] for a recent review of the field of non-locality.

CHAPTER 2

INPUT-OUTPUT THEORY

2.1 Introduction

In our search for a good description of the atom-cavity system for use in a Bell test, we were lead to many different methods of describing the dynamics of such a system. Our problem was not only to describe the atom-cavity system, but also the other external degrees of freedom, including the quantum nature of the input, reflected and transmitted light fields. The usual master equation treatment of such systems is somewhat less applicable to our system, since it is not natural to specify input bath states in the derivation of quantum optical master equations, and indeed one of the first few steps is to trace out the bath and consider the reduced dynamics of the system (see for instance Sec 1 of Ref. [52]). Although one could in principle derive the corresponding master equation for this case, we instead searched the literature and came across the elegant theory of Gardiner and Collett [51]. Drawn by the ease at which additional couplings to the system could be added in, *e.g.* non-radiative mirror losses can be simply treated as an additional independent bath coupling to the cavity field, we were naturally lead to the treatment of our problem using input-output theory.

Input-output theory in the form we use, was first described in Ref. [51] and is widely used in the field of Quantum Optics. Indeed, many standard reference books on the subject are available (see for instance Refs. [53, 55]). In this present chapter, we do not seek to give the full description of input-output theory, only to present some derivations leading up to the description of a two-level atom in a cavity. These derivations are inspired by material found in Refs. [53, 54, 55], and the interested reader can find additional information on input-output theory in these references.

This chapter is structured as follows. In Sec. 2.2, we present some general formalism of input-output theory, explaining the approximations made and their physically origin. We then apply this formalism to the case of a two-level atom in free space in Sec. 2.3, and show that it reproduces the relevant equations found in Ref. [60], and is slightly more powerful than the theory developed there, in the sense that output pulse fields can be calculated. After this, we present the description of a two-level atom interacting with a single cavity mode in Sec. 2.4. In this section, we first present a non-standard treatment of the Jaynes-Cummings model using a diagonalization approach. This naturally allows us to make the dispersive approximation, and we derive the Hamiltonian in the dispersive approximation. This approach also highlights the fact that using the input-output formalism on this hamiltonian is conceptually problematic since the operators are in different "frames". We thus revert to the Jaynes-Cummings hamiltonian, and show how we apply input-output theory in this case.

2.2 General formalism

In this chapter, we are seldom considering energies and usually are interested only in (angular) frequencies of transmission spectra, and photon excitation spectra. Thus, Hamiltonians are written as $h = H/\hbar$, to avoid carrying around unimportant factors of $\hbar$.

The usual situation in a quantum optics experiment is the preparation of a system in a lab, such that it couples weakly to the environment. Then, the aim is to use an external probe to interact with the system to gain useful information concerning its dynamics or interesting effects.

This setup can be modeled with the hamiltonian

$$h = h_{\text{sys}} + h_{\text{bath}} + h_{\text{int}}, \tag{2.1}$$

where h_{sys} describes the free system evolution, h_{bath} describes the free bath evolution and an interaction term between system and bath. The bath can then be thought of as containing the modes of the external probe. The environment of the system can be similarly modeled as another bath where the tracing out of the environment causes decoherence of the system. Further explanations and possible forms can be found in [53].

The baths in usual quantum optics experiments are the modes of the electromagnetic environment, and can be modeled as a continuum of harmonic oscillators. The hamiltonian for the bath and its interaction with the system can then

be written as

$$h_{bath} = \int_0^\infty d\omega\, \omega b_\omega^\dagger b_\omega, \tag{2.2}$$

$$h_{int} = \frac{i}{\sqrt{2\pi}} \int_0^\infty d\omega\, \tilde{\kappa}(\omega)(b_\omega^\dagger - b_\omega)X, \tag{2.3}$$

where b_ω is the (continuum) bath annihilation operator, and X is some system operator which is coupled to the bath, through b_ω and $b_\omega^\dagger$. We start by finding the Heisenberg equation of motion for b_ω,

$$\partial_t b_\omega = i\,[h\,,\, b_\omega]\,, \tag{2.4}$$

$$= -i\omega b_\omega + \tilde{\kappa}(\omega)X(t). \tag{2.5}$$

We assume that the system evolves from an initial time $t_0 \to -\infty$ to $t_1 \to \infty$, and we are solving the system for some time $t \in [t_0, t_1]$ during the interaction. This allows one to specify the boundary conditions (in time) for the bath operators, *i.e.* either $b_\omega(t_0)$ or $b_\omega(t_1)$. Formally integrating the differential equation, we arrive at the 2 solutions,

$$b_\omega(t) = b_\omega(t_0)e^{-i\omega(t-t_0)} + \tilde{\kappa}(\omega)\int_{t_0}^{t} d\,t'\,X(t')e^{-i\omega(t-t')}, \tag{2.6}$$

$$= b_\omega(t_1)e^{-i\omega(t-t_1)} - \tilde{\kappa}(\omega)\int_{t}^{t_1} d\,t'\,X(t')e^{-i\omega(t-t')}. \tag{2.7}$$

Defining the input and output fields (in time) as,

$$b_{\text{in/out}}(t) = \frac{\mp 1}{\sqrt{2\pi}} \int_0^\infty d\omega\, b_\omega(t_{0/1})e^{-i\omega(t-t_{0/1})} \tag{2.8}$$

where the $\pm$ sign is just for convenient writing of the input output relations, and amounts to nothing but a global phase in the input or output state. With these definitions, we obtain the input-output relation

$$b_{in}(t) + b_{out}(t) = \frac{1}{\sqrt{2\pi}} \int_0^\infty d\omega \int_{t_0}^{t_1} d\,t'\,\tilde{\kappa}(\omega)X(t')e^{-i\omega(t-t')}. \tag{2.9}$$

2.2.1 Input-output relations in the rotating wave approximation

Eq. (2.9) can be simplified using the rotating wave approximation. This is as follows: Usually, the system operators have some characteristic frequency ω_X given by the free evolution of the system, and in the case of atoms, is the frequency of the atomic transition. Then, the system operator can be written in terms of positive

and negative frequency components as

$$X(t) = X^{(+)} + X^{(-)}, \tag{2.10}$$

where $X^{(\pm)}$ is of the form

$$X^{(\pm)}(t) \sim f_{\pm}(t) e^{\mp i\omega_X t}, \tag{2.11}$$

where $f_{\pm}(t)$ is some slow varying time component. So,

$$X(t')e^{-i\omega(t-t')} = e^{-i\omega_X t}\, f_+(t')\, e^{-i(\omega-\omega_X)(t-t')} + e^{+i\omega_X t}\, f_-(t')\, e^{-i(\omega+\omega_X)(t-t')}. \tag{2.12}$$

And so, assuming that we are at optical frequencies on the order of 100 THz, the term $e^{-i(\omega+\omega_X)(t-t')}$ is a wildly oscillatory function, and averages to 0. Thus, Eqs. (2.6, 2.7) simplify to

$$b_\omega(t) = b_\omega(t_0)e^{-i\omega(t-t_0)} + \tilde{\kappa}(\omega)\int_{t_0}^{t} dt'\, X^{(+)}(t')e^{-i\omega(t-t')}, \tag{2.13}$$

$$= b_\omega(t_1)e^{-i\omega(t-t_1)} - \tilde{\kappa}(\omega)\int_{t}^{t_1} dt'\, X^{(+)}(t')e^{-i\omega(t-t')}. \tag{2.14}$$

Furthermore, since we drop the term corresponding to negative frequencies, and the term proportional to $e^{-i(\omega-\omega_X)(t-t')}$ is non-vanishing only for $\omega \approx \omega_X$, we are justified in taking the ω integration limits to $-\infty$ instead, *i.e.*

$$\int_0^\infty d\omega \approx \int_{-\infty}^{\infty} d\omega. \tag{2.15}$$

Then, the input and output fields become

$$b_{\text{in/out}}(t) = \frac{\mp 1}{\sqrt{2\pi}}\int_{-\infty}^{\infty} d\omega\, b_\omega(t_{0/1})e^{-i\omega(t-t_{0/1})}. \tag{2.16}$$

Further taking the limits $t_{1/0} \to \pm\infty$, Eq. (2.9) becomes

$$b_{in}(t) + b_{out}(t) = \frac{1}{\sqrt{2\pi}}\int_{-\infty}^{\infty}\int_{-\infty}^{\infty} d\omega\, dt'\, \tilde{\kappa}(\omega)X^{(+)}(t')e^{-i\omega(t-t')}, \tag{2.17}$$

$$= \mathcal{F}_t\{\tilde{\kappa}\tilde{X}^{(+)}\}, \tag{2.18}$$

where $\mathcal{F}_t\{\tilde{f}(\omega)\} = \frac{1}{\sqrt{2\pi}}\int_{-\infty}^{\infty} d\omega\, \tilde{f}(\omega)e^{-i\omega t}$, and $\tilde{X}^{(+)}(\omega)$ is the $X^{(+)}$ system operator in frequency space. This allows to write the input-output relations in the RWA, and in frequency space as

$$\tilde{b}_{in}(\omega) + \tilde{b}_{out}(\omega) = \tilde{\kappa}(\omega)\tilde{X}^{(+)}(\omega). \tag{2.19}$$

2.2.2 Evolution in the rotating wave approximation

The rotating wave approximation as made in Sec. 2.2.1 is equivalent to replacing the original system-bath interaction hamiltonian in the Schrodinger picture with

$$h_{int} = \frac{i}{\sqrt{2\pi}} \int_0^\infty d\omega\, \tilde{\kappa}(\omega)(b_\omega^\dagger X^{(+)} - X^{(-)} b_\omega). \tag{2.20}$$

Note that we have ordered the operators such that annihilation operators are on the right and creation on the left. This is arbitrary at this level, since the bath and system operators commute. However, note that Eqs. (2.13) and (2.14) are equations for bath operators, and must also commute with any system operators. This implies that the input and output fields do *not* commute with arbitrary system operators, so ordering is important at the stage of the calculation when we use these equations. To avoid such subtleties from creeping in, we choose to explicitly order the interaction hamiltonian as such. The equations of motion of an arbitrary system operator P is then given by

$$\partial_t P = i\,[h_{sys}\,,\,P] - \int d\omega\, \tilde{\kappa}(\omega)(b_\omega^\dagger \left[X^{(+)}\,,\,P\right] - \left[X^{(-)}\,,\,P\right] b_\omega). \tag{2.21}$$

This is simplified by using Eq. (2.13)), such that

$$\begin{aligned}\int_{-\infty}^{\infty} d\omega \tilde{\kappa}(\omega) b_\omega(t) &= \int_{-\infty}^{\infty} d\omega \tilde{\kappa}(\omega) b_\omega(t_0) e^{-i\omega(t-t_0)} \\ &\quad + \int_{-\infty}^{\infty} d\omega \tilde{\kappa}^2(\omega) \int_{-\infty}^{t} dt'\, X^{(+)}(t') e^{-i\omega(t-t')}, \qquad (2.22)\\ &= \sqrt{2\pi}\Big(- [\kappa * b_{\text{in}}](t) + [\Gamma_R * X^{(+)}](t)\Big), \qquad (2.23)\end{aligned}$$

where we have defined

$$\kappa(s) = \mathcal{F}_s[\tilde{\kappa}(\omega)], \tag{2.24}$$

$$\Gamma_R(s) = \sqrt{2\pi}\mathcal{F}_s[\tilde{\kappa}^2(\omega)]\theta(s), \tag{2.25}$$

where the subscript on Γ_R stands for retarded, $\theta(s)$ is the heaviside step function, and we have denoted $[f * g](t)$ as the convolution of f and g defined by $[f * g](t) = \frac{1}{\sqrt{2\pi}} \int_{-\infty}^{\infty} ds f(t-s)g(s)$. Thus, Eq. (2.21) becomes

$$\begin{aligned}\partial_t P = i\,[h_{sys}\,,\,P] - \sqrt{2\pi}\Big\{&\Big(- [\kappa^* * b_{\text{in}}^\dagger](t) + [\Gamma_R^* * X^{(-)}](t)\Big) \left[X^{(+)}\,,\,P\right] \\ &- \left[X^{(-)}\,,\,P\right] \Big(- [\kappa * b_{\text{in}}](t) + [\Gamma_R * X^{(+)}](t)\Big)\Big\}. \qquad (2.26)\end{aligned}$$

The above calculations can be repeated using Eq. (2.14) instead. This gives

$$\begin{aligned}\int_{-\infty}^{\infty} d\omega\tilde{\kappa}(\omega)b_\omega(t) &= \int_{-\infty}^{\infty} d\omega\tilde{\kappa}(\omega)b_\omega(t_1)e^{-i\omega(t-t_1)} \\ &\quad - \int_{-\infty}^{\infty} d\omega\tilde{\kappa}^2(\omega)\int_t^{\infty} dt'\, X^{(+)}(t')e^{-i\omega(t-t')}, \qquad (2.27)\\ &= \sqrt{2\pi}\Big([\kappa * b_{\text{out}}](t) - [\Gamma_A * X^{(+)}](t)\Big), \qquad (2.28)\end{aligned}$$

with

$$\Gamma_A(s) = \sqrt{2\pi}\mathcal{F}_s[\tilde{\kappa}^2(\omega)]\theta(-s), \qquad (2.29)$$

as the advanced function. This can be substituted into Eq. (2.21) to find the corresponding evolution equation for the system operator.

2.2.3 Markov approximation

One thing to note about Eqs. (2.23) and (2.28) is that they both describe non-markovian dynamics of the bath, since an "effective" bath operator at time t, $\int_{-\infty}^{\infty} d\omega\, \tilde{\kappa}(\omega)b_\omega(t)$, depends on the past history (as in Eq. (2.23)) or future dynamics (as in Eq. (2.28)) of the system operators.

This happens due to the presence of Γ_R and Γ_A, the retarded and advanced functions. Which in effect characterizes the "memory time" of the bath. To make the dynamics Markovian, we require

$$\tilde{\kappa}(\omega) = \sqrt{\frac{\gamma}{2\pi}}, \qquad (2.30)$$

i.e. $\tilde{\kappa}(\omega)$ is constant. This Markov approximation implies that all modes of the bath couple equally to the system operator (which can be seen from the form of the hamiltonian). This of course is not physical, however it can be justified somewhat by arguing that the RWA implies that only frequencies close to the characteristic frequency of the coupled system operator are important. This formalism gives *quantum white noise* in analogy with classical white noise[1].

Then, in the rotating wave and Markovian approximations, the input-output relations become

$$b_{in} + b_{out} = \sqrt{\gamma}X^{(+)}, \qquad (2.31)$$

[1]This approximation is usually referred to as the first Markov approximation, however since there does not seem to be a second markov approximation, I drop the reference to order. Further discussions of the physical implications of the Markov approximation can be found in Refs. [51, 53].

and are valid in the both the time and frequency domains. Further more, Eq. (2.26) becomes

$$\begin{aligned}\partial_t P - i\left[h_{sys}\,,\,P\right] &= \Big(\sqrt{\gamma}b^{\dagger}_{\rm in}(t) - \frac{\gamma}{2}X^{(-)}(t)\Big)\Big[X^{(+)}\,,\,P\Big] \\ &\quad - \Big[X^{(-)}\,,\,P\Big]\Big(\sqrt{\gamma}b_{\rm in}(t) - \frac{\gamma}{2}X^{(+)}(t)\Big), \quad \text{and,} \qquad (2.32)\\ &= \Big(-\sqrt{\gamma}b^{\dagger}_{\rm out}(t) + \frac{\gamma}{2}X^{(-)}(t)\Big)\Big[X^{(+)}\,,\,P\Big] \\ &\quad - \Big[X^{(-)}\,,\,P\Big]\Big(-\sqrt{\gamma}b_{\rm out}(t) + \frac{\gamma}{2}X^{(+)}(t)\Big). \qquad (2.33)\end{aligned}$$

2.2.4 Causality

Now, with Eq. (2.32), an arbitrary system operator $P(t)$ is solved in terms of system operators, and the input operator $b_{\rm in}(t')$. Thus, it must be the case that

$$[P(t), b_{\rm in}(t')] = 0 \qquad \text{for } t' > t, \qquad (2.34)$$

which is to say that a system operator at some time t does not depend on the input operator at some later time t', and is intuitively obvious. Also, Eq. (2.33) in terms of the output fields are a kind of backward evolution equation and so

$$[P(t), b_{\rm out}(t')] = 0 \qquad \text{for } t' < t. \qquad (2.35)$$

Furthermore, since the two equations

$$\begin{aligned}\int_{-\infty}^{\infty} d\omega\, \frac{\gamma}{\sqrt{2\pi}} b_\omega(t) &= -\sqrt{\gamma}b_{\rm in}(t) + \frac{\gamma}{2}X^{(+)}(t), \quad \text{and,} \qquad (2.36)\\ &= \sqrt{\gamma}b_{\rm out}(t) - \frac{\gamma}{2}X^{(+)}(t), \qquad (2.37)\end{aligned}$$

both commute with any system operator at the same time t, we arrive at

$$\begin{aligned}[P(t), b_{\rm in}(t')] &= \theta(t-t')\sqrt{\gamma}[P(t), X^{(+)}(t')], \qquad (2.38)\\ [P(t), b_{\rm out}(t')] &= \theta(t'-t)\sqrt{\gamma}[P(t), X^{(+)}(t')], \qquad (2.39)\end{aligned}$$

where we again use the heaviside step function defined as

$$\theta(s) = \begin{cases} 0, & s < 0 \\ \frac{1}{2}, & s = 0 \\ 1, & s > 0. \end{cases} \qquad (2.40)$$

This completes the general treatment of a system in the input-output formalism. We now use this theory in two specific examples, a two-level atom in free-space and in a cavity.

2.3 Two level atom in free space

In this section, we consider the interaction of a two-level atom with transition frequency ω_a with the continuum of the electromagnetic field. The hamiltonian in the rotating wave approximation is

$$h = \omega_a \sigma^\dagger \sigma + \int d\omega\, \omega a_\omega^\dagger a_\omega + i \int d\omega\, \kappa_\omega (a_\omega^\dagger \sigma - \sigma^\dagger a_\omega), \tag{2.41}$$

where as usual a is the annihilation operator of the field, and $\sigma = |g\rangle\langle e|$ is the atomic lowering operator. Using the general formalism of Sec. 2.2, making the Markov approximation and identifying the atomic transition rate Γ as

$$\kappa_w = \sqrt{\frac{\Gamma}{2\pi}}, \tag{2.42}$$

we directly write

$$\dot{\sigma} = (-\frac{\Gamma}{2} - i\omega)\sigma(t) - \sqrt{\Gamma}\sigma_z a_{\text{in}}(t), \quad \text{or,} \tag{2.43}$$

$$= (\frac{\Gamma}{2} - i\omega)\sigma(t) + \sqrt{\Gamma}\sigma_z a_{\text{out}}(t), \tag{2.44}$$

and also,

$$\dot{\sigma_z} = -\Gamma(\sigma_z + \mathbb{1}) + 2\sqrt{\Gamma}(a_{\text{in}}^\dagger \sigma(t) + \sigma^\dagger a_{\text{in}}(t)) \quad \text{or,} \tag{2.45}$$

$$= \Gamma(\sigma_z + \mathbb{1}) - 2\sqrt{\Gamma}(a_{\text{out}}^\dagger \sigma(t) + \sigma^\dagger a_{\text{out}}(t)), \tag{2.46}$$

where as a reminder, the input and output fields are defined as

$$a_{\text{in}}(t) = -\frac{1}{\sqrt{2\pi}} \int d\omega\, a_\omega(t_0) e^{-i\omega(t-t_0)}, \tag{2.47}$$

$$a_{\text{out}}(t) = \frac{1}{\sqrt{2\pi}} \int d\omega\, a_\omega(t_1) e^{-i\omega(t-t_1)}. \tag{2.48}$$

As an example on its use, let us assume that the initial state of the atom-bath system is

$$|\psi_0\rangle = |\phi\rangle_{\text{atom}} \otimes |\{\alpha\}\rangle, \tag{2.49}$$

where

$$|\{\alpha\}\rangle = \exp\left[\alpha \int d\omega \tilde{f}(\omega)\tilde{a}^{\dagger}_{\text{in}}(\omega) - \tilde{f}^{*}(\omega)\tilde{a}_{\text{in}}(\omega)\right]|0\rangle, \tag{2.50}$$

is a continuous mode coherent state which represents an input pulse with temporal shape $f(t) = \mathcal{F}_t[\tilde{f}(\omega)]$, with $\int dt\,|f(t)|^2 = 1$; $\tilde{a}_{\text{in}}(\omega)$ is the input operator in (angular) frequency space. This allows one to write the the following set of equations for the expectations

$$\partial_t \vec{s}(t) = M(t)\vec{s}(t) + \vec{c}, \tag{2.51}$$

where,

$$\vec{s} = \begin{pmatrix} \langle\sigma\rangle \\ \langle\sigma^{\dagger}\rangle \\ \langle\sigma_z\rangle \end{pmatrix}, \tag{2.52}$$

$$M(t) = \begin{pmatrix} -\frac{\Gamma}{2} - i\omega & 0 & -\sqrt{\Gamma}\alpha f(t) \\ 0 & -\frac{\Gamma}{2} + i\omega & -\sqrt{\Gamma}\alpha f^{*}(t) \\ 2\sqrt{\Gamma}\alpha f^{*}(t) & 2\sqrt{\Gamma}\alpha f(t) & -\Gamma \end{pmatrix}, \tag{2.53}$$

$$\vec{c} = \begin{pmatrix} 0 \\ 0 \\ -\Gamma \end{pmatrix}. \tag{2.54}$$

This matrix equation is exactly the same ones as in Ref. [60], and the variation of different input pulses forms the basis of the analysis in that paper.

However, the present formalism is more powerful in the sense that it additionally also solves for the output field after the interaction. This can be done by using the input-output relation

$$a_{in}(t) + a_{out}(t) = \sqrt{\Gamma}\sigma(t). \tag{2.55}$$

Then, since $\langle a_{in}(t)\rangle = \alpha f(t)$, we have

$$\langle a_{out}(t)\rangle = \sqrt{\Gamma}\,\langle\sigma(t)\rangle - \alpha f(t). \tag{2.56}$$

Furthermore, since

$$|a_{in}(t) + a_{out}(t)|^2 = \Gamma\sigma^{\dagger}\sigma, \tag{2.57}$$

$$a^{\dagger}_{in}a_{in} + a^{\dagger}_{out}a_{out} + a^{\dagger}_{in}a_{out} + a^{\dagger}_{out}a_{in} = \Gamma\sigma^{\dagger}\sigma, \tag{2.58}$$

we can further compute

$$\left\langle a_{out}^{\dagger} a_{out} \right\rangle = \Gamma \left\langle \sigma^{\dagger}\sigma \right\rangle - |\alpha f(t)|^2 - \alpha f^*(t) \left\langle a_{out} \right\rangle - \alpha \left\langle a_{out}^{\dagger} \right\rangle f(t), \tag{2.59}$$

$$= \Gamma \left\langle \sigma^{\dagger}\sigma \right\rangle - |\alpha f|^2 - \alpha f^*(\sqrt{\Gamma} \left\langle \sigma \right\rangle - \alpha f) - (\sqrt{\Gamma} \left\langle \sigma^{\dagger} \right\rangle - \alpha f^*)\alpha f, \tag{2.60}$$

$$= \Gamma \left\langle \sigma^{\dagger}\sigma \right\rangle - \alpha\sqrt{\Gamma}\Big(f^* \left\langle \sigma \right\rangle + \left\langle \sigma^{\dagger} \right\rangle f\Big) + \alpha^2 |f|^2, \tag{2.61}$$

which is solvable from the set of equations (2.51). This can be scaled up even further to calculate *any* correlation function of the output fields using the commutation relations Eqs. (2.38) and (2.39), and the fact that $\mathbb{1}, \sigma, \sigma^{\dagger}$ and σ_z span the system space, in the sense that any product of atomic operators can be expressed as linear combinations of these operators. Further use of the well-known quantum regression theorem also allows multi-time correlation functions to be computed. Also, one can define multiple independent bath modes representing pulses propagating in different directions and scale up the computation in a multitude of ways.

2.4 Two level atom in a cavity

In this section, we study the interaction of a two-level atom in a cavity. This section represents work done in the proposal for a loophole-free Bell test in Chapters 3-5. In that work, what is required is the full description of the quantum state after the interaction of an input pulse with the system. As previously described, in the free-space case, we were able to calculate all measurable correlation functions of the output fields. However, this formalism alone is not enough to accurately describe the fields produced in the atom-cavity system, since this is a highly non-linear system and fully analytical solutions of the open cavity system are not known. Then, using the dispersive measurements of qubits in cavities as inspiration, we seek to perform the interaction in the dispersive regime of the atom-cavity system.

This section proceeds as follows. We first show the usual Jaynes-Cummings hamiltonian which describes the closed atom-cavity system, presenting an unusual method to solve this Hamiltonian using a diagonalization method found in [61]. This method allows one to derive the dispersive hamiltonian while clearly showing the approximations made. We briefly discuss this Hamiltonian and our reasons for not applying it directly to our problem. We next discuss the approximations we make and show that they necessarily imply that we are working in the dispersive regime. We then go on to solve the problem of a dispersively coupled atom-cavity system coupled to multiple baths.

2.4.1 The Jaynes Cummings Hamiltonian

This subsection is essentially a reproduction of the appendix of Ref. [61]. In that work, they were concerned with the validity of the dispersive approximation in certain parameters ranges, and were trying to find higher order corrections. However, since this formalism is not widely discussed in books, I reproduce it here for completeness.

Our starting point is the Jaynes Cummings model hamiltonian, which models the interaction of a single atom and a single mode of the cavity

$$h_{sys} = \omega_c a^\dagger a + \omega_a \sigma^\dagger \sigma + g(a^\dagger \sigma + a\sigma^\dagger), \tag{2.62}$$

where ω_c is the frequency of the cavity mode, ω_a is the frequency of the atomic transition, and g is the coupling strength of the atom-cavity system. Using the same notation as Ref. [61], we reexpress the above as,

$$h_{sys} = h_0 + gI_+, \tag{2.63}$$

where

$$h_0 = \omega_c a^\dagger a + \omega_a \sigma^\dagger \sigma, \quad \text{and,} \tag{2.64}$$
$$I_+ = a^\dagger \sigma + a\sigma^\dagger. \tag{2.65}$$

We would like to diagonalize the hamiltonian in Eq. (2.62) by applying a time independent unitary. As is well known, one constant of motion in this closed system is the total number of excitations, $\hat{N} = a^\dagger a + \sigma^\dagger \sigma$. Using this fact, we seek a unitary of the form

$$U = e^{-\Lambda(\hat{N})I_-}, \tag{2.66}$$

for some unknown $\Lambda(\hat{N})$, which is a function of $\hat{N}$ to be determined, and $I_- = a^\dagger \sigma - a\sigma^\dagger$, such that $U^\dagger h_{sys} U$ is diagonal. Note that I_- is anti-hermitian, and so U is unitary by construction. The following are useful identities in the computation.

$$\left[I_\pm\,,\,\hat{N}\right] = 0 \quad , \quad [I_-\,,\,I_+] = -2\hat{N}\sigma_z, \tag{2.67}$$
$$[I_-\,,\,\sigma_z] = 2I_+ \quad , \quad [I_-\,,\,h_0] = \Delta I_+, \tag{2.68}$$
$$\mathcal{L}(\hat{B}) = \left[\hat{A}\,,\,\hat{B}\right] \quad , \quad \mathcal{L}^n(\hat{B}) = \left[\hat{A}\,,\,\mathcal{L}^{n-1}(\hat{B})\right], \tag{2.69}$$
$$e^{a\hat{A}}\hat{B}e^{-a\hat{A}} = \sum \frac{(a)^n}{n!}\mathcal{L}^n(\hat{B}), \tag{2.70}$$

and we have defined the atom cavity detuning $\Delta = \omega_a - \omega_c$. Direct application of the unitary then leads to

$$U^\dagger h_0 U = h_0 + \frac{\Delta}{2}\Big(\frac{I_+}{\sqrt{\hat{N}}}\sin\Phi - \sigma_z(1-\cos\Phi)\Big), \quad \text{and,} \tag{2.71}$$

$$U^\dagger I_+ U = I_+\cos\Phi - \sigma_z\sqrt{\hat{N}}\sin\Phi, \tag{2.72}$$

with $\Phi = 2\Lambda\sqrt{\hat{N}}$. Combining both equations, we finally arrive at

$$U^\dagger h_{sys} U = h_0 + I_+\Big(g\cos\Phi + \frac{\Delta}{2\sqrt{\hat{N}}}\sin\Phi\Big) - \sigma_z\Big(g\sqrt{\hat{N}}\sin\Phi + \frac{\Delta}{2}(1-\cos\Phi)\Big). \tag{2.73}$$

Now, since h_0 and σ_z contain only "uncoupled" terms, we set

$$\tan 2\Lambda\sqrt{\hat{N}} = -2\lambda\sqrt{\hat{N}}, \tag{2.74}$$

where $\lambda = \frac{g}{\Delta}$, such that the coefficient of I_+ vanishes. Thus, the hamiltonian after applying the unitary operation and using (2.74) is

$$h^D_{sys} = h_0 - \frac{\Delta}{2}\sigma_z\Big(1 - \sqrt{1+4\lambda^2\hat{N}}\Big). \tag{2.75}$$

Since the hamiltonian is now diagonal, the eigenstates are just the bare states atom-cavity states. However, since the unitary amounts to a change in the frame, to obtain the eigenstates of the Jaynes-Cummings hamiltonian in terms of the "real" states of the atom and cavity, $|\pm, n\rangle$, we apply the unitary to the bare states. This gives

$$\begin{aligned}\begin{pmatrix}|+,n\rangle\\ |-,n\rangle\end{pmatrix} &= U\begin{pmatrix}|g,n\rangle\\ |e,n-1\rangle\end{pmatrix},\\ &= \begin{pmatrix}\cos\frac{\Phi}{2} & \sin\frac{\Phi}{2}\\ -\sin\frac{\Phi}{2} & \cos\frac{\Phi}{2}\end{pmatrix}\begin{pmatrix}|g,n\rangle\\ |e,n-1\rangle\end{pmatrix},\end{aligned} \tag{2.76}$$

where $\Phi = 2\Lambda\sqrt{\hat{N}}$, and Eq. (2.74) is used. These are the usual eigenstates of the Jaynes-Cummings model, as can be verified by the reader. Although the method of deriving this well-known result is undoubtedly fairly complicated, it allows for conveniently reading off the eigenstates of the system. It is also the first step in making the dispersive approximation, as we show in the next subsection.

2.4.2 Dispersive regime

As is evident in Eqs. (2.74) and (2.76), the main parameter which characterizes the dynamics of the system after the unitary transform is a factor of the form, $\Lambda\sqrt{\hat{N}}$, and is related to physical system parameters through Eq. (2.74). Eq. (2.74) is a non-linear equation relating Λ to λ, and is not useful on its own. However, in the limit of small $\lambda\sqrt{\hat{N}}$, *i.e.* when $2\lambda\sqrt{\hat{N}} \ll 1$, we have

$$\begin{aligned} \tan 2\Lambda\sqrt{\hat{N}} &= -2\lambda\sqrt{\hat{N}}, \\ \Rightarrow 2\Lambda\sqrt{\hat{N}} &\approx -2\lambda\sqrt{\hat{N}}, \qquad (2.77) \\ \Rightarrow \Lambda\sqrt{\hat{N}} &= -\lambda\sqrt{\hat{N}}. \qquad (2.78) \end{aligned}$$

In this limit, equations (2.75) and (2.76) to first order in λ become,

$$h^D_{sys} \approx h_0 + \frac{g^2}{\Delta}\hat{N}\sigma_z, \quad \text{and}, \qquad (2.79)$$

$$\begin{pmatrix} |+,n\rangle \\ |-,n\rangle \end{pmatrix} \approx \begin{pmatrix} 1 & -\sqrt{n}\frac{g}{\Delta} \\ \sqrt{n}\frac{g}{\Delta} & 1 \end{pmatrix} \begin{pmatrix} |g,n\rangle \\ |e,n-1\rangle. \end{pmatrix} \qquad (2.80)$$

This means that in the dispersive regime, the bare eigenstates of h_0 very closely resemble the new eigenstates, and thus characterizes a situation of weak atom-cavity coupling.

Furthermore, if one is able to adiabatically "turn on" the interaction between atom and cavity, the atomic state will adiabatically follow the eigenstates of the new system with a suppression of energy exchange between atom and cavity by a factor $\frac{g}{\Delta}$. This observation is used extensively in the readout of cavity fields in the experiments of Serge Haroche [62, 63, 64].

2.4.3 Interaction with external baths

The above derivation of the dispersive Hamiltonian shows that one cannot directly apply input-output theory to this Hamiltonian. This is because a unitary has been done on the system, and so the system operators a and σ in this frame, are *not* the annihilation operators of the field and atomic excitation respectively! Thus, the coupling to baths is not straightforward. Ref. [61] recognizes this fact, and has expressions for the system operators (a and σ) in the dispersive picture. However, it is not clear to the author if these expansions are applicable, since the expansions assume small λ, and not $\lambda\sqrt{\hat{N}}$ which should be the case in the dispersive approximation. Furthermore, on using the expansions of these operators

found in Ref. [61], one is lead to non-linear terms with coefficients such as $g\lambda^2$, and there is no clear indication if such terms can be safely ignored.

Due to these reasons, we seek another route to the same goal. We first fall back to the Jaynes-Cummings Hamiltonian as our system Hamiltonian, and assume that the atom and the cavity field each individually couple to a bath. The full hamiltonian being

$$h_{\text{total}} = h_{\text{sys}} + h_{\text{bath}} h_{\text{int}}, \tag{2.81}$$

$$h_{\text{sys}} = \omega_c a^\dagger a + \omega_a \sigma^\dagger \sigma + g(a^\dagger \sigma + \sigma^\dagger a), \tag{2.82}$$

$$h_{\text{bath}} = \int d\omega\, \omega (b_\omega^\dagger b_\omega + r_\omega^\dagger r_\omega), \tag{2.83}$$

$$h_{\text{int}} = i \int d\omega\, \tilde{\kappa}(\omega)(b_\omega^\dagger a - b_\omega a^\dagger) + \tilde{\Gamma}(r_\omega^\dagger \sigma - r_\omega \sigma^\dagger). \tag{2.84}$$

Using the formalism developed in Sec. 2.2, we can write the Heisenberg equations of motion of the system operators in terms of the input bath fields. These are

$$\partial_t a = -(\frac{\kappa}{2} + i\omega_c)a - ig\sigma + \sqrt{\kappa} b_{\text{in}}, \tag{2.85}$$

$$\partial_t \sigma = -(\frac{\Gamma}{2} + i\omega_a)\sigma + ig\sigma_z a - \sqrt{\Gamma}\sigma_z r_{\text{in}}. \tag{2.86}$$

Note that this system of equations is not closed, since we also need equations of motions for the $\sigma_z a$ term. A quick check will show that if we would like to solve these operator equations directly, we need an infinite set of equations. In the Jaynes-Cummings model without external interactions, the infinite set of equations can be avoided by identifying the total excitation number $N = a^\dagger a + \sigma^\dagger \sigma$ and $C = \Delta\sigma^\dagger\sigma + g(a^\dagger\sigma + \sigma^\dagger a)$ as constants of motion [6]. However, the open system has no obvious constants of motion other than the total excitation number.

A drastic approximation

Instead of trying to directly solve this system for the general case, we try to attack this problem in the dispersive regime as studied in Sec. 2.4.2. This approach is largely motivated by the fact that we wish to use this system again in Chapter 4 for the preparation of a specific state.

We first assume that the atom stays essentially only in the ground state throughout the interaction. This can be weakly translated to the condition $\sigma_z(t) \approx -\mathbb{1}, \forall\, t$.

Under the approximation $\sigma_z \approx -\mathbb{1}$, Eqs. (2.85) and (2.86) simplify to

$$\partial_t a = -(\frac{\kappa}{2} + i\omega_c)a - ig\sigma + \sqrt{\kappa}b_{\text{in}}, \tag{2.87}$$

$$\partial_t \sigma = -(\frac{\Gamma}{2} + i\omega_a)\sigma - iga + \sqrt{\Gamma}r_{\text{in}}. \tag{2.88}$$

This approximation also makes these equations linear, and they can be most simply solved with Fourier transforms. Using the convention

$$f(t) = \frac{1}{\sqrt{2\pi}} \int_{-\infty}^{\infty} d\omega\, e^{-i\omega t} \tilde{f}(\omega), \tag{2.89}$$

where the tilde once again represents functions in frequency space, we can write immediately the matrix equation

$$\begin{pmatrix} \frac{\kappa}{2} - i(\omega - \omega_c) & ig \\ ig & \frac{\Gamma}{2} - i(\omega - \omega_a) \end{pmatrix} \begin{pmatrix} \tilde{a} \\ \tilde{\sigma} \end{pmatrix} = \begin{pmatrix} \sqrt{\kappa}\tilde{b}_{\text{in}} \\ \sqrt{\Gamma}\tilde{r}_{\text{in}} \end{pmatrix}. \tag{2.90}$$

This matrix equation can be solved by Cramer's rule to obtain

$$\tilde{a} = \frac{1}{\text{Det}(\omega)} \Big([\frac{\Gamma}{2} - i(\omega - \omega_a)]\sqrt{\kappa}\tilde{b}_{\text{in}} - ig\sqrt{\Gamma}\tilde{r}_{\text{in}} \Big), \tag{2.91}$$

$$\tilde{\sigma} = \frac{1}{\text{Det}(\omega)} \Big([\frac{\kappa}{2} - i(\omega - \omega_c)]\sqrt{\Gamma}\tilde{r}_{\text{in}} - ig\sqrt{\kappa}\tilde{b}_{\text{in}} \Big), \tag{2.92}$$

where $\text{Det}(\omega)$ is the determinant of the matrix in Eq. (2.90).

Self-consistency

The approximation $\sigma_z \approx -\mathbb{1}$ is a very drastic approximation, since it amounts to replacing an operator with the identity. It also gives the relation

$$[\sigma, \sigma^\dagger] = -\sigma_z \approx 1, \tag{2.93}$$

i.e. the fermionic two-level system acts like a boson. These two reasons alone should make the reader wonder how one can safely use such a drastic approximation of the system dynamics.

This subsection seeks to alleviate some of these concerns. We will show that, under some reasonable conditions, the dispersive approximation is a necessary condition for the validity of this approximation, thus implying that the bare atom-cavity states are approximate eigenstates of the dynamics. Although this alone does not fully justify the replacing of the operator σ_z with $-\mathbb{1}$, it certainly

is comforting that it necessarily requires the dispersive approximation for self-consistency, which is what we started out with.

Now, the approximation $\sigma_z \approx -\mathbb{1}$ must have the condition $\left\langle \sigma^\dagger \sigma \right\rangle \ll 1$ for self-consistency, and should hold both in the time and frequency domains. This implies that in the frequency domain, we have

$$\left\langle \tilde{\sigma}^\dagger \tilde{\sigma} \right\rangle = \frac{1}{|\mathrm{Det}(\omega)|^2} \left\langle \left| [\frac{\kappa}{2} - i(\omega - \omega_c)] \sqrt{\Gamma} \tilde{r}_{\mathrm{in}} - ig\sqrt{\kappa} \tilde{b}_{\mathrm{in}} \right|^2 \right\rangle \ll 1. \tag{2.94}$$

Now, we state and proof the following claim:

Lemma 1. *The conditions:*

C1: *The r bath is initially in the vacuum state, such that $\left\langle \hat{O}\, r \right\rangle = \left\langle r^\dagger \hat{O} \right\rangle = 0$.*

C2: *The b bath coupled to the cavity mode is initially non-empty only at frequencies close to the bare cavity frequency.*

C3: *The atom-cavity detuning $\Delta = \omega_c - \omega_a$ is much larger than the atomic transition linewidth Γ, i.e. $\Delta \gg \Gamma$.*

together with the self-consistency condition (2.94) for $\sigma_z \approx -\mathbb{1}$, is equivalent to the dispersive approximation.

Proof. Condition C1 allows us to simplify Eq. (2.94) to

$$\left\langle \tilde{\sigma}^\dagger \tilde{\sigma} \right\rangle = \frac{1}{|\mathrm{Det}(\omega)|^2} \left(g^2 \kappa \left\langle b_{\mathrm{in}}^\dagger b_{\mathrm{in}} \right\rangle \right), \tag{2.95}$$

which, on using the corresponding equation for $\left\langle \tilde{a}^\dagger \tilde{a} \right\rangle$, is

$$\left\langle \tilde{\sigma}^\dagger \tilde{\sigma} \right\rangle = \left\langle \frac{g^2}{(\frac{\Gamma}{2})^2 + (\omega - \omega_a)^2} \tilde{a}^\dagger \tilde{a} \right\rangle. \tag{2.96}$$

Then, applying conditions C2 and C3,

$$\left\langle \tilde{\sigma}^\dagger \sigma \right\rangle \approx \frac{g^2}{\Delta^2} \left\langle \tilde{a}^\dagger a \right\rangle. \tag{2.97}$$

Since $\left\langle \tilde{\sigma}^\dagger \tilde{\sigma} \right\rangle \ll 1$, we have $\left\langle \hat{N} \right\rangle \approx \left\langle a^\dagger a \right\rangle$. Then, Eq. (2.94) becomes

$$\left\langle \tilde{\sigma}^\dagger \sigma \right\rangle \approx \frac{g^2}{\Delta^2} \left\langle \hat{N} \right\rangle \ll 1. \tag{2.98}$$

Thus, the self-consistency of the approximation $\sigma_z \approx -\mathbb{1}$ is the dispersive approximation, if the conditions C1 - C3 are simultaneously satisfied. □

Remarks on conditions C1-C3: Condition C1 is usually a good approximation for optical transitions, since the environment is usually in a thermal state at a temperature usually around 300K, which has a very small occupancy in the optical frequency range (this is intuitively obvious from normal daily life, as a dark room is dark and not bursting with light.) The second condition C2 is an arbitrary restriction on the pumping frequencies, however, with the third conditions it becomes more natural, since we are in effect trying to keep the atom from being excited. Thus, cavity quanta and any pumping of the system should be far away from the atomic resonance.

Remark on lemma 1: It must be noted that what we have just shown in Lemma 1 is that the dispersive approximation is equivalent to conditions C1-C3 and Eq. (2.94), and thus a necessary condition for the approximation $\sigma_z \approx -\mathbb{1}$ to be true. It is however, not sufficient to show that the approximation is valid.

2.4.4 Transformation of inputs

Using the approximation $\sigma_z \approx -\mathbb{1}$ allowed us to write the matrix equation Eq. (2.90). However, we could just as well write the equations relating the system operators to the outputs instead, leading to

$$\begin{pmatrix} -\frac{\kappa}{2} - i(\omega - \omega_c) & ig \\ ig & -\frac{\Gamma}{2} - i(\omega - \omega_a) \end{pmatrix} \begin{pmatrix} \tilde{a} \\ \tilde{\sigma} \end{pmatrix} = - \begin{pmatrix} \sqrt{\kappa}\tilde{b}_{\text{out}} \\ \sqrt{\Gamma}\tilde{r}_{\text{out}} \end{pmatrix}. \tag{2.99}$$

Using some simple linear algebra gives

$$\begin{pmatrix} \sqrt{\kappa}\tilde{b}_{\text{in}} \\ \sqrt{\Gamma}\tilde{r}_{\text{in}} \end{pmatrix} = \frac{1}{D(\omega)} \begin{pmatrix} (\frac{\kappa}{2} - i\delta_c)(\frac{\Gamma}{2} + i\delta_a) - g^2 & ig\kappa \\ ig\Gamma & (\frac{\kappa}{2} + i\delta_c)(\frac{\Gamma}{2} - i\delta_a) - g^2 \end{pmatrix} \begin{pmatrix} \sqrt{\kappa}\tilde{b}_{\text{out}} \\ \sqrt{\Gamma}\tilde{r}_{\text{out}} \end{pmatrix}, \tag{2.100}$$

$$D(\omega) = (\frac{\kappa}{2} + i\delta_c)(\frac{\Gamma}{2} + i\delta_a) + g^2, \tag{2.101}$$

and we have also defined $\delta_a = \omega - \omega_a$ and $\delta_c = \omega - \omega_c$. Thus, an input state of the form

$$|\psi\rangle = f(b_{\text{in}})|0\rangle \otimes g(r_{\text{in}})|0\rangle \tag{2.102}$$

transforms to the output state according to Eq. (2.100).

2.4.5 Multiple field couplings

The previous section was for when the cavity field is coupled to a single bath. However, this is an unrealistic assumption in experiments, since a cavity is made of two independent mirrors, so there should be at least two baths representing couplings to the individual mirrors. On top of this, we also include the possibility of non-radiative mirror losses to better model experiments.

To treat the case of multiple field couplings to the cavity, we return to the matrix solution (Eq. (2.100)). This solution is derived using

$$\begin{pmatrix} \frac{\kappa}{2} - i\delta_c & ig \\ ig & \frac{\Gamma}{2} - i\delta_a \end{pmatrix}^{-1} \begin{pmatrix} \sqrt{\kappa}\tilde{b}_{\text{in}} \\ \sqrt{\Gamma}\tilde{r}_{\text{in}} \end{pmatrix} = \begin{pmatrix} -\frac{\kappa}{2} - i\delta_c & ig \\ ig & -\frac{\Gamma}{2} - i\delta_a \end{pmatrix}^{-1} \begin{pmatrix} -\sqrt{\kappa}\tilde{b}_{\text{out}} \\ -\sqrt{\Gamma}\tilde{r}_{\text{out}} \end{pmatrix}. \tag{2.103}$$

We note that with multiple field couplings to the cavity, we have $\sqrt{\kappa}b_{\text{in/out}} = \sum_i \sqrt{\kappa_i}b_{i,\text{in/out}}$ and $\kappa = \sum_i \kappa_i$. However, it still is not an equation for individual inputs in terms of outputs. Notice that converting from input to output operators, we require the following replacements, $\sqrt{\kappa_i}b_{i,\text{in}} \to -\sqrt{\kappa_i}b_{i,\text{out}}$ and $\kappa_i \to -\kappa_i$. Defining $k_i = \kappa - 2k_i$, and using the abbreviations

$$v_{\text{in}\to} = \sum_i \sqrt{\kappa_i}\tilde{b}_{i,\text{in}}, \tag{2.104}$$

$$v_{\text{out}\to} = \sum_i \sqrt{\kappa_i}\tilde{b}_{i,\text{out}}, \tag{2.105}$$

$$v_{\{i\},\text{in}} = \sqrt{\kappa_i}\tilde{b}_{i,\text{in}} - \sum_{j\neq i} \sqrt{\kappa_j}\tilde{b}_{j,\text{out}}, \tag{2.106}$$

we can write,

$$\begin{pmatrix} -\frac{k_i}{2} - i\delta_c & ig \\ ig & \frac{\Gamma}{2} - i\delta_a \end{pmatrix}^{-1} \begin{pmatrix} v_{\{i\},\text{in}} \\ \sqrt{\Gamma}\tilde{r}_{\text{in}} \end{pmatrix} = \begin{pmatrix} -\frac{\kappa}{2} - i\delta_c & ig \\ ig & -\frac{\Gamma}{2} - i\delta_a \end{pmatrix}^{-1} \begin{pmatrix} -v_{\text{out}\to} \\ -\sqrt{\Gamma}\tilde{r}_{\text{out}} \end{pmatrix}, \tag{2.107}$$

where we have converted all inputs $\to$ outputs except the i^{th} mode in the LHS of Eq. (2.103). Then, we can write

$$\begin{pmatrix} v_{\{i\},\text{in}} \\ \sqrt{\Gamma}\tilde{r}_{\text{in}} \end{pmatrix} = \frac{1}{D(\omega)} \begin{pmatrix} -(\frac{k_i}{2} + i\delta_c)(\frac{\Gamma}{2} + i\delta_a) - g^2 & ig\kappa_i \\ ig\Gamma & (\frac{\kappa}{2} + i\delta_c)(\frac{\Gamma}{2} - i\delta_a) - g^2 \end{pmatrix} \begin{pmatrix} v_{\text{out}\to} \\ \sqrt{\Gamma}\tilde{r}_{\text{out}} \end{pmatrix}. \tag{2.108}$$

With the above relation, we can write the input evolution equations as,

$$\begin{pmatrix} \vec{v}_{\text{in}} \\ \tilde{r}_{\text{in}} \end{pmatrix} = \begin{pmatrix} U_{\text{in}\to\text{out}}(\omega) & \vec{n}^T(\omega) \\ \vec{n}(\omega) & \sigma_{\text{in}\to\text{out}}(\omega) \end{pmatrix} \begin{pmatrix} \vec{v}_{\text{out}} \\ \tilde{r}_{\text{out}} \end{pmatrix}, \tag{2.109}$$

with

$$\vec{v}^T_{\text{in/out}} = (b_{1,\text{in/out}}, b_{2,\text{in/out}} \ldots, b_{N,\text{in/out}}), \tag{2.110}$$

$$\vec{n}^T(\omega) = \frac{ig\sqrt{\Gamma}}{D(\omega)}(\sqrt{\kappa_1}, \sqrt{\kappa_2}, \ldots, \sqrt{\kappa_N}); \tag{2.111}$$

the unitary matrix $U_{\text{in}\to\text{out}}$ defined as

$$U_{\text{in}\to\text{out},ij} = t_i(\omega) + \delta_{ij}(r_i(\omega) - t_i(\omega)), \tag{2.112}$$

and the various coefficients are

$$\sigma_{\text{in}\to\text{out}}(\omega) = \frac{1}{D(\omega)}\Big[(\frac{\kappa}{2} + i\delta_c)(\frac{\Gamma}{2} - i\delta_a) - g^2\Big], \tag{2.113}$$

$$t_i(\omega) = \frac{\kappa_i(\frac{\Gamma}{2} + i\delta_a)}{D(\omega)}, \quad \text{and} \tag{2.114}$$

$$r_i(\omega) = \frac{-1}{D(\omega)}\Big[(\frac{k_i}{2} + i\delta_c)(\frac{\Gamma}{2} + i\delta_a) + g^2\Big]. \tag{2.115}$$

CHAPTER 3

BELL TEST - SCENARIO

As explained in the introduction, we seek another route to the closure of the loopholes in Bell tests. We first note that atomic, ionic and solid state systems can be detected with high efficiencies, but are in essence stationary. Photons on the other hand are small packets of energy which usually only perturb the medium in which it travels slightly, thus making them hard to detect. But at the same time, able to travel large distances with relatively low loss. One could then imagine entangling a propagation light field with one of these stationary systems and performing a bell state on the resultant atom-photon state. The propagating light field would then help to close the locality loophole, and the efficient detection on the stationary system would help to close the detection loophole.

To perform the Bell test, we use the CHSH inequality:

$$\mathcal{B} = \sum_{i,j \in \{0,1\}} (-1)^{i \cdot j} \langle A_i B_j \rangle \leq 2, \tag{3.1}$$

where A_i and B_j are local measurement operators that each party Alice and Bob can perform on the state. The violation of this inequality in an experiment without any loopholes would then imply that nature does not satisfy both locality and realism simultaneously. This inequality is a two party inequality, with each party having two measurements and each measurement having two outcomes. We use the CHSH inequality as an example, to illustrate that atom-photon states are indeed viable candidates to be used in bell tests. In principle however, one could try other inequalities for such a system, since the photon dimension is infinite.

3.1 Atomic measurements

As may be well known to the reader, the violation of the Bell's inequalities is highly dependent not only on the quantum state measured, but also on the measurements done on the state. Thus, we first describe the set of measurements we would like to perform on the state before going into the details of the state.

We assume that the stationary system can be well approximated by a two-level system. In this case, measurements on this system can be described by vectors on the bloch sphere of the form

$$A_0 = \sin\gamma\sigma_x + \cos\gamma\sigma_z, \quad \text{and,} \tag{3.2}$$

$$A_1 = \sin\gamma\sigma_x - \cos\gamma\sigma_z, \tag{3.3}$$

where σ_x and σ_z are the usual pauli matrices; we further make the simplification that these measurements are restricted to the $x-z$ plane of the bloch sphere, and are simply parametrized by a single γ angle. This vastly simplifies the search space of possible measurements.

3.2 Photonic measurements

To measure the photonic degrees of freedom, we take inspiration from [65] and first consider photocounting and homodyne measurements. The photocounting measurement is done simply by letting the propagating light impinge on a photon-number resolving detector, while the homodyne measurement is done by combing the signal with a strong local oscillator on a beam splitter, and measuring the difference in intensity signals on both beam splitter outputs. Because of the intense local oscillator, the homodyne measurement can be made highly efficient even though the underlying photodetectors are not as efficient [66]. The efficiency of the photocounting measurement however, *is* the photodetector efficiency. The efficiency of commercially available, photon-number resolving, Si avalanche detectors are on the order of 30% for optical frequencies[1]. Although highly efficient detectors are available [67, 68], these work on the physical process of detecting a superconducting phase transition, and require that the detector be temperature stabilized at cryogenic temperatures, thus making such detectors difficult to implement experimentally.

[1] See for instance, Thor labs SPCM20A/M and SPCM50A/M.

However, both of these photonic measurements have infinite outcomes and require dichotomization of the outcomes to be suitable for use in the CHSH inequality. The homodyne measurement produces an outcome on the real line, the dichotomization is then taken as partitioning the real line into bins. We choose a symmetric binning such that the $+1$ outcome is when the measurement is $\in [-b, b]$, and the -1 outcome when it falls outside. The measurement operator would then look like

$$B_{\text{homodyne}} = 2\int_{-b}^{b} dx\, |x_\theta\rangle\langle x_\theta| - \mathbb{1}, \tag{3.4}$$

where $|x_\theta\rangle$ is the eigenstate of the operator $x_\theta = \frac{ae^{-i\theta}+a^\dagger e^{i\theta}}{\sqrt{2}}$. Usually, the most inefficient photonic measurement is the photocounting measurement. We thus choose the measurement operator to output $+1$ when nothing is detected, and -1 otherwise. As we will show in a later section, this choice does help in the detection efficiency problem. The measurement operator can then be written as

$$B_{\text{counting}} = 2|0\rangle\langle 0| - \mathbb{1}, \tag{3.5}$$

where $|0\rangle$ denotes the vacuum state of the field.

3.3 The state

With the atomic measurements (3.2, 3.3) and photonic measurements (3.4, 3.5), it has been shown previously in [58, 69], that there exists a state of the form

$$|\Phi\rangle = \cos\nu|g, 0\rangle + \sin\nu|e, \Xi\rangle, \tag{3.6}$$

which achieves the maximum quantum CHSH value of $2\sqrt{2}$. The states $|g\rangle$ and $|e\rangle$ represent the two energy levels of a two-level system; $|0\rangle$ represents the vacuum state of the electromagnetic field and $|\Xi\rangle$ is another state of the field whose exact form is unimportant in the following discussion. The same authors also prove that the state which maximizes the CHSH inequality unfeasible, since the total photon number of $|\Xi\rangle$ diverges. They then proceeded to approximate the photonic part with a cat state, since the fock state representation of $|\Xi\rangle$ consisted of either even or odd photon numbers. However, propagating cat states are non-trivial states of the electromagnetic field and are not easy to produce experimentally. We instead consider the state

$$|\psi\rangle = \cos\nu|g, 0\rangle + \sin\nu|e, \alpha\rangle, \tag{3.7}$$

where

$$|\alpha\rangle = e^{-|\alpha|^2/2} \sum_{n=0}^{\infty} \frac{\alpha^n}{\sqrt{n!}} |n\rangle \tag{3.8}$$

is a coherent state with amplitude α. We now proceed to compute the CHSH value using the state (3.7) and the measurements (3.2,3.3, 3.4 and 3.5)

3.4 Optimization methodology

With the above constraints, we now show a semi-analytical optimization procedure which not only simplifies numerical optimizations but also allows us derive a surprising theorem. The semi-analytical procedure we use is just the sequential maximization of the function $\mathcal{B}$ over the measurement parameters.

We first notice that the structure of the atomic measurements (3.2) and (3.3) allows one to optimize directly over the measurement angle γ. To see this, we substitute equations (3.2) and (3.3), and rewrite Eq. (3.1) as

$$\mathcal{B} = \langle (A_0 + A_1)B_1 + (A_0 - A_1)B_0 \rangle \tag{3.9}$$

$$= 2\cos\gamma \langle \sigma_z B_1 \rangle + 2\sin\gamma \langle \sigma_x B_0 \rangle , \tag{3.10}$$

where B_0 and B_1 are either the homodyne measurement (3.4) or photocounting (3.5). Since the terms $\langle \sigma_z B_1 \rangle$ and $\langle \sigma_x B_0 \rangle$ are just numbers, the maximum $\mathcal{B}$ over γ is simply

$$\mathcal{B}_\gamma = 2\sqrt{\Big(\mathrm{Tr}(\rho\sigma_x B_0)\Big)^2 + \Big(\mathrm{Tr}(\rho\sigma_z B_1)\Big)^2}, \tag{3.11}$$

where the subscript denotes the variable which has been optimized over, and we have used the fact that $\left\langle \hat{O} \right\rangle = \mathrm{Tr}(\rho\hat{O})$, with $\rho = |\psi\rangle\langle\psi|$. Inserting (3.7) for $|\psi\rangle$ and defining

$$c_1 = \frac{1}{2}\mathrm{Tr}\Big((|0\rangle\langle\alpha| + |\alpha\rangle\langle 0|)B_0\Big), \tag{3.12}$$

$$c_2 = \mathrm{Tr}(|0\rangle\langle 0|B_1), \tag{3.13}$$

$$c_3 = \mathrm{Tr}(|\alpha\rangle\langle\alpha|B_1), \tag{3.14}$$

we get,

$$\mathcal{B}_\gamma = 2\sqrt{(2c_1\cos\nu\sin\nu)^2 + (c_2\cos^2\nu - c_3\sin^2\nu)^2}. \tag{3.15}$$

This allows us to optimize (3.15) again over the angle ν. We first rewrite the above equation as

$$\mathcal{B}_\gamma = 2\sqrt{A\sin^4\nu + B\sin^2\nu + c_2^2}, \tag{3.16}$$

where $A = (c_2 + c_3)^2 - 4c_1^2$ and $B = 4c_1^2 - 2c_2(c_2 + c_3)$. This function has at most 3 extrema, is symmetric about $\sin\nu = 0$, and has $\mathcal{B}_\gamma = 2|c_2| \leq 2$ for $\sin\nu = 0$, and $\mathcal{B}_\gamma = 2|c_3| \leq 2$ for $\sin\nu = 1$. With these conditions, we can write down the following claim:

Claim. *The necessary condition for $\mathcal{B}_\gamma > 2$ is for the function $\mathcal{B}_\gamma$ to have two maxima between $\sin\nu \in (-1, 1)$.*

Proof. To proof this claim, we first rewrite Eq. (3.16) as

$$\mathcal{B}_\gamma = 2\sqrt{f}, \tag{3.17}$$

where $f = A\sin^4\nu + B\sin^2\nu + c_2^2$. Writing Eq. (3.16) in this form makes it clear that if $f > 1$, $\mathcal{B}_\gamma > 2$. Since $c_2, c_3 \leq 1$, f must exceed both c_2 and c_3 to be greater

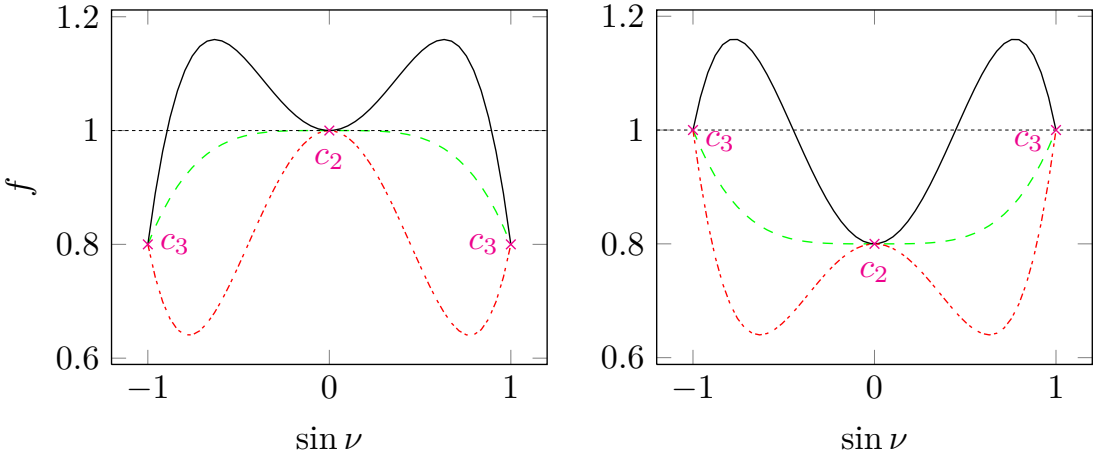

Figure 3.1: The above plots show the possible plots of the function f given $f(\sin\nu = 0) = |c_2|$, and $f(\sin\nu = \pm 1) = |c_3|$. The left graph shows the case when $|c_2| > |c_3|$ and the right graph is when $|c_2| < |c_3|$. As is evident from these graphs, the only possible case for $f \geq 1$ is when f and consequently $\mathcal{B}_\gamma$ has 2 maxima in $\sin\nu \in [-1, 1]$. Note that in both graphs we have let the larger of $|c_2|$ and $|c_3|$ be 1. This is not necessarily the case, and depends on the specific measurements used. Thus, the condition of 2 maxima is a necessary but insufficient condition for $\mathcal{B}_\gamma > 2$.

than 1. Plotting f as a function of $\sin\nu$ in Fig. 3.1 shows that the only type of curve which has $f > c_2, c_3$ is the one with 2 maxima, thus proving claim (3.4). □

Simple differentiation shows that the extrema satisfy the condition

$$(2A\sin^2\nu + B)\sin\nu = 0. \tag{3.18}$$

Thus, the conditions for (3.16) to have two maxima are

$$0 < \frac{B}{-2A} < 1 \quad \text{and,} \tag{3.19}$$

$$A < 0. \tag{3.20}$$

Rewriting the above in terms of c_1, c_2 and c_3 gives,

$$\text{C1:} \qquad c_3(c_2 + c_3) < 2c_1^2$$

$$\text{C2:} \qquad c_2(c_2 + c_3) < 2c_1^2$$

as the necessary conditions for $\mathcal{B} > 2$. From Fig. 3.1, it is evident that if either $c_2 = 1$ or $c_3 = 1$, and both conditions (C1) and (C2) are satisfied, we have immediately $\mathcal{B} > 2$.

If both conditions (C1) and (C2) are met, the maximum $\mathcal{B}$ achievable is given by

$$\mathcal{B}_{\nu,\gamma} = 2\sqrt{\frac{[2c_1^2 - c_2(c_2 + c_3)]^2}{4c_1^2 - (c_2 + c_3)^2} + c_2^2}. \tag{3.21}$$

Notice that we have yet to specify the operators B_0 and B_1, and so the above argument is applicable to any choice of these operators. We will consider two cases; one of these operators is a photocounting measurement and the other is a homodyne measurement, and when both measurements are homodyne measurements.

3.5 One photocounting measurement

In this section, we consider the case where one of the measurements performed on the light state is photocounting. In this case, we note that choosing B_1 to be the photocounting measurement operator given by Eq. (3.5) immediately gives us $c_2 = 1$. Then, satisfying both conditions (C1) and (C2) is sufficient to show a violation of the CHSH inequality.

In the Bell test scenario we consider, we assume that the light field suffers from losses due to imperfect intensity transmission, T_{line}. Next, to study the effect of inefficient photocounting, we assume the atomic detection (A_0,A_1) and homodyne detection (B_0) have perfect detection efficiency, and that photocounting (B_1) has efficiency η. Although this is not a realistic assumption in practice, the high efficiencies of atomic and homodyne measurements would imply that the main detection efficiency problem will come from the photocounting measurement.

We model both the transmission and detection losses as beamsplitters with transmitivities $\sqrt{T_{\text{line}}}$ and $\sqrt{\eta}$. Since the transmission loss is symmetric, the state

just before the detection event is

$$|\Psi\rangle = \cos\nu|g,0\rangle \otimes |0\rangle_{\text{env}} + \sin\nu|e,\sqrt{T_{\text{line}}}\alpha\rangle \otimes |\sqrt{1-T_{\text{line}}}\alpha\rangle_{\text{env}}, \tag{3.22}$$

where $|\rangle_{\text{env}}$ represents the part of the state which is loss to the environment. Tracing out the environment, we arrive at

$$\rho = V|\psi'\rangle\langle\psi'| + (1-V)\sigma, \tag{3.23}$$

where

$$|\psi'\rangle = \cos\nu|g,0\rangle + \sin\nu|s,\sqrt{T_{\text{line}}}\alpha\rangle, \tag{3.24}$$

$$\sigma = \cos^2\nu|g,0\rangle\langle g,0| + \sin^2\nu|s,\sqrt{T_{\text{line}}}\alpha\rangle\langle s,\sqrt{T_{\text{line}}}\alpha|, \quad \text{and} \tag{3.25}$$

$$V = \exp\left[-(1-T_{\text{line}})\frac{|\alpha|^2}{2}\right]. \tag{3.26}$$

Then, the equations (3.12-3.14) become

$$\begin{aligned} c_1 &= \frac{V}{2}\text{Tr}\Big((\Big|0\Big\rangle\Big\langle\sqrt{T_{\text{line}}}\alpha\Big| + \Big|\sqrt{T_{\text{line}}}\alpha\Big\rangle\Big\langle 0\Big|)B_0\Big), \\ &= V\Big(\frac{2}{\sqrt{\pi}}\int_{-b}^{b} dx\, e^{-x^2}\cos(\sqrt{2}x\sqrt{T_{\text{line}}}|\alpha|) - e^{-\frac{T_{\text{line}}|\alpha|^2}{2}}\Big), \end{aligned} \tag{3.27}$$

and

$$c_2 = \text{Tr}(|0\rangle\langle 0|B_1) = 1, \tag{3.28}$$

$$c_3 = \text{Tr}(|\sqrt{\eta T_{\text{line}}}\alpha\rangle\langle\sqrt{\eta T_{\text{line}}}\alpha|B_1) = 2e^{-\eta T_{\text{line}}\frac{|\alpha|^2}{2}} - 1. \tag{3.29}$$

The form of c_1 is derived using the convention that, $\hat{x} = \frac{a+a^\dagger}{\sqrt{2}}$ (see appendix A.1 for details of the derivation). It should further be noted that we have used α completely imaginary in Eq. (3.27). The intuition for this comes from the form of B_0, which is a measurement of the X quadrature, and the form of c_1, which is the trace of B_0 and the "off-diagonal" terms $|0\rangle\langle\alpha| + |\alpha\rangle\langle 0|$. Drawing the phase space distributions of $|0\rangle$ and $|\alpha\rangle$ would then show that using $i\alpha \in \mathbb{R}$ must give the largest overlap of the projections of the distributions onto the X quadrature. This also implies that the absolute phase of α is not important, but as long as the relative phases between the quadrature measurement and α is $\frac{\pi}{2}$, the c_1 term will be maximized. To satisfy conditions (C1) and (C2), we need to maximize c_1^2. This can be done by looking for the maximum of (3.27) over the binning parameter, b. Taking the partial derivative of Eq. (3.27) with respect to b and setting the

resultant to 0, we get

$$\frac{\partial c_1}{\partial b} = V\frac{2}{\sqrt{\pi}}\left(2e^{-b^2}\cos(\sqrt{2}b\sqrt{T_{\text{line}}}|\alpha|)\right) = 0, \tag{3.30}$$

$$\rightarrow \cos(\sqrt{2}b\sqrt{T_{\text{line}}}|\alpha|) = 0. \tag{3.31}$$

Eq. (3.31) has an infinite number of solutions, and in principle one can go through the route of finding the second derivatives to find the maxima of this function. However, graphing the integrand

$$e^{-x^2}\cos(\sqrt{2}x\sqrt{T_{\text{line}}}|\alpha|), \tag{3.32}$$

shows that the integral as a function of b must first increase from 0 with b, and then oscillate with period equal to $\cos(\sqrt{2}x\sqrt{T_{\text{line}}}|\alpha|)$ around its $b \to \infty$ value, since the integral is essentially adding up the positive and negative contributions of the integrand.

Then, the maximum value of the integral must occur for the first zero of Eq. (3.31) which occurs at $b = \frac{\pi}{2\sqrt{2}|\alpha|}$. With this optimal value of the binning b, we are left with the optimization over $|\alpha|$. However, the functions (3.27-3.29) then become too cumbersome to deal with analytically, and further optimization over α is done numerically. The results are shown in figure 3.2. The maximum CHSH violation is 2.324, for $|\alpha| = 2.1$. For a line transmission of 52.2%, and perfect detector efficiency, this scheme still achieves a violation of the CHSH inequality. From Fig. 3.2, one see that the numerical optimizations curiously allows violation for small η when the line transmission is almost perfect. We next show that this is not a numerical artifact, and that it is always possible to achieve a violation for perfect line transmission, regardless of the detector efficiency.

Theorem 1. *If* $T_{\text{line}} = 1$*, we have*

$$\mathcal{B} > 2, \tag{3.33}$$

irrespective of the value of η*.*

Proof. We first note that since $c_2 = 1$, the only condition we need to satisfy to show that $\mathcal{B} > 2$ is condition (C2). This can been seen since

$$c_3 \leq 1 = c_2, \tag{3.34}$$

$$\implies c_3(c_2 + c_3) \leq c_2(c_2 + c_3), \tag{3.35}$$

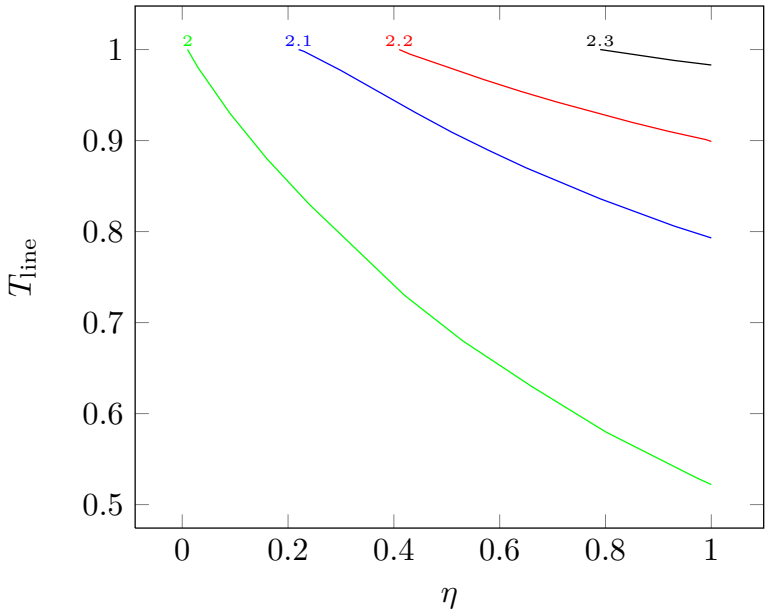

Figure 3.2: Contour plot of $\mathcal{B}$ vs the line transmission and the photocounting efficiency. The maximum CHSH violation is 2.324 for $|\alpha| = 2.1$.

i.e. that condition (C2) true implies condition (C1) true. Also, for $T_{\text{line}} = 1$, we have

$$c_1 = \Big(\frac{2}{\sqrt{\pi}}\int_{-b}^{b} dx\, e^{-x^2}\cos(\sqrt{2}x|\alpha|) - e^{-\frac{|\alpha|^2}{2}}\Big), \quad \text{and} \tag{3.36}$$

$$c_3 = 2e^{-\eta\frac{|\alpha|^2}{2}} - 1. \tag{3.37}$$

Then, for $|\alpha| \to \infty$, we have

$$\frac{2}{\sqrt{\pi}}\int_{-b}^{b} dx\, e^{-x^2}\cos(\sqrt{2}x|\alpha|) \approx \frac{2}{\sqrt{\pi}}\int_{-b}^{b} dx\, \cos(\sqrt{2}x|\alpha|), \tag{3.38}$$

$$= \sqrt{\frac{2}{\pi}}\frac{2}{|\alpha|}, \tag{3.39}$$

where we have used $b = \frac{\pi}{2\sqrt{2}|\alpha|} \to 0$ for $|\alpha| \to \infty$, and the approximation that in the limit of small b, the term e^{-x^2} can be approximated to unity. The condition (C2) then becomes

$$e^{-\eta\frac{|\alpha|^2}{4}} < \sqrt{\frac{2}{\pi}}\frac{2}{|\alpha|}, \tag{3.40}$$

where we have made the approximation that for $|\alpha| \gg 1$, $e^{-\frac{|\alpha|^2}{2}} \approx 0$. Since the left hand side of the inequality is exponentially decreasing in $|\alpha|$, and the right hand side is decreasing as $\frac{1}{|\alpha|}$, for any η, $\exists$ some $|\alpha| \gg 1$ such that condition (C2) holds. Thus, since $c_2 = 1$, for $T_{\text{line}} = 1$ and *any* η, there exists some $|\alpha|, \gamma$ and ν, which

gives $\mathcal{B} > 2$. □

One interesting remark is that in the limit of $|\alpha| \to \infty$, the state (3.7) resembles a maximally entangled Bell state, since in this same limit, the states $|0\rangle$ and $|\alpha\rangle$ are approximately orthogonal.

3.6 Two homodyne measurements

Theorem 1 shows that when transmission is perfect and for any η, there exists a α which can violate the CHSH inequality. This naturally leads one to wonder if its possible to violate the CHSH inequality using two homodyne measurements. Moreover, the setup we have been considering is a highly asymmetric measurement setup, where the light field is subject to either photodetection or homodyne measurement. We thus ask if we can perform the Bell test in a symmetric manner, using two homodyne measurements on the photonic side, eliminating the need to consider inefficient photocounting.

3.6.1 Perfect atomic measurements

In the case of two homodyne measurements and perfect atomic measurements, the optimization is straightforward. We first redefine the measurement operators on the photonic side as

$$B_0 = 2\int_{-b}^{b} dx\, |x\rangle\langle x| - \mathbb{1}, \tag{3.41}$$

$$B_1 = 2\int_{-\infty}^{\frac{|\alpha|}{\sqrt{2}}} dp\, |p\rangle\langle p| - \mathbb{1}, \tag{3.42}$$

and consider only α imaginary as in Sec. 3.4. This form of the B_1 measurement operator and binning is arbitrary, and we do not claim that it is optimal. The intuition for using this form of the B_1 measurement comes from the form of Eq. (3.5). This photocounting operator perfectly discriminates the state $|0\rangle$, and partially discriminates $|\alpha\rangle$. We thus choose Eq. (3.42) to measure the P quadrature to discriminate the states $|0\rangle$ and $|\alpha\rangle$, and choose a binning based on this intuition.

This choice of the B_1 operator is also particularly convenient, since the symmetric nature of the limits of the integral gives immediately $c_2 = -c_3$. Then, $\mathcal{B}$ after optimization over γ is

$$\mathcal{B}_\gamma = 2\sqrt{c_1^2 \sin^2(2\nu) + c_2^2}, \tag{3.43}$$

which is trivially maximized by $\sin^2(2\nu) = 1$ and $b = \frac{\pi}{2\sqrt{2}|\alpha|}$. Thus

$$\mathcal{B}_{\nu,\gamma} = 2\sqrt{c_1^2 + c_2^2}, \tag{3.44}$$

where c_1 is given in Eq. (3.27), and

$$c_2 = \mathrm{erf}(\sqrt{\frac{T_{\mathrm{line}}}{2}}|\alpha|). \tag{3.45}$$

Differentiation of Eq. (3.44) over $|\alpha|$ is possible, and the resulting equation for $|\alpha|$ is easy to write down. However, it is not possible to solve for the value of $|\alpha|$ which maximizes $\mathcal{B}_{\nu,\gamma}$ analytically. Thus, we directly optimize Eq. (3.44) numerically over $|\alpha|$. We then plot $\mathcal{B}_{\nu,\gamma,|\alpha|}$ vs T_{line} in Fig. 3.3. It shows that the largest violation attainable is 2.29, and the minimum required transmission which still yields a violation to be $T_{\mathrm{line}} = 0.678$. This measurement protocol can be directly compared to the one presented in Ref. [59], and one can see that there is both an improvement on the maximum violation and the minimum transmission (2.26 and 78%). One important remark is that in this measurement scenario, we no longer need to produce the state (3.7) exactly, and a state of the form

$$|\psi\rangle = \cos\nu|s, 0+\beta\rangle + \sin\nu|g, \alpha+\beta\rangle \tag{3.46}$$

for any complex β is also a possible candidate, since this corresponds to an appropriate shift in the binnings. However, the two coherent states need to be in the same mode for the results to be applicable. This will be relevant in Sec. 4.

The discussions above has assumed that atomic detection can be done with near unit efficiency. However, the drawback of having high detection efficiencies in the atomic detection usually necessitates long detection times. Although schemes exists to implement fast and efficient atomic detection [70], such techniques might not always be an option. In the next subsection, we treat the problem of inefficient atomic detection, and show that it quickly degrades the achievable CHSH violation.

3.6.2 Inefficient atomic detection

To treat inefficient atomic detection, one assumes that with probability η_{a}, we measure the state ρ given by Eq. (3.23), and with probability $1 - \eta_{\mathrm{a}}$, we measure

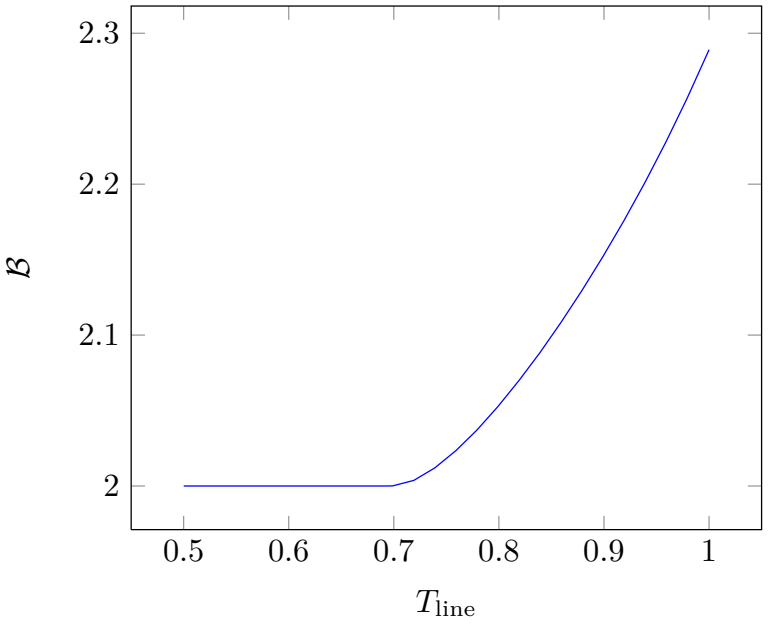

Figure 3.3: $\mathcal{B}$ vs Transmission diagram. This figure shows that the maximum CHSH violation is 2.29, and the minimum transmission required for the violation of the CHSH inequality is $T_{\text{line}} = 0.678$. $\mathcal{B}$ is computed by numerically optimizing Eq. (3.44) over $|\alpha|$.

only the partial state of the photon *i.e.*

$$\mathcal{B} = \text{Tr}\Big[\Big((A_0 + A_1)B_0 + (A_0 - A_1)B_1\Big)\rho_{\text{loss}}\Big], \tag{3.47}$$

$$\rho_{\text{loss}} = \eta_{\text{a}}\rho + (1 - \eta_{\text{a}})\mathbb{1}_{\text{atom}} \otimes \text{Tr}_{\text{atom}}(\rho), \tag{3.48}$$

where in Eq. (3.48) Tr_{atom} denotes the partial trace of the state over the atomic degrees of freedom. Then, the CHSH quantity after optimization over the atomic measurement angle gives

$$\mathcal{B}_\gamma = 2\Big(\eta_{\text{a}}\sqrt{c_1^2 \sin^2(2\nu) + c_2^2} + (1 - \eta_{\text{a}})c_2 \cos(2\nu)\Big), \tag{3.49}$$

where c_1 and c_2 are once again given by Eqs. (3.27) and (3.45). The optimization over the angle ν can once again be done analytically, and the resulting expression numerically optimized over α. Fig. 3.4 summarizes the results of the final optimization. It shows that the atomic detection efficiency must at least be above $\eta_{\text{a}} = 0.817$ to observe any CHSH violation, since it is the atomic detection efficiency for perfect line transmission. This result is not ideal, as a simple calculation would show that it does not reach the Eberhard bound, $\eta T_{\text{line}} = 2/3$ [71]. Next, we show a possible scheme to circumvent inefficient atomic detection.

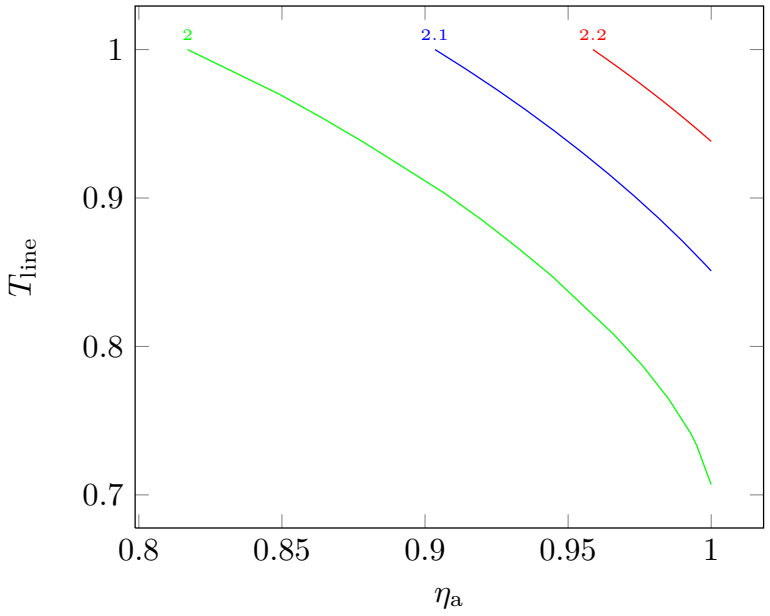

Figure 3.4: Contour plot of $\mathcal{B}$ vs the line transmission and the atomic detection efficiency. It shows that the minimum atomic detection efficiency is 0.817 for perfect line transmission.

3.7 Atomic system as a state preparator

A possible way to avoid the problem of inefficient atomic detection is to use the atomic system as a state preparator to produce entangled coherent states [72]. One could then imagine performing Bell tests on these states [73, 74].

3.7.1 Coherent state superpositions

Consider the system prepared in the state (3.7). If the atom is measured in the $\frac{1}{\sqrt{2}}(|s\rangle \pm |g\rangle)$ basis, and post-selected on the $\frac{1}{\sqrt{2}}(|s\rangle \pm |g\rangle)$ outcome, the resultant photonic state after a suitable displacement operation is,

$$N(\alpha)(\cos\nu|-\alpha\rangle \pm \sin\nu|\alpha\rangle), \tag{3.50}$$

where $N(\alpha)$ is a normalization factor, dependent on α. This state is known as a coherent state superposition (or Schrödinger's cat state) [72], and has been well studied in the literature, with much experimental progress in creating these states [75, 76, 77, 78]. However, producing such states with values of $|\alpha| \geq 1.5$ has proven to be a big experimental hurdle. Our state production protocol thus provides an alternative route to achieving such states with a larger $|\alpha|$. Notice that with the postselection of the atomic measurement, we do not loose the state due to inefficient atomic detection. Furthermore, for a state of the form of Eq. (3.23), the

post selection on the ± result creates the state

$$\rho_{\text{photon},\pm} = V|\tilde{\psi}_\pm\rangle\langle\tilde{\psi}_\pm| + (1-V)\sigma_\pm, \tag{3.51}$$

$$|\tilde{\psi}_\pm\rangle = N(\alpha)\Big(\cos\nu|0\rangle \pm \sin\nu|\tilde{\alpha}\rangle\Big), \tag{3.52}$$

$$\sigma_\pm = |N(\alpha)|^2\Big[\cos^2\nu|0\rangle\langle 0| + \sin^2\nu|\tilde{\alpha}\rangle\langle\tilde{\alpha}|\Big]. \tag{3.53}$$

Thus, losses of the state due to transmission or production imperfections are trivially carried forward by this postselection.

3.7.2 Splitting the cat

One interesting thing about this state is that, by sending the state (3.50) to a 50/50 beamsplitter, one can create entangled coherent states of the form

$$N(\alpha)(\cos\nu|-\tfrac{\alpha}{\sqrt{2}},-\tfrac{\alpha}{\sqrt{2}}\rangle + \sin\nu|\tfrac{\alpha}{\sqrt{2}},\tfrac{\alpha}{\sqrt{2}}\rangle), \tag{3.54}$$

which is reminiscent of the Bell states with polarization entanglement [79]. It is also worth noting, that such a route to producing a coherent state superposition with the help of atoms is not new, and a similar proposal has been previously studied in [80].

Notice that this operation of splitting the state (3.50) using a single beamsplitter can, in principle, be repeated *ad infinitum*, leading one to envision the case of n beamsplitters as in Fig. 3.5. Denoting the transmittivity and reflectivity of the

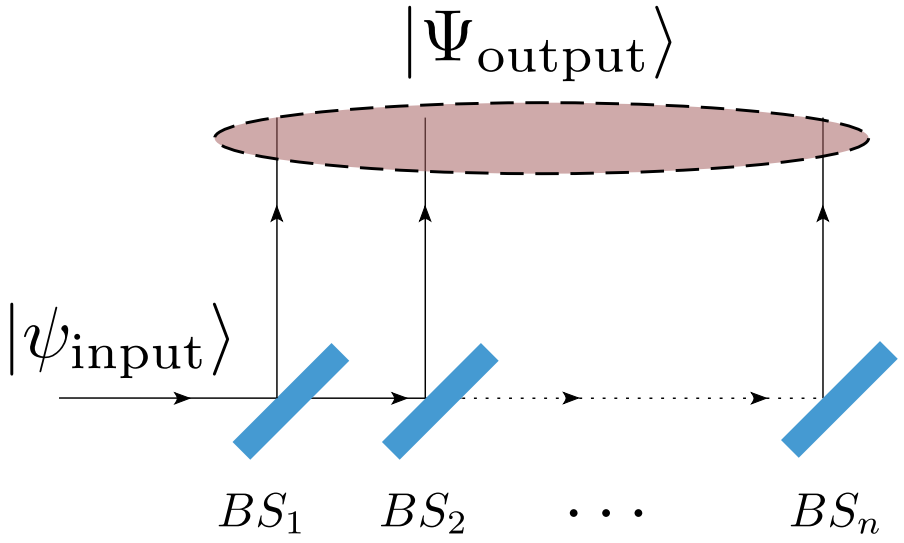

Figure 3.5: The above setup of n beamsplitters creates a path-entangled, n-partite state $|\Psi_{\text{output}}\rangle$.

i^{th} beamsplitter as t_i and r_i, with $t_i^2 + r_i^2 = 1$, we write the state $|\Psi_{\text{output}}\rangle$ produced

at the output given the input state (3.50), as

$$|\Psi_{\text{output}}\rangle = N(\alpha)(\cos\nu|-f_1\alpha, -f_2\alpha, \ldots - f_N\alpha\rangle + \sin\nu|f_1\alpha, f_2\alpha, \ldots f_N\alpha\rangle), \tag{3.55}$$

where we have used the shorthand $f_k = r_k\Pi_{i=1}^{k-1}t_i$. If one desires to create a state with equal output amplitudes, the condition $f_k = f_{k-1}$ must be satisfied. Some simple algebra then shows that to create a state with equal amplitudes in each mode requires that the transmittivity of the k^{th} and $k-1^{th}$ beamsplitters satisfy $t_k^2 = 2 - \frac{1}{t_{k-1}^2}$, thus producing a state of the form

$$|\Psi\rangle = N(\alpha)(\cos\nu|-\tilde{\alpha}, -\tilde{\alpha}\ldots - \tilde{\alpha}\rangle + \sin\nu|\tilde{\alpha}, \tilde{\alpha}\ldots \tilde{\alpha}\rangle). \tag{3.56}$$

Such a multipartite entangled state could be used to test Bell inequalities for multiple parties, which may yield interesting findings.

3.7.3 Testing the entangled coherent states

In appendix A, we detail our methodology for the testing of states of the form Eq. (3.54). We show that for the states and measurements considered, no violation of the CHSH inequality was found.

3.7.4 Other inequalities

The CHSH inequality represents a very restricted class of Bell inequalities, and is not overly suited to the problem at hand, since we have an entangled system which is infinite dimensional. The use of the CHSH inequality, which is a discrete outcome inequality, thus necessarily requires that we dichotomize the outcomes regardless of the physical measurement performed and can be regarded as somewhat inelegant to a theorist.

One possible extension would then be, to test other Bell inequalities which may be more suited to this state. In Appendix A.3, we test one particular Bell inequality found in Ref. [81]. It seemed suitable, due to its allowance for continuous outcomes. However, the result of the numerical search found that it is not possible to violate this inequality for the class of states we considered.

CHAPTER 4

BELL TEST - STATE PREPARATION

In this chapter, we detail our methodology for state production. Our state production setup, first thought of by one of our collaborators Marcelo Santos, and refined by us, is inspired by the dispersive measurements in cavity and circuit QED setups. We first describe the dispersive measurement of atoms, showing how such a non-demolition measurement of the atomic state can be performed. Then, we describe how the ideas of this measurement directly allows one to create a state of the form Eq. (3.7).

4.1 Intuition from the dispersive measurements of the atom-cavity system

We first start by describing the dispersive measurement of an atomic state. From Sec. 2.4.2, we can write the eigenstates of the Jaynes-Cummings hamiltonian in the dispersive approximation as

$$\begin{pmatrix} |+,n\rangle \\ |-,n\rangle \end{pmatrix} \approx \begin{pmatrix} 1 & -\sqrt{n}\frac{g}{\Delta} \\ \sqrt{n}\frac{g}{\Delta} & 1 \end{pmatrix} \begin{pmatrix} |g,n\rangle \\ |e,n-1\rangle \end{pmatrix}, \tag{4.1}$$

where g is the coupling constant between the cavity mode and the $|e\rangle - |g\rangle$ transition and $\Delta = \omega_a - \omega_c$ is the detuning between the cavity mode and the atomic transition frequency; the dispersive approximation is the condition $g/\Delta\sqrt{n} \ll 1$.

The energy of these eigenstates are

$$E_{+,n} \approx \hbar(\omega_c - \frac{g^2}{\Delta})n + 0, \quad \text{and} \tag{4.2}$$

$$E_{-,n} \approx \hbar(\omega_c + \frac{g^2}{\Delta})(n-1) + \hbar(\omega_a + \frac{g^2}{\Delta}). \tag{4.3}$$

Writing the eigenstates and energies of these eigenstates in this way allows the following observations: Firstly, the dispersive approximation essentially states that the atom-cavity system is not strongly coupled, and the eigenstates of the system are approximately the "bare" states of the atom and cavity. Next, looking only at the frequency of the cavity mode shows that the frequency of the cavity mode is shifted positively or negatively depending on the state of the atom and the sign of the atom-cavity detuning! Conversely, the cavity field shifts the energy levels of the atom.

This latter point has been used to produce amazing experimental results in the work of Serge Haroche in Paris [62, 63, 64]. However, these works used atoms to probe a cavity field by traversing atoms across the cavity. A simple calculation shows that for an atomic measurement time of 1μs, a minimum propagation distance of about 300m is required to close the locality loophole. Moving an atom at the speed of sound would mean keeping the entire propagation coherent for at least 1s. This makes it propagating atoms unfeasible for a loophole-free Bell test.

However, the same dispersive approximation of the atom-cavity system also allows one to infer the state of the atom by measuring transmission of photons through the cavity. This is done routinely in Circuit QED setups [82, 83], where the two-level system is built from Josephson junctions. The basic idea here is that due to the shift in the frequency of the cavity mode, probing the cavity with a probe sharp in frequency would reveal a shift in the transmission from the cavity due to the state of the atom. This shift in the transmission of the cavity is utilized to infer the state of the two-level system. Then, the two-level system is left in the cavity, and the light exits the cavity and is free to propagate. It is this effect that we use in the next section.

4.2 State production formalism

As mentioned in the last section, we seek to use the ideas of the dispersive measurements of two level systems to create the desired atom-photon entangled state. We consider the dispersive interaction of a cavity mode with a three-level atom. The energy level diagram of the atom is shown in Fig. 4.1.

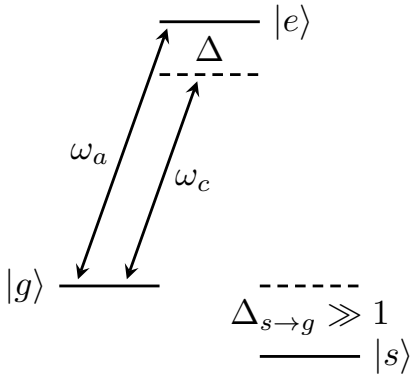

Figure 4.1: Atomic level diagram showing the relations of the $|e\rangle$, $|g\rangle$ and $|s\rangle$ energy levels. The atomic $|g\rangle - |e\rangle$ transition is coupled to the cavity mode, while the atomic $|s\rangle$ state is assumed to be uncoupled to the cavity. ω_c is the frequency of the cavity mode, and $\Delta = \omega_c - \omega_a$ the detuning between the cavity field and the $|g\rangle - |e\rangle$ transition.

The atom is assumed to have two metastable states $|g\rangle$ and $|s\rangle$, and one excited $|e\rangle$ state. The atomic $|g\rangle - |e\rangle$ transition is coupled to the cavity mode with frequency ω_c, while the atomic $|s\rangle$ state is assumed to be decoupled from the cavity. The use of the third level is used to reduce decoherence from atomic spontaneous emission from the $|e\rangle$ state if we were to directly use a two-level atom. Then, the atom can be prepared in a superposition of $|s\rangle$ and $|g\rangle$ before the start of the interaction with a pump field.

The full setup with have in mind is shown in Fig. 4.2. Using an input field

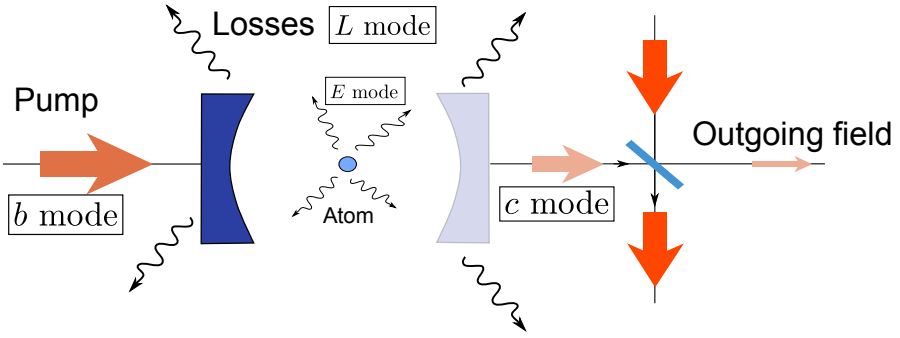

Figure 4.2: An input field is incident on the atom-cavity system. This causes some reflection and some transmission of the cavity field. We assume that the mirror on the right has a lower reflectivity than the mirror on the left, such that the field predominantly leaves the cavity to the right. The final beam splitter performs a displacement operation which creates the required propagating vacuum and coherent state as in Eq. (3.7).

incident on the atom cavity system, with the energies and frequencies arranged as in Fig. 4.1, one can create a state where the light field escapes the system

predominantly through only one cavity mirror. The need of both the asymmetric cavity and the displacement operation after the field has left the cavity are not *a priori* obvious, and will be detailed below.

We first give an intuitive description of the interaction. Then, using this description as a guide, we write down the full description of the setup using input-output theory.

4.2.1 Intuitive description

We consider transmission of a coherent pump beam through a cavity containing the atom. Since we assumed that the $|e\rangle - |g\rangle$ transition is dispersively coupled to the cavity mode, we can approximate the atom as a state dependent refractive index, such that the optical length and hence the resonance frequency of the cavity is dependent on the atomic state. So if the atom is in the $|s\rangle$ state, the transmission profile is centered around ω_c, and if the atom is in the $|g\rangle$ state, it is centered around $\omega_c - \frac{g^2}{\Delta}$. This is illustrated in Fig. 4.3.

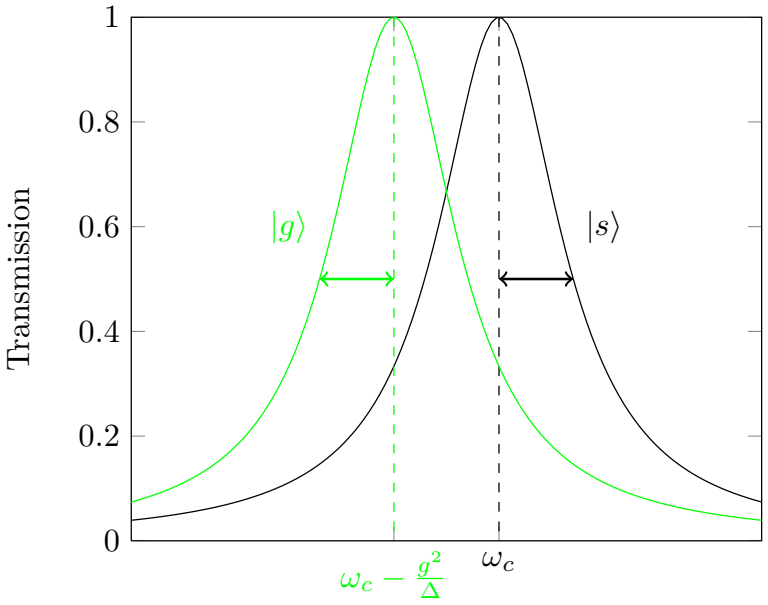

Figure 4.3: Approximate transmission profiles of the atom-cavity system in the dispersive regime can approximately described by Lorenztian profiles, shifted depending on the atomic state.

This dependence allows the following intuitive description of the transmission of a pump beam through the cavity:

$$|\alpha_L\rangle_{\text{in}}|g\rangle|0\rangle_{\text{trans}} \rightarrow |r_g\alpha_L\rangle_{\text{refl}}|g\rangle|t_g\alpha_L\rangle_{\text{trans}}, \tag{4.4}$$

$$|\alpha_L\rangle_{\text{in}}|s\rangle|0\rangle_{\text{trans}} \rightarrow |r_s\alpha_L\rangle_{\text{refl}}|s\rangle|t_s\alpha_L\rangle_{\text{trans}}, \tag{4.5}$$

where $|\alpha_L\rangle$ is a coherent pump field, and r_i and t_i are state dependent reflection and transmission coefficients.

Due to linearity, any superposition of $|g\rangle$ and $|s\rangle$ will then transform according to the above set of equations. The state of the transmitted field and atom after this interaction is then obtained by tracing out the reflected field. The Bell test can then be done on the atomic state in the $|g\rangle - |s\rangle$ subspace, and the transmitted field.

4.2.2 The need to displace the field

Fig. 4.3 shows that if we were to pump the cavity highly off resonance, it could be possible to approximately create a state of the form Eq. (3.7). In this subsection, we show that it is not optimal to directly produce the state using only the atom-cavity system. This can be seen from the following simple argument. The two Lorenztian profiles in Fig. 4.3 have peaks which are $\frac{g^2}{\Delta}$ apart, and each have a linewidth on the order of κ. From the properties of these transmission profiles, we observe the following problems:

- If we wish to have each line spectroscopically well-resolved with respect to the input field, we require the input field to have γ_{L} (bandwidth of the input field) much smaller that κ (decay rate of the cavity).
  - This implies that the length of the input pulse will be very much longer than the cavity decay rate, making the required propagation distance to close the locality loophole and thus the transmission losses large.
- If we wish to have smaller propagation distances, we want $\gamma_{\mathrm{L}} \approx \kappa$ for a given cavity setup, since the outgoing pulse length will be inversely proportional to the larger of the two bandwidths. In that case, we need the difference in the resonant frequencies to be bigger than the cavity decay rate. *i.e.* $g^2/\Delta \gg \kappa$, or
$$\frac{g}{\Delta} \gg \frac{\kappa}{g}. \tag{4.6}$$
  - Since the dispersive approximation requires $g/\Delta \ll 1$, Eq. (4.6) gives $g/\kappa \gg 1$. Since optical cavities have g/κ on the order of 10 or below, this condition makes optical cavities (and thus the possibility of low-loss transmission in optical fibres) unusable in this setting.

The above argument, although conceptually appealing, is only qualitative. To further convince ourselves of the need to use a displacement, we next perform a short feasibility check of just using an atom-cavity system to produce the state.

Approximating transmission through a cavity

Let us consider the following situation. A laser of some central frequency $\omega_{\rm L}$ and some linewidth $\gamma_{\rm L}$ impinges on a cavity (may or may not be empty) of some frequency $\omega_{\rm cav}$ and linewidth κ.

Since we would like to perform only a feasibility study, we assume the laser has a Lorentzian spectrum of the form:

$$\mathcal{L}_{\rm laser}(\omega) \propto \frac{1}{(\frac{\omega-\omega_{\rm L}}{\gamma_{\rm L}})^2+1}. \tag{4.7}$$

We also further assume that the dispersive approximation gives nothing but a Lorenztian spectrum with linewidth κ, and central frequency $\omega_{\rm cav} = \omega_c$ or, $\omega_c - \frac{g^2}{\Delta}$.

The transmission of the laser passing through the cavity is then given by the convolution of the two Lorentzian profiles, and will be proportional to

$$\begin{aligned} T &\sim \int_{-\infty}^{\infty} d\omega\, \mathcal{L}_{\rm laser}(\omega)\, \mathcal{L}_{\rm cavity}(\omega), \\ &\sim \int_{-\infty}^{\infty} d\omega \left(\frac{1}{(\frac{\omega-\omega_{\rm L}}{\gamma_{\rm L}})^2+1}\right)\left(\frac{1}{(\frac{\omega-\omega_{\rm cav}}{\kappa})^2+1}\right). \end{aligned} \tag{4.8}$$

This equation can be integrated with the calculus of residues, and we arrive at

$$T \sim \frac{\pi}{2}\frac{\Gamma_{hm}}{(\frac{\delta_{\rm L}}{\gamma_{\rm L}+\kappa})^2+1}, \tag{4.9}$$

where $\Gamma_{hm} = \frac{2}{\frac{1}{\gamma_{\rm L}}+\frac{1}{\kappa}}$ is the harmonic mean of the two linewidths, and $\delta_{\rm L} = \omega_{\rm L} - \omega_{\rm cav}$. This allows us to write the normalized transmission as

$$t = \frac{1}{(\frac{\delta_L}{\gamma_{\rm L}+\kappa})^2+1}. \tag{4.10}$$

We would like to compare 2 quantities, the transmission when the cavity is empty, *i.e.* $\omega_{\rm cav} = \omega_c$ and the transmission when the cavity is shifted by a dispersively coupled atom, *i.e.* $\omega_{\rm cav} = \omega_c - \frac{g^2}{\Delta}$. These are,

$$t_{\rm empty} = \frac{1}{(\frac{\delta_{\rm L}}{\gamma_{\rm L}+\kappa})^2+1} \tag{4.11}$$

$$t_{\rm shifted} = \frac{1}{(\frac{\delta_{\rm L}+\frac{g^2}{\Delta}}{\gamma_{\rm L}+\kappa})^2+1} \tag{4.12}$$

To create a state of the form of Eq. (3.7) only with a atom-cavity system, we need

$$\frac{t_{\text{shifted}}}{t_{\text{empty}}} := N \gg 1. \tag{4.13}$$

We first eliminate the variable δ_{L}, since we are free to control the frequency of the laser. Eq. (4.11) then becomes

$$\frac{\delta_L}{\gamma + \kappa} = -\sqrt{\frac{1}{t_e} - 1}, \tag{4.14}$$

where we choose the negative sign so we can assume $\Delta > 0$. Now, we choose a few parameters for numerical computation:

1. We assume the laser linewidth is much more narrow than cavity, so we set, $\gamma = \frac{1}{10}\kappa$.
2. The dispersive limit is satisfied, so that we set $\frac{g}{\Delta} = 0.1$.

Combining these with Eq. (4.14), we have

$$\left(\frac{g}{11\kappa} - \sqrt{\frac{N}{t_{\text{shifted}}} - 1}\right)^2 = \frac{1}{t_s} - 1. \tag{4.15}$$

Notice that given some N and t_{shifted}, the above equation has 2 roots of $\frac{g}{\kappa}$, both $+ve$ (For $N > 1$). Since we are looking for the cavity parameters (g/κ) which is able to produce the desired state, we ignore the larger root, and plot the contour lines of N vs t_{shifted} given some g/κ, such that they satisfy Eq. (4.15) in Fig. 4.4.

Fig. 4.4 shows that to be in a regime where we can approximate the state (3.7), we need to have $g/\kappa \sim 50$. Furthermore, since the length of the outgoing pulse in time is basically limited by the cavity decay rate, we would like κ large for smaller transmission losses (since a longer measurement time implies a longer propagation distance and thus larger transmission losses). Since we need g/κ large to produced the desired state, and we want κ large to reduce transmission distance, we need g to be substantial. We note that current optical cavities have g/κ less than 10 [84, 85], which from Fig. 4.4 implies that they are not suitable. Although microwave cavities can reach $g/\kappa \sim 100$, long-distance low-loss microwave propagation is not viable, and thermal effects become more prominent at microwave frequencies.

Thus, we cannot hope to reach the desired regime just with an atom-cavity system alone. In the next section, we investigate the possibility of an imperfect state preparation on the Bell test, and show that as expected, these effects are extremely detrimental to the achievable CHSH violation.

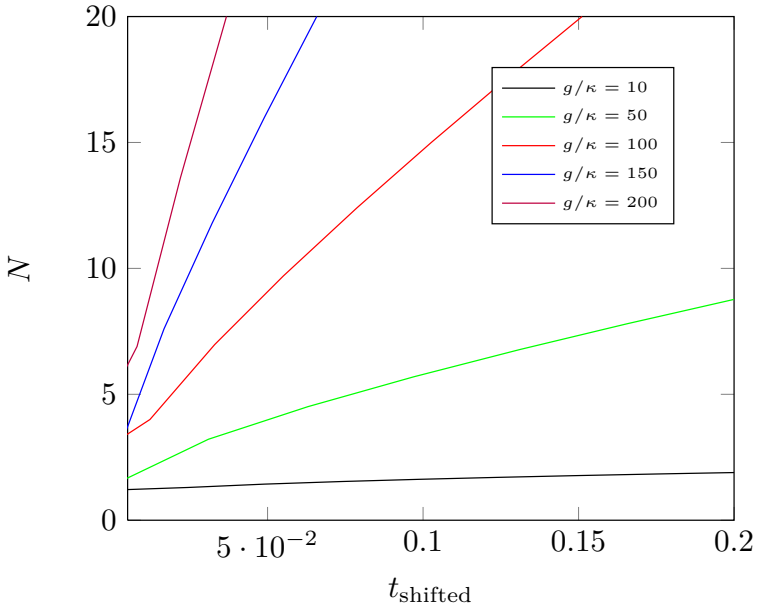

Figure 4.4: Plots of the values of N and t_{shifted} for a given g/κ, which satisfy Eq. (4.15). The plot shows that the cavity needs to have a large g/κ to have a large N and small t_{shifted}, which is the desired situation to approximate a state of the form Eq. (3.7).

Imperfect state preparation

In this section, we assume that the previous section prepares a state of the form

$$|\psi_{im}\rangle = \cos\nu|s, t_s\, p\rangle + \sin\nu|g, t_g\, p\rangle, \tag{4.16}$$

and we perform a Bell test on this state. This form ignores decoherence due to reflection of the pump beam, but is useful to check for the feasibility of using this state to perform the Bell test. One thing to note is that this difference is only meaningful in the scenario with photocounting and homodyning, since the effect of this difference from zero in the double homodyne scenario can be compensated by suitable choice of binning. Note that we are assuming that both coherent states $|t_s p\rangle$ and $|t_g p\rangle$ have the same spectrum, which is not the case in a real setup, and there will be additional decoherence effects due to the slight difference in the modes of the coherent states. We now test the scenario with

$$B_1 = 2|0\rangle\langle 0| - \mathbb{1}, \quad \text{and} \tag{4.17}$$

$$B_0 = 2\int_{-b+\chi}^{b+\chi} dx\, |x\rangle\langle x| - \mathbb{1}, \tag{4.18}$$

where χ in the integration limits is suitable change in the binning such that it matches the measurement (3.4). Following the steps in Sec. 3.4, we arrive at

$$c_1 = \frac{1}{2}\mathrm{Tr}\Big((|0\rangle\langle\alpha| + |\alpha\rangle\langle 0|)B_0\Big), \tag{4.19}$$

$$c_2 = \mathrm{Tr}(|\epsilon_s\rangle\langle\epsilon_s|B_1), \tag{4.20}$$

$$c_3 = \mathrm{Tr}(|\epsilon_g\rangle\langle\epsilon_g|B_1), \tag{4.21}$$

and

$$\mathcal{B}_\gamma = 2\sqrt{(2c_1\cos\nu\sin\nu)^2 + (c_2\cos^2\nu - c_3\sin^2\nu)^2}, \tag{4.22}$$

with $\epsilon_s = t_s p$, $\epsilon_g = t_g p$ and $|\alpha| = |\epsilon_g - \epsilon_s|$. This is exactly the same form as in Sec. 3.4, and thus we again have the same necessary conditions for violation. We now choose a small value of $t_s = 0.01$, and for each $g/\kappa \in [1, 300]$, we first solve for N according to Eq. (4.15) and maximize Eq. (4.22) over p. This gives a maximum of $\mathcal{B} = 2.02$. Note that in this test, we did not consider decoherence due to reflection of the pump field. Thus, we expect that when we use the state produced, only with the atom cavity system, for the Bell test, we will obtain $\mathcal{B} < 2.02$ for any transmission and detection efficiency.

The previous subsections clearly shows that directly using the atom-cavity system to create the state to perform the Bell test is not possible. However, as was pointed out in Ref. [86], we can combine the outgoing field with another field as in Fig. 4.2, effectively performing a displacement operation on the outgoing field. This is the approach we follow. We next give a brief description of the more complete theory for this setup.

4.2.3 Results from input-output theory

We use input-output theory to model this interaction. Following the procedures in [53] and [55], we assume that the single mode cavity field is coupled to multiple independent harmonic oscillator baths describing not only cavity transmission, but also non-radiative mirror losses. The atomic $|g\rangle - |e\rangle$ transition is treated as being coupled to the cavity mode and another independent bath of harmonic oscillators to model spontaneous emission; the atomic $|s\rangle$ state is assumed to be uncoupled to the rest of the dynamics. The full details of this model, including a discussion of the approximations we make are expounded on in Sec. 2.4, and we only quote the results relevant to the present situation.

When the atom is in the $|s\rangle$ state, we have

$$b_{in}(\omega) = r_s(\omega)b_{out}(\omega) + t_s(\omega)c_{out}(\omega) + l_s(\omega)L_{out}(\omega), \tag{4.23}$$

where

$$r_s(\omega) = -\frac{\frac{\kappa-2\kappa_b}{2} + i\delta_c}{\frac{\kappa}{2} + i\delta_c}, \tag{4.24}$$

$$t_s(\omega) = \frac{\sqrt{\kappa_b\kappa_c}}{\frac{\kappa}{2} + i\delta_c}, \quad \text{and} \tag{4.25}$$

$$l_s(\omega) = \frac{\sqrt{\kappa_L\kappa_b}}{\frac{\kappa}{2} + i\delta_c}. \tag{4.26}$$

When the atom is in the $|g\rangle$ state,

$$\begin{aligned} b_{in}(\omega) = {} & r_g(\omega)b_{out}(\omega) + t_g(\omega)c_{out}(\omega) \\ & + l_g(\omega)L_{out}(\omega) + n_g(\omega)E_{out}(\omega), \end{aligned} \tag{4.27}$$

with

$$\chi_g(\omega) = \chi_s(\omega)\frac{(\frac{\Gamma}{2} + i\delta_a)(\frac{\kappa}{2} + i\delta_c)}{(\frac{\Gamma}{2} + i\delta_a)(\frac{\kappa}{2} + i\delta_c) + g^2}, \tag{4.28}$$

$$r_g(\omega) = -\frac{(\frac{\kappa-2\kappa_b}{2} + i\delta_c)(\frac{\Gamma}{2} + i\delta_a) + g^2}{(\frac{\kappa}{2} + i\delta_c)(\frac{\Gamma}{2} + i\delta_a) + g^2}, \tag{4.29}$$

$$n_g(\omega) = i\frac{g\sqrt{\Gamma\kappa_b}}{(\frac{\Gamma}{2} + i\delta_a)(\frac{\kappa}{2} + i\delta_c) + g^2}, \tag{4.30}$$

where $\chi \in \{t, l\}$, and all the results above are in the frequency domain. The a, b, c, L and E modes are the cavity, left (input/reflected), right (transmitted), loss (in both mirrors) and environment (spontaneous emission loss) modes respectively. The coupling rates of the cavity field to the left, right and non-radiative baths are respectively, κ_b,κ_c, and κ_L; Γ is the spontaneous emission rate of the atom, and $\delta_{\mathrm{c/a}} = \omega_{\mathrm{L}} - \omega_{\mathrm{c/a}}$. Eqs. (4.23) and (4.27) can be written in the slightly more concise form:

$$\begin{aligned} b_{in}(\omega) = {} & \tilde{r}(\omega)b_{out}(\omega) + \tilde{t}(\omega)c_{out}(\omega) \\ & + \tilde{l}(\omega)L_{out}(\omega) + \tilde{n}(\omega)E_{out}(\omega), \end{aligned} \tag{4.31}$$

where the transformation coefficients are given by

$$\tilde{\chi} = \chi_s|s\rangle\langle s| + \chi_g|g\rangle\langle g|, \qquad \chi \in \{r, t, l, n\} \tag{4.32}$$

$$n_s(\omega) = 0. \tag{4.33}$$

One should notice that Eq. (4.31) is a linear equation transforming inputs to outputs. This implies that if the input pump field is in a coherent state, all output modes would be coherent states as well. This point can be seen from the following calculation. Assume that the input pump field is in a coherent state with spectrum $s_{\mathrm{L}}(\omega)$. The input state is then written as

$$|\{\alpha_{\mathrm{L}}\}\rangle \otimes |\Phi\rangle_{\mathrm{atom}} = \exp\left[\alpha_{\mathrm{L}} \int d\omega \left(s_{\mathrm{L}}(\omega) b^{\dagger}_{\mathrm{in}}(\omega) - s^{*}_{\mathrm{L}}(\omega) b_{\mathrm{in}}(\omega)\right)\right] |0\rangle \otimes |\Phi\rangle_{\mathrm{atom}}, \tag{4.34}$$

where the curly brackets on α_{L} denote the continuous frequency nature of the state, and the spectrum is normalized such that $\int_0^\infty d\omega\, |s_{\mathrm{L}}(\omega)|^2 = 1$ and the coherent state amplitude is α_{L}. Upon inserting Eq. (4.31), the output state after the field has left the cavity is

$$\begin{aligned} |\{\alpha_{\mathrm{L}}\}\rangle \otimes |\Phi\rangle_{\mathrm{atom}} \to \exp\Bigg[\alpha_{\mathrm{L}} \int d\omega \Big(s_{\mathrm{L}}(\omega)\{\tilde{r}^{*}(\omega) b^{\dagger}_{out}(\omega) + \tilde{t}^{*}(\omega) c^{\dagger}_{out}(\omega) \\ + \tilde{l}^{*}(\omega) L^{\dagger}_{out}(\omega) + \tilde{n}^{*}(\omega) E^{\dagger}_{out}(\omega)\} - \mathrm{h.c.}\Big)\Bigg] |0\rangle \otimes |\Phi\rangle_{\mathrm{atom}}. \end{aligned} \tag{4.35}$$

Since the baths are assumed to be independent, this implies that not only do the operators b_{out}, c_{out}, L_{out} and E_{out} commute, but also $[x_{\mathrm{out}}, y^{\dagger}_{\mathrm{out}}] = 0$, where $x, y \in \{b_{\mathrm{out}}, c_{\mathrm{out}}, L_{\mathrm{out}}, E_{\mathrm{out}}\}$ and $x \neq y$. Taking the example of $|\Phi\rangle_{\mathrm{atom}} = |g\rangle$, we can rewrite Eq. (4.35) as

$$|\{\alpha_{\mathrm{L}}\}\rangle \otimes |g\rangle \to |\{r_g \alpha_{\mathrm{L}}\}\rangle_{\mathrm{refl}} \otimes |\{t_g \alpha_{\mathrm{L}}\}\rangle_{\mathrm{trans}} \otimes |\{l_g \alpha_{\mathrm{L}}\}\rangle_{\mathrm{loss}} \otimes |\{n_g \alpha_{\mathrm{L}}\}\rangle_{\mathrm{emiss}} \otimes |g\rangle, \tag{4.36}$$

where the initial pump coherent state becomes coherent states in the other modes, with different spectra and amplitudes. A quick consistency check shows that

$$|\tilde{r}|^2 + |\tilde{t}|^2 + |\tilde{l}|^2 + |\tilde{n}|^2 = \mathbb{1}, \tag{4.37}$$

as expected. These equations show that as in beamsplitters, pure coherent states are mapped to pure coherent states, which justifies the intuitive equations (4.4) and (4.5). Then, the state production protocol would be to first prepare the atom in a suitable superposition of $|g\rangle$ and $|s\rangle$, $\cos\nu|s\rangle + \sin\nu e^{i\phi}|g\rangle$ then pump the cavity with a coherent pump field $|\{\alpha_{\mathrm{L}}\}\rangle$, and lastly, to perform a displacement

operation on the outgoing field. The state after this interaction is

$$\begin{aligned}|\Psi\rangle = &\cos\nu|s,0\rangle \otimes |\{r_s\alpha_{\rm L}\}\rangle_{\rm refl} \otimes |\{l_s\alpha_{\rm L}\}\rangle_{\rm loss}|0\rangle_{\rm emiss}|\tfrac{1}{r_{\rm BS}}\{t_s\alpha_{\rm L}\}\rangle_{\rm BS} \\ &+ \sin\nu e^{i\phi}|g, t_{\rm BS}(\{t_s\alpha_{\rm L}\} - \{t_g\alpha_{\rm L}\})\rangle \otimes |\{r_g\alpha_{\rm L}\}\rangle_{\rm refl}|\{l_g\alpha_{\rm L}\}\rangle_{\rm loss}|\{n_g\alpha_{\rm L}\}\rangle_{\rm emiss} \\ &|\tfrac{t_{\rm BS}^2}{r_{\rm BS}}\{t_s\alpha_{\rm L}\} + r_{\rm BS}\{t_g\alpha_{\rm L}\}\rangle_{\rm BS},\end{aligned} \tag{4.38}$$

where the states with $|\{\} - \{\}\rangle_{\rm BS}$ stand for the displacement of coherent states with different spectra (and thus are in different modes), and the subscript refers to the port of the beamsplitter which is not detected. We have assumed that the displacement of the transmitted field is done with a large coherent state $|\{\beta\}\rangle$, in an identical spectral mode as $|\{t_s\alpha_{\rm L}\}\rangle$, and has amplitude β such that

$$r_{\rm BS}\beta = t_{\rm BS}\alpha_L \int d\omega\, |t_s(\omega)s_{\rm L}(\omega)|^2. \tag{4.39}$$

This is a necessary requirement to achieve the vacuum state in one of the superposition states. Since only the atom and the outgoing field are detected, we trace away all other modes and obtain the final atom-light state

$$\rho = V|\psi_f\rangle\langle\psi_f| + (1-V)\sigma, \tag{4.40}$$

with

$$|\psi_f\rangle = \cos\nu|s,0\rangle + \sin\nu e^{i(\phi+\theta)}|g,\{\alpha\}\rangle, \tag{4.41}$$

$$\sigma = \cos^2\nu|s,0\rangle\langle s,0| + \sin^2\nu|g,\{\alpha\}\rangle\langle g,\{\alpha\}|, \tag{4.42}$$

where the visibility V is

$$V = \exp\Big[-\frac{|\alpha|^2}{2t_{BS}^2}F\Big], \tag{4.43}$$

$$F = r_{BS}^2 + f_{cav} + I_{s_{\rm L}}\frac{1}{4C}(1+f_{cav}), \tag{4.44}$$

$$I_{s_{\rm L}} = \frac{\int d\omega|s_{\rm L}(\omega)\frac{1}{D(\omega)}|^2}{\int d\omega|s_{\rm L}(\omega)\frac{1}{D(\omega)}\frac{1}{1+2i(\omega-\omega_c)/\kappa}|^2}, \tag{4.45}$$

where C is the usual single-atom cooperativity $C = \frac{g^2}{\Gamma\kappa}$, $f_{cav} = \frac{\kappa_b+\kappa_L}{\kappa_c}$ is a factor which describes the asymmetry of the cavity; with the continuous frequency

coherent state $|\{\alpha\}\rangle$ in Eq. (4.41) given by

$$|\{\alpha\}\rangle = e^{-\frac{|\alpha|^2}{2}} \exp\Big\{\int d\omega\, \alpha(\omega) c^\dagger_{out}(\omega)\Big\}|0\rangle, \tag{4.46}$$

$$\alpha(\omega) = t_{BS}\alpha_L(t_s(\omega) - t_g(\omega))s_{\mathrm{L}}(\omega), \tag{4.47}$$

$$|\alpha|^2 = \int d\omega\ |\alpha(\omega)|^2 . \tag{4.48}$$

The additional phase angle θ in equation (4.41) arises from tracing of the undetected field modes, and can in principle be compensated by a suitable choice of the phase of the initial atomic superposition ϕ. Eq. (4.43) is derived simply by noticing that to trace out undetected modes of the following pure state

$$|\xi\rangle = \alpha|\phi\rangle_{\mathrm{sys}} \otimes |\tilde{\phi}\rangle_{\mathrm{undetected}} + \beta|\zeta\rangle_{\mathrm{sys}} \otimes |\tilde{\zeta}\rangle_{\mathrm{undetected}}, \tag{4.49}$$

gives the reduced state

$$\rho_{\mathrm{sys}} = V|\tilde{\xi}\rangle\langle\tilde{\xi}| + (1-V)\sigma, \tag{4.50}$$

$$\tilde{\xi} = \alpha|\phi\rangle + \beta e^{i\theta}|\zeta\rangle, \tag{4.51}$$

$$\sigma = |\alpha|^2|\phi\rangle\langle\phi| + |\beta|^2|\zeta\rangle\langle\zeta|, \tag{4.52}$$

$$V = |\langle\tilde{\phi}|\tilde{\zeta}\rangle|, \quad \text{and} \tag{4.53}$$

$$\theta = \arg(V). \tag{4.54}$$

Then, we need to compute inner products of the form

$$\langle\{\alpha\}|\{\beta\}\rangle, \tag{4.55}$$

where $|\{\alpha\}\rangle$ and $|\{\beta\}\rangle$ are continuous frequency coherent states with spectra given by $\alpha(\omega)$ and $\beta(\omega)$. We then use the Baker-Campbell-Hausdorff formula with the commutation relation

$$[\int d\omega\, \alpha^*(\omega)a(\omega), \int d\omega\, \beta(\omega)a^\dagger(\omega)] = \int d\omega\, \alpha^*(\omega)\beta(\omega) = \chi, \tag{4.56}$$

to derive the identity

$$D(\alpha(\omega))D(\beta(\omega)) = D(\alpha(\omega) + \beta(\omega)) \exp[\frac{1}{2}(\chi - \chi^*)], \tag{4.57}$$

where

$$D(\alpha(\omega)) = \exp\left[\int d\omega\, \alpha(\omega)a^\dagger(\omega) - \alpha^*(\omega)a(\omega)\right] \tag{4.58}$$

is the continuous frequency displacement operator. The inner product in Eq. (4.55) is then

$$\langle\{\alpha\}|\{\beta\}\rangle = \langle 0|D(-\alpha(\omega))D(\beta(\omega))|0\rangle, \tag{4.59}$$

$$= \langle 0|D(\beta(\omega)-\alpha(\omega))|0\rangle \exp[\frac{1}{2}(\chi-\chi^*)], \tag{4.60}$$

$$= \exp[-\frac{1}{2}\int d\omega\, |\beta(\omega)-\alpha(\omega)|^2] \exp[i\,\mathrm{Im}\left(\int d\omega\, \alpha^*(\omega)\beta(\omega)\right)], \tag{4.61}$$

where we separated out the magnitude and phase of the inner product. Then, the visibility (4.43) is given by

$$\log(V) = -\frac{\alpha_{\mathrm{L}}^2}{2}\int d\omega \Big(|(r_s-r_g)s_{\mathrm{L}}|^2 + |(l_s-l_g)s_{\mathrm{L}}|^2 + |n_g s_{\mathrm{L}}|^2 + r_{\mathrm{BS}}^2\,|(t_s-t_g)s_{\mathrm{L}}|^2 \Big). \tag{4.62}$$

Using Eqs. (4.47) and (4.48), we can write

$$\alpha_{\mathrm{L}}^2 = \frac{|\alpha|^2}{t_{\mathrm{BS}}^2 \int d\omega\ |(t_s-t_g)s_{\mathrm{L}}|^2}. \tag{4.63}$$

Then, the major simplification of the visibility comes from noticing that in the derivation of the transmission, reflection and loss coefficients in Eq. (2.109), the following relation can be derived

$$\frac{t_{s/g}}{\sqrt{\kappa_c}}, \frac{l_{s/g}}{\sqrt{\kappa_L}} = \frac{r_{s/g}}{\sqrt{\kappa_b}} + 1. \tag{4.64}$$

This implies that

$$\frac{\int d\omega\ |(r_s-r_g)s_{\mathrm{L}}|^2 + |(l_s-l_g)s_{\mathrm{L}}|^2}{\int d\omega\ |(t_s-t_g)s_{\mathrm{L}}|^2}, \tag{4.65}$$

$$= \frac{\int d\omega\, \frac{\kappa_b}{\kappa_c}\,|(t_s-t_g)s_{\mathrm{L}}|^2 + \frac{\kappa_L}{\kappa_c}\,|(t_s-t_g)s_{\mathrm{L}}|^2}{\int d\omega\ |(t_s-t_g)s_{\mathrm{L}}|^2}, \tag{4.66}$$

$$= \frac{\kappa_b+\kappa_L}{\kappa_c} := f_{\mathrm{cav}}. \tag{4.67}$$

Then, we have,

$$\log(V) = -\frac{\alpha_{\mathrm{L}}^2}{2}\int d\omega \Big(|(r_s - r_g)s_{\mathrm{L}}|^2 + |(l_s - l_g)s_{\mathrm{L}}|^2 + |n_g s_{\mathrm{L}}|^2 + r_{\mathrm{BS}}^2 |(t_s - t_g)s_{\mathrm{L}}|^2 \Big), \tag{4.68}$$

$$= -\frac{\alpha^2}{2t_{\mathrm{BS}}^2} \frac{\int d\omega \Big(|(r_s - r_g)s_{\mathrm{L}}|^2 + |(l_s - l_g)s_{\mathrm{L}}|^2 + |n_g s_{\mathrm{L}}|^2 + r_{\mathrm{BS}}^2 |(t_s - t_g)s_{\mathrm{L}}|^2 \Big)}{\int d\omega \ |(t_s - t_g)s_{\mathrm{L}}|^2}, \tag{4.69}$$

$$= -\frac{\alpha^2}{2t_{\mathrm{BS}}^2}\Big[r_{\mathrm{BS}}^2 + f_{\mathrm{cav}} + \frac{\int d\omega \ |n_g s_{\mathrm{L}}|^2}{\int d\omega \ |(t_s - t_g)s_{\mathrm{L}}|^2}\Big]. \tag{4.70}$$

Simplifying the integrals gives the final visibility Eq. (4.43). From equation (4.43), it is easy to see that for $F \to 0$, we have $V \to 1$. And for $F \to 0$, we need the three conditions, $r_{BS} \to 0$, $f_{cav} \to 0$ and $C \to \infty$. In practice, the first condition means that one should use a small value of the beam splitter reflectivity and adjust the amplitude of the local oscillator, such that the condition

$$r_{\mathrm{BS}}\beta = t_{\mathrm{BS}}\alpha_L \int d\omega \, |t_s(\omega)s_{\mathrm{L}}(\omega)|^2, \tag{4.71}$$

is still satisfied. The second condition is the requirement of the asymmetric cavity, and is dependent only on the transmission of the cavity mirrors used. The third condition means that one needs large single-atom cooperativity. One remarkable feature of this result is that for $C \gg 1$, the visibility V (but of course not the state) is independent of the details of the spectrum of the input pulse. Lastly, one can also analyze the form of the spectrum dependent part of the Visibility, $I_{s_{\mathrm{L}}}$, which is given by the expression

$$I_{s_{\mathrm{L}}} = \frac{\int d\omega |s_{\mathrm{L}}(\omega)\frac{1}{D(\omega)}|^2}{\int d\omega |s_{\mathrm{L}}(\omega)\frac{1}{D(\omega)}\frac{1}{1+2i(\omega-\omega_c)/\kappa}|^2}. \tag{4.72}$$

Notice that $I_{s_{\mathrm{L}}}$ is a ratio of 2 positive integrals differing only by the Lorenztian spectrum of the empty cavity in the denominator, and thus has range $I_{s_{\mathrm{L}}} \in [1, \infty)$. Furthermore, we want this factor to be small, since the larger this factor, the smaller the Visibility will be. Some analysis reveals that for a laser spectrum s_{L} centered far from the cavity resonance, the denominator $\to 0$, and so $I_{s_{\mathrm{L}}} \to \infty$. Thus, it must achieve its smallest value for s_{L} sufficiently narrow and centred at ω_c. This implies that to reduce the overall visibility, the pump should have a narrow frequency spectrum centred on the empty cavity resonance.

CHAPTER 5

BELL TEST - FEASIBILITY

In this chapter, we first derive a parameter space which is feasible in a real experiment to perform a Bell test. We then show that our proposal is feasible to produce a state of the form (3.7), in the sense that existing cavity setups can produce the required state with a high visibility.

We note that in a realistic experiment, the relevant parameters which play a role in the interaction are $g, \kappa, \Gamma, f_{\text{cav}}$ and γ_{L}. The first four parameters are cavity parameters, and are the coupling strength of the cavity to the $|e\rangle - |g\rangle$ transition, the total cavity decay rate, the atomic $|e\rangle - |g\rangle$ transition decay rate and the cavity asymmetry which is related to the specific mirrors used in the setup, respectively. The fifth parameter is the bandwidth of the input laser field. This parameter not only determines the spectral width of the outgoing field, but also the achievable fidelity (for a given amplitude) of the output state.

Although in principle all experimental parameters are tunable, one must agree that some parameters are more easily tuned then others. We assume that we are free to control the parameters of the laser, namely, the laser central frequency w_{L} and bandwidth γ_{L}. Further, we assume that we can choose the detuning between the atomic $|e\rangle - |g\rangle$ transition and the cavity mode, Δ, to be large enough to satisfy the dispersive approximation. This last point can be achieved by a slight change in the cavity length, or by using an additional laser and considering the AC stark shift of the energy levels due to the laser.

To quantify our claims, we assume that the input pulse has the Gaussian spectrum

$$|s_{\text{L}}(\omega)|^2 = \frac{1}{\gamma_{\text{L}}\sqrt{\pi}} e^{-\left(\frac{\omega-\omega_{\text{L}}}{\gamma_{\text{L}}}\right)^2}, \tag{5.1}$$

where ω_{L} is the laser central frequency, and γ_{L} is the bandwidth of the laser. This

form of the input spectrum is arbitrary, and one could use different types of input to different degrees of success. However, our main aim in the rest of this section is to show the effect of the laser bandwidth on the dynamics and output fields of this system.

We consider two main issues:

1. Validity of analysis: To have the system evolve as described in the previous sections, we need that our approximations hold for possible experimental parameters.

2. Locality loophole: We seek to perform a Bell test which closes the locality loophole. As such, this sets further constraints on possible experimental parameters.

5.1 Validity of approximations

The most important requirement is the description of the dynamics we derive is valid. Since the major approximation used in our calculations is $\sigma_z \approx -\mathbb{1}$, we have to show that the set of experimental parameters we specify can achieve a regime where our description is appropriate.

As previously showed in Lemma 1 in Chapter 2, the self consistency of our description under some reasonable conditions is equivalent to saying we are working in the dispersive regime of cavity QED. Since our scheme is inspired by and very similar to dispersive measurements of two-level systems as described in Sec. 4.1, we claim that our approach is justified whenever the conditions of Lemma 1 and

$$P_{\text{excite}} := \max_t \left\langle \sigma^\dagger(t)\sigma(t) \right\rangle \ll 1, \tag{5.2}$$

is satisfied, where P_{excite} is the maximum probability of the atom being in the $|e\rangle$ state throughout the duration of the interaction, and $\sigma(t) = |g\rangle\langle e|$ is the lowering operator for the $|e\rangle - |g\rangle$ transition. Using the methods and notation of Sec. 2.4.5, we can write

$$\begin{pmatrix} \tilde{a} \\ \tilde{\sigma} \end{pmatrix} = \begin{pmatrix} \frac{\kappa}{2} - i\delta_c & ig \\ ig & \frac{\Gamma}{2} - i\delta_a \end{pmatrix}^{-1} \begin{pmatrix} v_{\text{in}\rightarrow} \\ \sqrt{\Gamma}\tilde{r}_{\text{in}} \end{pmatrix}, \tag{5.3}$$

$$= \frac{1}{D^*(\omega)} \begin{pmatrix} \frac{\Gamma}{2} - i\delta_a & -ig \\ -ig & \frac{\kappa}{2} - i\delta_c \end{pmatrix} \begin{pmatrix} v_{\text{in}\rightarrow} \\ \sqrt{\Gamma}\tilde{r}_{\text{in}} \end{pmatrix}, \tag{5.4}$$

and thus

$$\sigma(t) = \int \frac{d\omega}{\sqrt{2\pi}} e^{-i\omega t} \frac{1}{D^*(\omega)} \Big(- ig(\sqrt{\kappa_b}\tilde{b}_{\text{in}} + \sqrt{\kappa_c}\tilde{c}_{\text{in}} + \sqrt{\kappa_L}\tilde{L}_{\text{in}}) + (\frac{\kappa}{2} - i\delta_c)\sqrt{\Gamma}\tilde{r}_{\text{in}}) \Big). \tag{5.5}$$

The assumption that the input modes of all modes other than the b_{in} mode are in the vacuum state translates to assuming the initial state of the system is

$$|\xi\rangle_{\text{initial}} = |\Phi\rangle_{\text{atom}} \otimes |\{\alpha_{\text{L}}\}\rangle \otimes |0\rangle. \tag{5.6}$$

Then the maximum probability of excitation becomes

$$P_{\text{excite}} = \max_t \left| \int \frac{d\omega}{\sqrt{2\pi}} e^{-i\omega t} \frac{1}{D^*(\omega)} \Big(- ig\sqrt{\kappa_b}\alpha_{\text{L}} s_{\text{L}}(\omega) \Big) \right|^2. \tag{5.7}$$

The dependence of the maximum excitation probability on specific experimental parameters can quantified by defining the following dimensionless quantities

$$\tilde{\kappa} = \frac{\kappa}{g}, \tag{5.8}$$

$$\tilde{\gamma}_{\text{L}} = \frac{\gamma_{\text{L}}}{g}, \quad \text{and} \tag{5.9}$$

$$C = \frac{g^2}{\Gamma\kappa}, \tag{5.10}$$

which are the decay rate of the cavity and bandwidth of the laser with respect to the coupling strength of the cavity to the atom, and the single atom cooperativity respectively. Using this allows us to write the maximum excitation probability as

$$P_{\text{excite}} = \frac{\kappa_b}{\kappa} \frac{|\alpha_{\text{L}}|^2}{2\pi^{3/2}} \frac{\tilde{\kappa}}{\tilde{\gamma}_{\text{L}}} \max_t \left| \int d\tilde{\omega} e^{-i\tilde{\omega}gt} \frac{e^{-\frac{1}{2}(\tilde{\omega}/\tilde{\gamma}_{\text{L}})^2}}{(\frac{\tilde{\kappa}}{2} - i\tilde{\omega})(\frac{1}{2C\tilde{\kappa}} - i(\tilde{\omega} - \frac{\Delta}{g})) + 1} \right|^2. \tag{5.11}$$

In Fig. 5.1, we numerically integrate the above integral to find the maximum excitation probability for $\frac{g}{\kappa} \in [-1, 20]$, assuming $C = 25/9$ and $\frac{\kappa_b}{\kappa} = \frac{5}{115}$ (which are the values in the experiment of [84, 87]), for $\frac{g}{\Delta} \in \{\frac{1}{10}, \frac{1}{100}, \frac{1}{1000}\}$ and $|\alpha| = 2.1$, which is the value of $|\alpha|$ for which $\langle \mathcal{B} \rangle$ achieves its maximum value in the ideal case of Sec. 3.5. The left panel is for $\tilde{\gamma}_{\text{L}} = \frac{1}{20}$ and the right panel for $\tilde{\gamma}_{\text{L}} = \tilde{\kappa}$.

We now take $P_{\text{excite}} < 0.1$ to be the region where our approximations are self-consistent. This choice is arbitrary, which might strike the pedantic as unsatisfactory. However, we could as well look for a range of parameters for which the probability is below 5%, which is also arbitrary. This reduction can be carried through *ad infinitum* all the way to 0^+, and it is impossible to find a satisfactory end-point without in-depth analysis of both the approximate and full models.

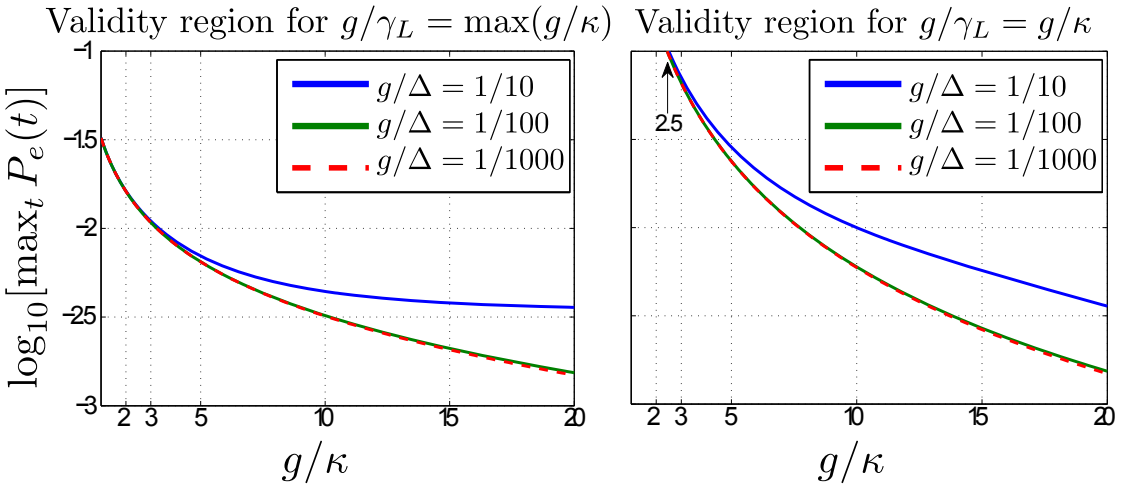

Figure 5.1: Plots of the log of the maximum excitation probability for $\frac{g}{\kappa} \in [-1, 20]$, assuming $C = 25/9$ and $\frac{\kappa_b}{\kappa} = \frac{5}{115}$ (which are the values in the experiment of [84, 87]), for $\frac{g}{\Delta} \in \{\frac{1}{10}, \frac{1}{100}, \frac{1}{1000}\}$ and $|\alpha| = 2.1$. The left panel is for $\tilde{\gamma}_{\mathrm{L}} = \frac{1}{20}$ and the right panel for $\tilde{\gamma}_{\mathrm{L}} = \tilde{\kappa}$. As is evident from both graphs, when $\frac{g}{\Delta}$ becomes sufficiently small, further reduction in this parameter with all other parameters constant, will have a negligible effect on the maximum excitation probability.

Thus, to quantify the performance of a set of cavity parameters on the state-production, we (reluctantly) make this arbitrary choice.

Fig. 5.1 clearly shows that for a small value of γ_{L}, it is always possible to find a set of cavity parameters for which $P_{\mathrm{excite}} < 0.1$. However, for $\gamma_{\mathrm{L}} = \kappa$, this is not always the case, and $\frac{g}{\kappa} < 2.5$ does not satisfy our criteria. This can be explained intuitively as follows, a small value of γ_{L} corresponds to a sharp pulse in frequency. This would mean that the spectrums $t_s(\omega)$ and $t_g(\omega)$ corresponding to the atom in the $|s\rangle$ and $|g\rangle$ state respectively are resolvable by the pulse. Thus, the pump intensity $|\alpha_{\mathrm{L}}|^2$ required to achieve $|\alpha|^2 = 2.1^2$ is lower and consequently, the maximum excitation probability of the atom is also lower.

Fig. 5.1 also shows that there exists some threshold of the atom-cavity detuning, $\frac{\Delta}{g}$, such that further increase in the detuning negligibly affects the maximum excitation probability.

5.2 Locality loophole and finite detection times

As was explained in the previous subsection, a small value of γ_{L} can achieve the required self-consistency threshold for a large range of cavity parameters. However, a small value of γ_{L} corresponds not only to a short pulse in frequency, but also to a long pulse duration. Since the duration of the pulse is necessarily the lower bound

on the measurement time of the outgoing pulse, to close the locality loophole, one would prefer a situation with larger values of γ_L.

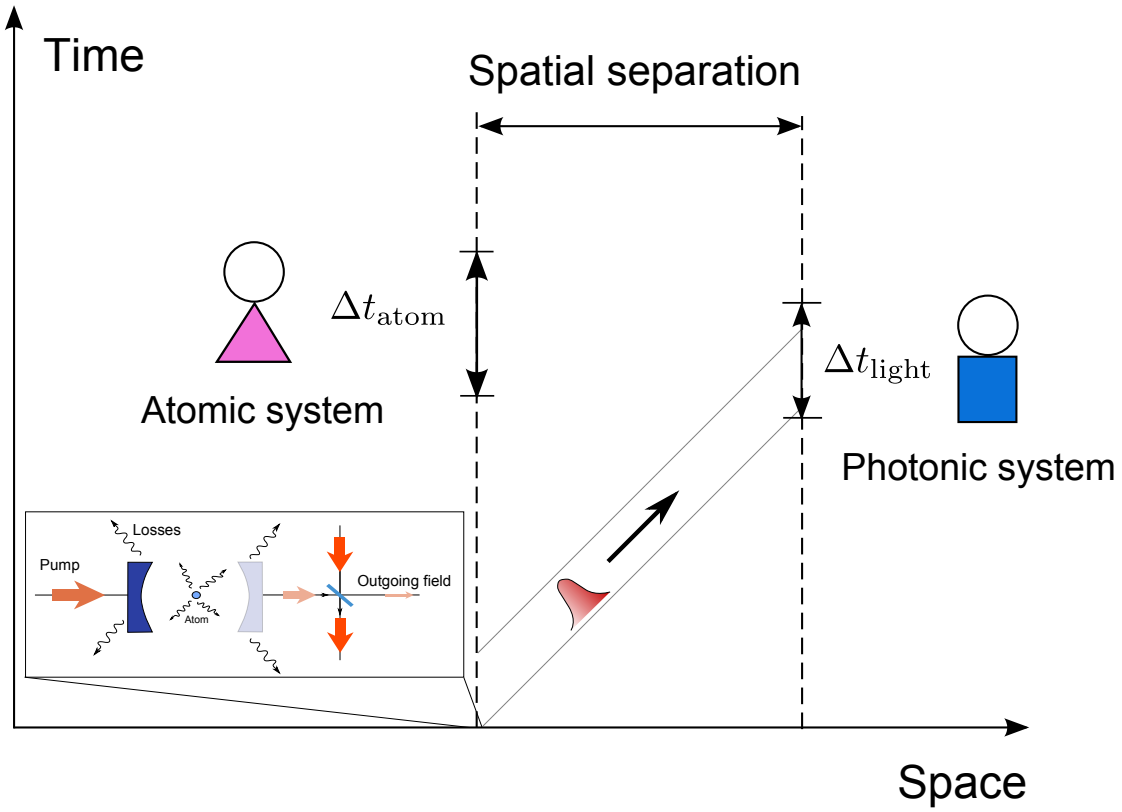

Figure 5.2: The above space-time diagram represents two parties, Alice and Bob, involved in the Bell test. Alice entangles the atom and the outgoing field at her lab, and sends the outgoing pulse to Bob, who measures it. Alice upon sending the pulse, waits an appropriate time before making her measurement on the atomic system, such that both measurements are space-like separated.

The condition for the measurements to be independent is for the event representing the start of the measurement on one system is space-like separated from the event representing the end of the measurement on the other system. This translates to a minimum spatial separation, d, between the measurement events such that the distance d satisfies

$$d = c \max\{\Delta t_{\text{atomic}}, \Delta t_{\text{light}}\}, \tag{5.12}$$

i.e. that the distance be larger than the larger of the atomic and light measurement times multiplied by the speed of light. This separation is then necessary to close the locality loophole. Fig. 5.2 summarizes this point.

Thus, with these considerations in mind we seek to find a compromise in the laser bandwidth γ_L such that the required propagation distances can be reduced.

The reduction in the propagation distance also slightly reduces the constraints on the experiment, since this would also reduce losses due to transmission. One could seek to reduce the propagation distances by reducing the measurement times on either side. The effect of a finite detection time can be modeled by assuming that the detector records some current (which consists of both noise and signal) in some time period and "turns off" outside of this time period. Then, a smaller detection time implies that the signal to noise ratio of the detection must be less than or equal to an infinite measurement time, since less signal is recorded over the detection time period. This implies that the detection efficiency is reduced, and will contribute to errors in the experimental result. We now show that the measurement time of the outgoing pulse can be reduced to $< 1\mu$s with negligible effect on the overall visibility.

To include the effect of finite pulse measurement time, we note that the outgoing pulse after the displacement operation has a frequency spectrum given by Eq. (4.47). The detected intensity would then be a convolution of the actual detector response function and the pulse spectrum. However, this would depend on the actual detector used, and an involved calculation would not give much insight into the physics of the process. Instead, we assume that the detector acts as a perfect detector for a particular time interval $(t_0, t_0 + \Delta t_{\text{det}})$, where t_0 is the start time of the detection. With this approximation, the detected integrated pulse intensity can be written as

$$I_{\text{det}} = \max_{t_0} \int_{t_0}^{t_0+\Delta t_{\text{det}}} dt \left| \frac{1}{\sqrt{2\pi}} \int d\omega \, e^{-i\omega t} \alpha(\omega) \right|^2, \tag{5.13}$$

where we fourier transform the frequency spectrum $\alpha(\omega)$ to the time domain and sum up the Intensity distribution in time over the detection window. The maximization of the integral over the start time t_0 for a given detection duration corresponds physically to tuning the detection time window such that the maximum count rate on the detector is achieved. The visibility of such an experiment can then be written simply as

$$V_{\text{ext}} = V_{\text{prod}} \cdot I_{\text{det}}/I_0, \tag{5.14}$$

with the state production visibility V_{prod} given by Eq. (4.43), and I_0 is the total integrated pulse intensity given by

$$I_0 = \int_0^{\infty} dt \left| \frac{1}{\sqrt{2\pi}} \int d\omega \, e^{-i\omega t} \alpha(\omega) \right|^2. \tag{5.15}$$

In a realistic setup, the most pertinent quantities would then be $\gamma_{0.1}$, which is the largest laser bandwidth that satisfies condition $\max_t \left\langle \sigma^\dagger \sigma(t) \right\rangle \approx 0.1$, and the experimental visibility (5.14), which is computed using the laser bandwidth $\min(\kappa, \gamma_{0.1})$, assuming $|\alpha| = 2.1$, $|r_{\rm BS}|^2 = 0.001$ and a pulse measurement duration $\Delta t_{\rm det} = 1\mu$s.

The experimental setup of Ref. [84], has $(g, \Gamma, \kappa) = 2\pi \times (5, 3, 3)$MHz and $f_{\rm cav} = \frac{15}{100}$, where we have inferred the asymmetry factor $f_{\rm cav}$ by noticing that the various decay rates of the mirrors are inversely proportional to the mirror transmission and losses, such that

$$f_{\rm cav} = \frac{\kappa_b + \kappa_L}{\kappa_c} = \frac{T_b + L}{T_c}, \tag{5.16}$$

where T_i is the transmission of the i^{th} mirror, and L is the total non-radiative losses in the cavity. Then, using $(T_b, T_c, L) = (5, 100, 10)$ppm[1], we obtain $f_{\rm cav} = \frac{15}{100}$. With these experimental parameters, the visibility of state production and the laser bandwidth $\gamma_{0.1}$ can be computed to give $(V_{\rm prod}, \gamma_{0.1}/(2\pi)) = (0.56, 1.16\,\text{MHz})$, and $I_{\rm det}/I_0 = 0.9996$. Notice that we have $I_{\rm det}/I_0 \approx 1$ for $\Delta t_{\rm det} = 1\,\mu$s, and amounts to a negligible correction to $V_{\rm prod}$. Indeed, as shown in Fig. 5.3, for $\Delta t_{\rm det} > 800\,$ns, $I_{\rm det}/I_0 \approx 1$.

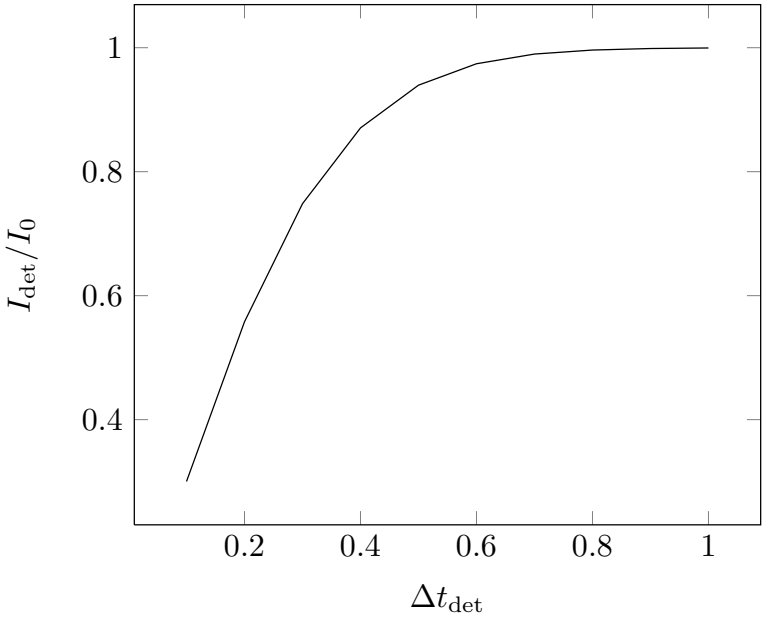

Figure 5.3: Plot of $I_{\rm det}/I_0$ against $\Delta t_{\rm det}$. It shows that for $\Delta t_{\rm det} > 0.8\,\mu$s, $I_{\rm det}/I_0$ is approximately equal to unity. The parameters used for this plot are $(g, \Gamma, \kappa, \gamma_{\rm L}) = 2\pi \times (5, 3, 3, 1.15)$MHz

[1]These numbers were communicated to me when I last visited their group in MPQ in July 2012, and might have since improved.

Since the larger of the atomic and photonic measurement time determines the propagation distance of the outgoing pulse, Fig. 5.3 also shows that the measurement time of the light field can be made smaller (up to about 800 ns) if required, without significant loss.

5.3 Using existing setups

5.3.1 State production and Visibilities

In this section, we use experimental parameters given in [85, 88, 84]. These experiments use 852 nm and 780 nm light respectively, which are subject to about 2 dB/km loss in optical fibers. In the following, we compare both experiments and possible modifications. As discussed previously, we will work in the large detuning regime, $\Delta \gg g$. We choose an arbitrary, but subjected to experimental constraints, value of $g/\Delta = 1/10$. This ensures that we respect all approximations used, as long as we also satisfy condition $\max_t P_e(t) \leq 0.1$. The figure of merit in both cases will be, $\gamma_{0.1}$, which is the largest laser bandwidth that satisfies condition $\max_t P_e(t) \approx 0.1$, and the state production visibility (4.43), which is computed using the laser bandwidth $\min(\kappa, \gamma_{0.1})$, assuming $|\alpha| = 2.1$ and $|r_{\rm BS}|^2 = 0.001$. Table 5.1 summarizes the results.

$g/(2\pi)$	$\kappa/(2\pi)$	$\Gamma/(2\pi)$	f_{cav}	$\gamma_{0.1}/(2\pi)$	V
34 MHz	4.1 MHz	2.6 MHz	10/4	13.3 MHz	0.4%
34 MHz	4.1 MHz	2.6 MHz	14/100	63.3 MHz	72.4%
34 MHz	4.1 MHz	2.6 MHz	4/100	65.2 MHz	90.4%
5 MHz	3 MHz	3 MHz	14/100	1.1 MHz	56.3%
5 MHz	3 MHz	3 MHz	4/100	1.3 MHz	71.3%
5 MHz	1.5 MHz	3 MHz	4/100	3.1 MHz	78.1%

Table 5.1: Expected visibilities for available experimental parameters for ^{133}Cs (first 3 rows) and ^{87}Rb (last 3 rows). All parameters $(g/(2\pi), \kappa/(2\pi), \Gamma/(2\pi), f_{cav})$ in the first and fourth row are actual cavity parameters (including mirror losses) obtained from [85, 88, 84]. The second row shows the effect on the Visibility and $\gamma_{0.1}$ by reducing f_{cav} to the current value in the experiment of Ref. [84]. The third row is obtained by neglecting the mirror losses, which further decreases the value of f_{cav}. The fifth row shows the effect of neglecting mirror losses, and the last row shows the effect of increasing g/κ. The state production visibility, V is computed assuming $|\alpha| = 2.1$ and $|r_{BS}|^2 = 0.001$, and using the laser bandwidth $\min(\kappa, \gamma_{0.1})$.

The parameters of Ref. [85, 88] are $(g/(2\pi), \kappa/(2\pi), \Gamma/(2\pi), f_{cav})$ = (34 MHz, 4.1 MHz, 2.6 MHz, 10/4) (we assume that the experiment performed implements a symmetric cavity). Due to the symmetry of the cavity, one obtains a small

effective visibility. Assuming that the cavity could be made asymmetric reducing f_{cav} to the current value in the experiment of Ref. [84], the visibility dramatically increases to 72.4% (second row). Neglecting the mirror losses, we show in the third row that V can be as high as 90.4%.

The parameters of Ref. [84] are $(g/(2\pi), \kappa/(2\pi), \Gamma/(2\pi), f_{cav}) = (5\,\text{MHz}, 3\,\text{MHz}, 3\,\text{MHz}, 14/100)$. As the setup stands, the visibility is 56.3%. However, neglecting the mirror losses, V increases to 71.3% (fifth row). If it were further possible to reduce the total cavity decay rate by a factor of 2, thus increasing the cooperativity, while maintaining the same asymmetry, the visibility further increases to 78.1% (sixth row). The required incident photon number can be calculated from (4.48). For the parameters in Table 5.1 and requiring the resulting photon number, $|\tilde{\alpha}|^2 = 2.1^2$, one requires $|\alpha_{in}|^2 \approx 25 - 400$ input photons.

For the specific case of ^{87}Rb, one might also identify possible states playing the role of $|g\rangle$, $|s\rangle$ and $|e\rangle$. We may choose for example the $|s\rangle$ state to be the hyperfine state $|5S_{1/2}, F = 1, m_F = 1\rangle$, the $|g\rangle$ state $|5S_{1/2}, F = 2, m_F = 2\rangle$ and the $|e\rangle$ state $|5P_{3/2}, F = 3, m_F = 3\rangle$. In this case, the input pulse and cavity field would have a σ_+ polarization coupling the $|g\rangle - |e\rangle$ transition. Due to the large detuning of the hyperfine states (6.8 Hz), and the fact that the s state is far-detuned to any other σ_+ transitions, these states are possible candidates for the experiment.

5.3.2 Performance of Bell tests

We now evaluate the performance of the experimental setup found in Ref. [84], assuming that there is no loss in the cavity mirrors. We assume that this setup is used to produce the desired entangled state, and then proceeding as in Sec. 3.4, we optimize the CHSH inequality for some sets of measurements. In this case, we use the cavity parameters $(g/(2\pi), \kappa/(2\pi), \Gamma/(2\pi), f_{cav}) = (5\,\text{MHz}, 3\,\text{MHz}, 3\,\text{MHz}, 5/100)$. Since we need to further optimize over α to find the maximum CHSH value, we do not use the calculated visibilities as in Table 5.1.

The optimization procedure is now a 4 step process as follows:

- For a range of α, find $\gamma_{0.1}$.
- With $\gamma_{0.1}$, compute V_{prod} according to Eq. (4.43).
- With the same range of α, compute V_{opt} using Eq. (3.26).
- Visibility is now $V = V_{\text{prod}} \times V_{\text{opt}}$, and optimization over α can now be done.

Using the case of one-photocounting measurement as an example, we find that the maximum achievable chsh value is $\langle \mathcal{B} \rangle = 2.16$, which occurs at $|\alpha| = 1.95$

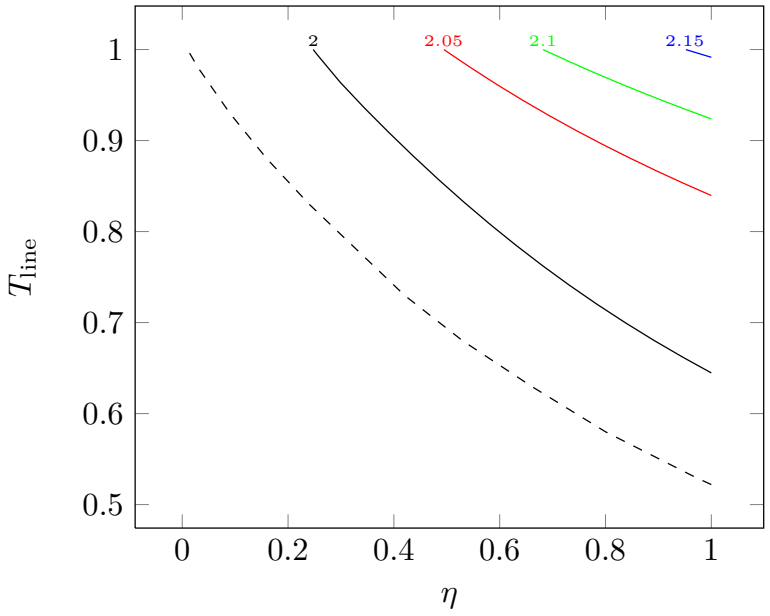

Figure 5.4: Contour plot of $\mathcal{B}$ vs the line transmission and the photocounting efficiency. The maximum CHSH violation is 2.16, which occurs at $|\alpha| = 1.95$ and $\gamma_{0.1} = (2\pi)1.46\text{MHz}$. The ideal state is included (dashed) for comparison. The parameters used are, $(g/(2\pi), \kappa/(2\pi), \Gamma/(2\pi), f_{cav}) = (5\,\text{MHz}, 3\,\text{MHz}, 3\,\text{MHz}, 5/100)$, and $|r_{\text{BS}}|^2 = 0.001$.

and $\gamma_{0.1} = (2\pi)1.46\text{MHz}$. Furthermore, the minimum detector efficiency required is $\eta = 0.247$ for perfect line transmission, and the minimum line transmission is $T_{\text{line}} = 0.64$ for perfect detector efficiency. Fig. 5.4 summarizes these results.

CHAPTER 6

THEORY OF ENTANGLED PHOTONS GENERATION WITH FOUR-WAVE MIXING

This chapter arose due to the results of Ref. [89], where they show a four-wave mixing experimental setup that produces a very narrow band source of entangled photon pairs. This review of the four-wave mixing literature was done by the author to clarify questions on the properties of the photon pairs that arose in discussions with the authors of Ref. [89].

This chapter is structured as follows. In Sec. 6.1, we first give a brief description of the results of Ref. [89]. Next, in Sec. 6.2, we write down the problem hamiltonian. Then, identifying slow-varying operators, we derive an effective hamiltonian for this system and the corresponding equations of motion for these operators. After this, we study the approach of Ref. [90] in Sec. 6.3, outlining the main conceptual steps taken in that thesis, showing how some of the results are qualitatively linked to those of Ref. [89]. We then give a conclusion of this work. Lastly, we present ongoing calculations in a different approach to this problem in Appendix B, inspired by the work of Gorshkov in Ref. [91].

6.1 The measurement

The physical situation situation to be considered is a cold atomic ensemble of ^{87}Rb gas with a diamond energy level configuration as in Fig. 6.1. We consider the four-wave mixing setup with 2 classical pump beams at 780nm and 776nm that pump the atoms from the $5S_{1/2}, F = 2$ energy level to the $5D_{3/2}, F = 3$ state and the entangled photon pair is on the 762nm signal and 795nm idler transitions.

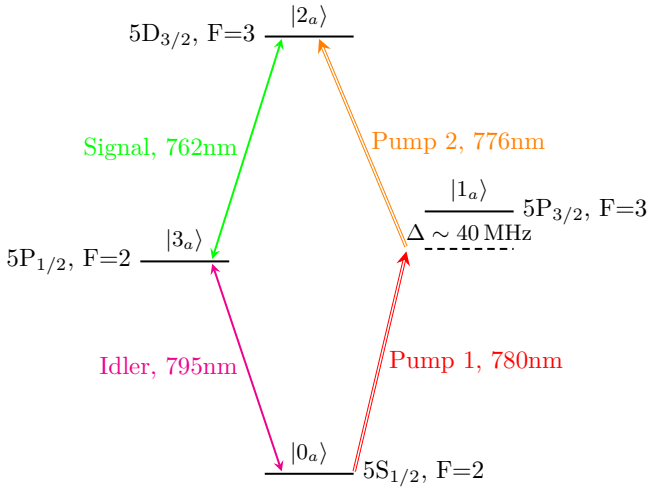

Figure 6.1: Relevant energy levels of the ^{87}Rb atom used in the experiment. Image adapted from Ref. [89].

Ref. [89] demonstrated that by having a cold atomic ensemble of ^{87}Rb atoms and pumping the ensemble with the two pump fields as shown in Fig. 6.1, and applying a small "seed" field on the idler transition, a high quality entangled photon pair source is created. Also, due to superradiant effects, the photons created have a narrower bandwidth than one would naively expect from the transition decay rates. Furthermore, due to the decay process, the photons produced are also correlated in the time domain as well. This implies that the detection of a signaller photon heralds the arrival of the idler photon. This later point is directly related to the 2$^{\text{nd}}$ order correlation function between the signaller and idler photons.

In the following sections, we derive the basic theory necessary to tackle this problem, keeping in mind the physical scenario.

6.2 Interaction of the ensemble and fields

We first denote the levels as the follows: Let $|0_a\rangle$ be the $|5S_{1/2}, F = 2\rangle$ state, $|1_a\rangle$ be the $|5P_{3/2}, F = 3\rangle$ state, $|2_a\rangle$ be the $|5D_{3/2}, F = 3\rangle$ state and $|3_a\rangle$ be the $|5P_{1/2}, F = 2\rangle$ state (counter-clockwise naming $0 \to 1 \to 2 \to 3 \to 0$). Then, the relevant transition frequencies are, $\frac{\omega_{01}}{c} \approx 780\text{nm}$, $\frac{\omega_{12}}{c} \approx 776\text{nm}$, $\frac{\omega_{23}}{c} \approx 762\text{nm}$ and $\frac{\omega_{04}}{c} \approx 795\text{nm}$.

6.2.1 Description of the problem in the rotating wave approximation

We approach the problem in a one-dimensional approximation, where $+z$ is the direction of propagation of the pump fields. Then, we assume implicitly one of the four-wave mixing phase matching conditions, which is $\hat{k}_{p1}+\hat{k}_{p2}=\hat{k}_s+\hat{k}_d$, where $\hat{k}_i$ is the direction of propagation of the i^{th} mode. With this, we define the relevant Electric field operators as

$$\vec{E}_{p1} = \epsilon_{p1}\mathcal{E}_{p1}(t-z/c)\cos(w_{p1}(t-z/c)), \tag{6.1}$$

$$\vec{E}_{p2} = \epsilon_{p2}\mathcal{E}_{p2}(t-z/c)\cos(w_{p2}(t-z/c)), \tag{6.2}$$

$$\vec{E}_s(z) = \epsilon_s\sqrt{\frac{\hbar\omega_s}{4\pi c\epsilon_0 A}}\int d\omega\, s_\omega e^{i\omega z/c} + \text{h.c.}, \quad \text{and,} \tag{6.3}$$

$$\vec{E}_i(z) = \epsilon_d\sqrt{\frac{\hbar\omega_d}{4\pi c\epsilon_0 A}}\int d\omega\, d_\omega e^{i\omega z/c} + \text{h.c..}, \tag{6.4}$$

where $\vec{E}_{p1}$ and $\vec{E}_{p2}$ are the Electric fields of the two classical pump fields, and $\vec{E}_s$ and $\vec{E}_i$ are the fields of the signaller and idler respectively such that s_ω and d_ω are the continuum annihilation operators in the signaller and idler modes and A is the effective cross-sectional area of the modes, which are assumed to be equal for simplicity. Then, we can write the Hamiltonian of this system (divided by $\hbar$), in the rotating wave approximation, as

$$h = h_0 + \hat{v}, \tag{6.5}$$

$$h_0 = \int d\omega\,\omega(s^\dagger_\omega s_\omega + d^\dagger_\omega d_\omega) + \sum_{i=1}^{N}\sum_{\mu\in\{1,2,3\}} w_{0\mu}\sigma_{\mu\mu,i}, \tag{6.6}$$

$$\hat{v} = -\sum_{i=1}^{N}\Big(\Omega_{p1}(t-\frac{z_i}{c})\sigma^\dagger_{01,i}e^{-iw_{p1}(t-\frac{z_i}{c})} + \Omega_{p2}(t-\frac{z_i}{c})\sigma^\dagger_{12,i}e^{-iw_{p2}(t-\frac{z_i}{c})}$$
$$\sqrt{\frac{L}{2\pi c}}\int d\omega\,\Big(g_s s_\omega\sigma^\dagger_{32,i}e^{iw\frac{z_i}{c}} + g_d d_\omega\sigma^\dagger_{03,i}e^{iw\frac{z_i}{c}}\Big)\Big) + \text{h.c}, \tag{6.7}$$

where $\Omega_{p1} = \langle 1_a|d\cdot\epsilon_{p1}|0_a\rangle\frac{\mathcal{E}_{p1}(t-\frac{z}{c})}{2\hbar}$, $\Omega_{p2} = \langle 2_a|d\cdot\epsilon_{p2}|1_a\rangle\frac{\mathcal{E}_{p2}(t-\frac{z}{c})}{2\hbar}$, $g_s = \langle 2_a|d\cdot\epsilon_s|3_a\rangle\sqrt{\frac{w_s}{2\hbar\epsilon_0 AL}}$ and $g_d = \langle 3_a|d\cdot\epsilon_d|0_a\rangle\sqrt{\frac{w_d}{2\hbar\epsilon_0 AL}}$; $\sigma_{\mu\nu} = |\mu_a\rangle\langle\nu_a|$.

6.2.2 Deriving an effective description

The above hamiltonian is fairly complex, and masks easily interpretable results. We then seek an effective Hamiltonian for slow-varying collective atomic operators, and effective quantum fields. We follow the approach of Gorshkov in Ref. [91], and

do the following: We first consider quantized sections of the z-axis, for $z \in [0, L]$, where L is the length of the atomic ensemble. The quantized sections are such that we have $N_z \gg 1$, where N_z is the number of atoms in the section $[z, z + dz]$. We further assume that the cells are large enough such that the fields can be considered continuous. We then write down the collective slow varying atomic operators evolving according to the applied and detected fields:

$$\tilde{\sigma}_{\mu,\mu}(z,t) = \frac{1}{N_z}\sum_{i=1}^{N_z}\sigma_{\mu,\mu,i}, \tag{6.8}$$

$$\tilde{\sigma}_{0,1}(z,t) = \frac{1}{N_z}\sum_{i=1}^{N_z}\sigma_{0,1,i}e^{i\omega_{p1}(t-z_i/c)}, \tag{6.9}$$

$$\tilde{\sigma}_{1,2}(z,t) = \frac{1}{N_z}\sum_{i=1}^{N_z}\sigma_{1,2,i}e^{i\omega_{p2}(t-z_i/c)}, \tag{6.10}$$

$$\tilde{\sigma}_{3,2}(z,t) = \frac{1}{N_z}\sum_{i=1}^{N_z}\sigma_{3,2,i}e^{i\omega_{s}(t-z_i/c)}, \tag{6.11}$$

$$\tilde{\sigma}_{0,3}(z,t) = \frac{1}{N_z}\sum_{i=1}^{N_z}\sigma_{0,3,i}e^{i\omega_{d}(t-z_i/c)}, \tag{6.12}$$

where $N_z = n(z)dz$, where we denote $n(z)$ as the column density of the ensemble. The Heisenberg equations of motion for these operators are easily derived to obtain,

$$\begin{aligned}
-i\partial_t\tilde{\sigma}_{01} &= -(\omega_{01}-\omega_{p1})\tilde{\sigma}_{01} + \Omega_{p1}(\tilde{\sigma}_{11}-\tilde{\sigma}_{00}) - \Omega_{p2}^*\Big[\frac{1}{N_z}\sum_{i=1}^{N_z}\sigma_{02,i}e^{i(\omega_{p1}+\omega_{p2})(t-\frac{z_i}{c})}\Big] \\
&\quad + g_d\sqrt{\frac{L}{2\pi c}}\int d\omega\, d_\omega e^{i\omega\frac{z}{c}}\Big[\frac{1}{N_z}\sum_{i=1}^{N_z}\sigma_{31,i}e^{i\omega_{p1}(t-\frac{z_i}{c})}\Big], \qquad (6.13)\\
-i\partial_t\tilde{\sigma}_{12} &= -(\omega_{12}-\omega_{p2})\tilde{\sigma}_{12} + \Omega_{p1}^*\Big[\frac{1}{N_z}\sum_{i=1}^{N_z}\sigma_{02,i}e^{i(\omega_{p1}+\omega_{p2})(t-\frac{z_i}{c})}\Big] + \Omega_{p2}(\tilde{\sigma}_{22}-\tilde{\sigma}_{11}) \\
&\quad - g_s\sqrt{\frac{L}{2\pi c}}\int d\omega\, s_\omega e^{i\omega\frac{z}{c}}\Big[\frac{1}{N_z}\sum_{i=1}^{N_z}\sigma_{13,i}e^{i\omega_{p2}(t-\frac{z_i}{c})}\Big], \qquad (6.14)\\
-i\partial_t\tilde{\sigma}_{32} &= -(\omega_{32}-\omega_s)\tilde{\sigma}_{32} - \Omega_{p2}\Big[\frac{1}{N_z}\sum_{i=1}^{N_z}\sigma_{31,i}e^{i(\omega_s-\omega_{p2})(t-\frac{z_i}{c})}\Big] \\
&\quad + g_s\sqrt{\frac{L}{2\pi c}}e^{i\omega_s(t-\frac{z}{c})}\int d\omega\, s_\omega e^{i\omega\frac{z}{c}}(\tilde{\sigma}_{22}-\tilde{\sigma}_{33}) \\
&\quad + g_d^*\sqrt{\frac{L}{2\pi c}}\int d\omega\, d_\omega^\dagger e^{-i\omega\frac{z}{c}}\Big[\frac{1}{N_z}\sum_{i=1}^{N_z}\sigma_{02,i}e^{i\omega_s(t-\frac{z_i}{c})}\Big], \qquad (6.15)\\
-i\partial_t\tilde{\sigma}_{03} &= -(\omega_{03}-\omega_d)\tilde{\sigma}_{03} + \Omega_{p1}\Big[\frac{1}{N_z}\sum_{i=1}^{N_z}\sigma_{13,i}e^{i(\omega_d-\omega_{p1})(t-\frac{z_i}{c})}\Big] \\
&\quad - g_s^*\sqrt{\frac{L}{2\pi c}}\int d\omega\, s_\omega^\dagger e^{-i\omega\frac{z}{c}}\Big[\frac{1}{N_z}\sum_{i=1}^{N_z}\sigma_{02,i}e^{i\omega_d(t-\frac{z_i}{c})}\Big] \\
&\quad + g_d\sqrt{\frac{L}{2\pi c}}e^{i\omega_d(t-\frac{z}{c})}\int d\omega\, d_\omega e^{i\omega\frac{z}{c}}(\tilde{\sigma}_{33}-\tilde{\sigma}_{00}), \qquad (6.16)
\end{aligned}$$

where we have denoted $\omega_{ij} = \omega_{0j} - \omega_{0i}$. The above set of equations implies that appropriate slow varying field operators should be given by,

$$\mathcal{S}(z,t) = \sqrt{\frac{L}{2\pi c}}e^{i\omega_s(t-\frac{z}{c})}\int d\omega\, s_\omega e^{i\omega\frac{z}{c}}, \quad \text{and,} \qquad (6.17)$$

$$\hat{\mathcal{D}}(z,t) = \sqrt{\frac{L}{2\pi c}}e^{i\omega_d(t-\frac{z}{c})}\int d\omega\, d_\omega e^{i\omega\frac{z}{c}}. \qquad (6.18)$$

We can also identify the two slow varying operators for the "indirect" transitions, *i.e.* $\tilde{\sigma}_{13}$ and $\tilde{\sigma}_{02}$, "indirect" since there are no physical fields directly coupling these states, and these states are coupled indirectly by 2 fields. We assume that we satisfy energy conservation in the 4-wave mixing, *i.e.* $\omega_{p1}+\omega_{p2} = \omega_s+\omega_d$. This also means that $\omega_d - \omega_{p1} = \omega_{p2} - \omega_s$. With this additional assumption, we

can write the two missing slow varying operators as

$$\tilde{\sigma}_{02} = \left[\frac{1}{N_z}\sum_{i=1}^{N_z}\sigma_{02,i}e^{i(\omega_{p1}+\omega_{p2})(t-\frac{z_i}{c})}\right], \quad \text{and,} \tag{6.19}$$

$$\tilde{\sigma}_{13} = \left[\frac{1}{N_z}\sum_{i=1}^{N_z}\sigma_{13,i}e^{i(\omega_{d}-\omega_{p1})(t-\frac{z_i}{c})}\right]. \tag{6.20}$$

These definitions are natural in the sense that they preserve the usual commutation relations for atomic operators, up to an additional z dependent scaling of $1/N_z$.

$$[\tilde{\sigma}_{ab}(z,t), \tilde{\sigma}_{cd}(z',t)] = \frac{\delta(z-z')}{N_z}(\delta_{bc}\tilde{\sigma}_{ad} - \delta_{da}\tilde{\sigma}_{bc}). \tag{6.21}$$

Similarly for the fields, we have

$$[\mathcal{S}(z,t), \mathcal{S}^\dagger(z',t)] = L\delta(z-z'), \tag{6.22}$$

and the corresponding one for $\hat{\mathcal{D}}$. Then, we can write the neater equations,

$$-i\partial_t\tilde{\sigma}_{01} = -(\omega_{01}-\omega_{p1})\tilde{\sigma}_{01} + \Omega_{p1}(\tilde{\sigma}_{11}-\tilde{\sigma}_{00}) - \Omega^*_{p2}\tilde{\sigma}_{02} + g_d\hat{\mathcal{D}}\tilde{\sigma}^\dagger_{13}, \tag{6.23}$$

$$-i\partial_t\tilde{\sigma}_{12} = -(\omega_{12}-\omega_{p2})\tilde{\sigma}_{12} + \Omega^*_{p1}\tilde{\sigma}_{02} + \Omega_{p2}(\tilde{\sigma}_{22}-\tilde{\sigma}_{11}) - g_s\mathcal{S}\tilde{\sigma}_{13}, \tag{6.24}$$

$$-i\partial_t\tilde{\sigma}_{32} = -(\omega_{32}-\omega_{s})\tilde{\sigma}_{32} - \Omega_{p2}\tilde{\sigma}^\dagger_{13} + g_s\mathcal{S}(\tilde{\sigma}_{22}-\tilde{\sigma}_{33}) + g^*_d\hat{\mathcal{D}}^\dagger\tilde{\sigma}_{02}, \tag{6.25}$$

$$-i\partial_t\tilde{\sigma}_{03} = -(\omega_{03}-\omega_{d})\tilde{\sigma}_{03} + \Omega_{p1}\tilde{\sigma}_{13} - g^*_s\mathcal{S}^\dagger\tilde{\sigma}_{02} + g_d\hat{\mathcal{D}}(\tilde{\sigma}_{33}-\tilde{\sigma}_{00}), \tag{6.26}$$

and,

$$-i\partial_t\tilde{\sigma}_{02} = -[\omega_{02}-(\omega_s+\omega_d)]\tilde{\sigma}_{02} + \Omega_{p1}\tilde{\sigma}_{12} - \Omega_{p2}\tilde{\sigma}_{01} - \mathcal{S}\tilde{\sigma}_{03} + \hat{\mathcal{D}}\tilde{\sigma}_{32}, \tag{6.27}$$

$$-i\partial_t\tilde{\sigma}_{13} = -[\omega_{13}-(\omega_d-\omega_{p1})]\tilde{\sigma}_{13} + \Omega^*_{p1}\tilde{\sigma}_{03} + \Omega_{p2}\tilde{\sigma}^\dagger_{32} - \mathcal{S}^\dagger\tilde{\sigma}_{12} - \hat{\mathcal{D}}\tilde{\sigma}^\dagger_{01}. \tag{6.28}$$

Field propagation

Eqs. (6.23-6.28) complete the required description for the atomic operators. In this short section, we outline the derivation of the field propagation equations in the slow-varying envelope approximation for completeness. The derivation can be broken down into a 5 step process as follows:

1. Start from Maxwell's equations with no free charge or current

$$\vec{\nabla}\times\vec{E} = -\frac{\partial\vec{B}}{\partial t} \quad , \quad \vec{\nabla}\times\vec{H} = \frac{\partial\vec{D}}{\partial t},$$
$$\vec{\nabla}\cdot\vec{D} = 0 \quad , \quad \vec{\nabla}\cdot\vec{B} = 0, \tag{6.29}$$

with the material equations,

$$\vec{D} = \epsilon_0 \vec{E} + \vec{P}, \quad \text{and,} \quad \vec{B} = \mu_0 \vec{H} + \vec{M}. \tag{6.30}$$

2. Assume material has no magnetization, only polarization (which is induced by the incoming field).

3. Write down wave equation for the electric field and make the slow varying envelope approximation (similar to paraxial approximation). Without additional approximations, we get

$$\left(\frac{1}{c^2}\frac{\partial^2}{\partial t^2} - \vec{\nabla}^2\right)\vec{E} = \frac{1}{\epsilon_0}\vec{\nabla}[\vec{\nabla}\cdot\vec{P}] - \mu_0\frac{\partial^2\vec{P}}{\partial t^2}. \tag{6.31}$$

Assume that the medium is homogenous, such that $\vec{\nabla}\cdot\vec{P} = 0$. Then, we get the wave equation

$$\left(\vec{\nabla}^2 - \frac{1}{c^2}\frac{\partial^2}{\partial t^2}\right)\vec{E} = \mu_0\frac{\partial^2\vec{P}}{\partial t^2}. \tag{6.32}$$

The slow-varying envelope approximation is as follows, assume that $\vec{E} = \mathcal{E}(x,y,z)e^{-i(wt-kz)}$, *i.e.* that it has an envelope function $\mathcal{E}$ and predominantly propagates in the z direction. This equation then becomes

$$\begin{aligned}&\left(\vec{\nabla}_\perp^2 + \frac{\partial^2}{\partial z^2} + 2ik\frac{\partial}{\partial z} - k^2 - \frac{1}{c^2}\left[\frac{\partial^2}{\partial t^2} - 2i\omega\frac{\partial}{\partial t} - \omega^2\right]\right)\vec{\mathcal{E}} \\ &= \mu_0[\frac{\partial^2}{\partial t^2} - 2i\omega\frac{\partial}{\partial t} - \omega^2]\vec{\mathcal{P}}.\end{aligned} \tag{6.33}$$

Where $\vec{\nabla}_\perp$ denotes the transverse spatial derivatives, $\mathcal{P}$ denotes the slow varying envelope of the polarization, and we have made the linear medium approximation, $P = \epsilon_0\chi E$. Then, the slow-varying envelope approximation are the four approximations

$$\left|\frac{\partial^2\mathcal{E}}{\partial z^2}\right| \ll \left|2ik\frac{\partial\mathcal{E}}{\partial z}\right|, \qquad \left|\frac{\partial^2\mathcal{E}}{\partial t^2}\right| \ll \left|2i\omega\frac{\partial\mathcal{E}}{\partial t}\right|, \tag{6.34}$$

$$\left|\frac{\partial^2\mathcal{P}}{\partial t^2}\right| \ll \left|2i\omega\frac{\partial\mathcal{P}}{\partial t}\right|, \qquad \left|\frac{\partial\mathcal{P}}{\partial t}\right| \ll |\omega\mathcal{P}|. \tag{6.35}$$

This approximation can be explained in a number of ways. One more interesting way is to say that this approximation is equivalent to ignoring backward propagation of the pulse[1]. With these approximations, we get the

[1]For an elaboration of this point and other interpretations, see for instance part F, sec. 68.2 of Ref. [92] and sec. 7 of Ref. [93]

wave equation

$$\left(\vec{\nabla}_{\perp}^{2} + 2ik\frac{\partial}{\partial z} + 2i\frac{k}{c}\frac{\partial}{\partial t}\right)\vec{E} = -\mu_0\omega^2\vec{P}. \tag{6.36}$$

Ignoring transverse variation of the pulse, we finally get

$$\left(\frac{\partial}{\partial z} + \frac{1}{c}\frac{\partial}{\partial t}\right)\vec{E} = -\frac{k}{2i\epsilon_0}\vec{P}. \tag{6.37}$$

4. Next, polarization is split into the quasi-resonant transition to the applied field, and all other possibly coupled transitions. The other transitions (*e.g.*other hyperfine states) constitute a higher order correction to the polarizability of the atom, and can be computed with 2^{nd} order perturbation theory. However, for the sake of this problem, we will ignore these corrections and only consider the quasi-resonant transition.

5. The polarization is simply defined as $P = \frac{\langle d \rangle}{V}$, *i.e.* the mean dipole density.

Using the above outline, including the quasi-resonant approximation, the propagation equations for the slow varying field operators in terms of the collective atomic operators are,

$$(c\partial_z + \partial_t)S(z,t) = ig_s Ln(z)\tilde{\sigma}_{32}(z,t), \quad \text{and,} \tag{6.38}$$

$$(c\partial_z + \partial_t)D(z,t) = ig_d Ln(z)\tilde{\sigma}_{03}(z,t). \tag{6.39}$$

We are now in place to derive a simpler effective Hamiltonian. Defining the detunings;

$$\delta_{p1} = \omega_{01} - \omega_{p1} \tag{6.40}$$

$$\delta_{p2} = \omega_{12} - \omega_{p2} \tag{6.41}$$

$$\delta_s = \omega_{32} - \omega_s \tag{6.42}$$

$$\delta_d = \omega_{03} - \omega_d \tag{6.43}$$

$$\Delta_2 = \omega_{02} - (\omega_s + \omega_d) \tag{6.44}$$

$$\Delta_w = \omega_{13} - (\omega_d - \omega_{p1}) \tag{6.45}$$

where δ's are single photon detunings, and Δ's are 2 photon detunings. Then, the effective Hamiltonian is,

$$\tilde{h}_{\text{eff}} = \tilde{h}_0 + \tilde{v}_{\text{int}}, \tag{6.46}$$

$$\tilde{h}_0 = \int d\omega\, \omega(s_\omega^\dagger s_\omega + d_\omega^\dagger d_\omega) - \int_0^L \frac{dz}{L}\left(\omega_s \mathcal{S}^\dagger \mathcal{S} + \omega_d \hat{\mathcal{D}}^\dagger \hat{\mathcal{D}}\right) + \int_0^L dz\, n(z)\left(\delta_{p1}\tilde{\sigma}_{11} + \Delta_2 \tilde{\sigma}_{22} + \delta_d \tilde{\sigma}_{33}\right), \tag{6.47}$$

$$\tilde{v}_{\text{int}} = -\int_0^L dz\, n(z)\Big(\Omega_{p1}(t - \frac{z}{c})\tilde{\sigma}_{01}^\dagger + \Omega_{p2}(t - \frac{z}{c})\tilde{\sigma}_{12} + g_s \mathcal{S}\tilde{\sigma}_{32}^\dagger + g_d \hat{\mathcal{D}}\tilde{\sigma}_{03}^\dagger + \text{h.c}\Big). \tag{6.48}$$

With this effective Hamiltonian, and the commutation relations Eqs. (6.21) and (6.22), the reader can verify that we obtain the equations of motion derived from the original Hamiltonian.

6.3 A tried and tested approach

In the thesis of Jen [90], this system was considered and solved first using an ansatz solution, and the solution verified by numerically solving the full system. The methods used and the situation considered is much more complex then the present one, since the rotating wave approximation is not used in this treatment. Since we do not consider this additional level of complexity, we shall only outline his methods without detailed derivations. The interested reader is referred to Ref. [90] and references therein for a detailed and complete treatment[2].

6.3.1 An analytical approach

Ref. [90] tackles this problem analytically using a conceptually simple approach. However, due to the complexity of the problem and the lack of the rotating wave approximation in the approach, the resultant equations rarely fit on one line and can be very daunting to an unsuspecting reader. As such, we break down the line of reasoning into 4 steps.

- Jen uses the ansatz that the atomic ensemble is only weakly excited, such that only a single entangled photon pair is produced.

  This allows to expand the atom-photon Hilbert space into the set of states, $\mathcal{S} = \{|0_a\rangle|0\rangle, |0_a\rangle|1_s, 1_d\rangle, |1_a\rangle|0\rangle, |2_a\rangle|0\rangle, |3_a\rangle|1_s, 0\rangle\}$, which is the set of states

[2]The reader is however, strongly advised to read through this outline before attempting to study the thesis.

allowable in the rotating wave approximation, starting from the atomic ensemble state in the ground state and signaler and idler fields in the vacuum state, given the constraint of a single entangled photon pair.

- With this ansatz, the set $\mathcal{S}$ now forms a complete basis for the atom-photon Hilbert space. We then write down the Schrödinger equation with this expansion, to obtain coupled differential equations for the state expansion coefficients.

- This set of equations are solved using an adiabatic and far detuned pump approximation, where the pump fields are assumed far detuned from the relevant atomic transitions and do not vary too fast in time[3].

- Since what is measured in the experiment is detection of either signaler or idler photon, triggered on the other photon, this measurement directly measures the 2^{nd} order correlation function of the fields.

  This correlation function is again related to the probability amplitude of the $|0_a\rangle|1_s, 1_d\rangle$. Using again the ansatz that the set $\mathcal{S}$ represents all allowable states, the $G^{(2)}$ for this measurement is calculated.

6.3.2 Numerical approach

This approach was developed to relax the ansatz of the previous subsection, and to numerically verify the results. However, it must be noted that in this part of Ref. [90], the rotating wave approximation is made. This approximation was likely made to simplify the already messy problem.

As is usual in the case of numerical work, the numerical approach taken here can be considered somewhat brute force, so the outline of this method will be brief.

- Write down the Hamiltonian in the rotating wave approximation describing this system.

- Assuming only atomic decay processes, and ignore any dephasing processes, write down the master equation of the system.

- Using known correspondences between the positive P representation and the master equation, write down a set of coupled equations for the characteristic function.

[3] See Appendix A2 of Ref. [90] for more precise conditions of the adiabatic approximation used in this context.

- With this in hand, derive a Fokker-Planck equation for the distribution, and with this, find c-number Langevin equations for the system operators.
- Identify the correlation functions of the Langevin forces (noise terms) from the corresponding terms in the Fokker-Planck equation, and confirm them using generalized Einstein relations.
- The system of equations are now fully specified and can be numerically solved. This complicated system is now solved using a host of numerical methods. See Ref. [90] for full details of the simulation[4].

6.4 Outcomes and continuation

Using the ansatz technique of Ref. [90], we were able to derive the exponentially decaying $G^{(2)}$ trace measured in Ref. [89]. This theory also gives the correct predictions for the detection of the signaller photon, triggered on the idler, that the resulting $G^{(2)}$ is a *rising* exponential pulse [94].

Reviewing the methods by which Ref. [90] derives the four-wave mixing results, one notices the following: Either the approximations seem rigid, assuming the ansatz in Sec. 6.3.1, or the problem is treated in its full generality (up to the rotating wave approximation) in Sec. 6.3.2. The rigidity of the approximate ansatz in Sec. 6.3.1 becomes apparent when one tries to glean further information from the system, for instance the conversion efficiency of the problem, which the numerical approach might reveal, but is cumbersome to use. This hints at some middle ground where useful results can be derived semi-analytically, without overly rigid approximations or completely general treatments. In Appendix B, we present an ongoing attempt to describe this system using techniques and ideas inspired from Ref. [91].

[4]However, as (possibly frustratingly) noted on pp 140, the system of equations has 19 variables, 64 diffusion matrix elements and 117 noise terms, so one might agree that this is not a simple problem to tackle.

CHAPTER 7

QUANTUM OPTIMAL CONTROL

7.1 Introduction

The work in this chapter was carried out in collaboration with Howard Wiseman in the Centre for Quantum Dynamics, Griffith University in Brisbane. It represents the author's attempt to learn the vast field of optimal control theory, particularly in quantum optimal control. The author seeks the understanding of the reader for any lapses in understanding of the material.

This chapter is structured as follows. We first discuss the measurement model of a qubit and the equations governing the dynamics of this system, with a short discussion on the control strategies in this system. Next we present Jacobs' problem of rapid stochastic purification [47], and show his solution and proof. We then show a complementary protocol by Wiseman and Ralph (WR) [49] with a modified control objective in mind. We then proceed to discuss a family of purification measures through the Rényi entropies, and show that it highlights non-intuitive features of quantum control theory.

7.2 Measurement model and control strategies

The physical model that we consider is identical to those considered previously in [47, 49, 50], which is the continuous measurement of a qubit in the z basis, with the ability to control the Hamiltonian evolution of the qubit. Without loss of generality, we assume that the initial state of the qubit satisfies $\mathrm{Tr}[\rho_0\sigma_y] = 0$. Then, to control the evolution of the qubit, we need only implement Hamiltonian controls in the y basis. The conditional master equation for the qubit state matrix

is then

$$d\rho = -i\frac{\Omega_t}{2}[\sigma_y, \rho]dt + (\sigma_z\rho\sigma_z - \rho)dt + (\sigma_z\rho + \rho\sigma_z - 2\mathrm{Tr}[\rho\sigma_z]\rho)dW, \tag{7.1}$$

where Ω_t is the control input, and dW is the stochastic Wiener increment satisfying $dW^2 = dt$. The above equation can be equivalently represented in terms of its Bloch components $(x, y, z) = \mathrm{Tr}[\rho(\sigma_x, \sigma_y, \sigma_z)]$

$$dx = (-2x + \Omega_t z)dt - 2xzdW, \tag{7.2}$$

$$dz = -\Omega_t x dt + 2(1 - z^2)dW, \tag{7.3}$$

and $y = 0$. Using the definition of the Bloch vector, we can define the purity P of the qubit as the square of the length of the Bloch vector, *i.e.* $P = \mathrm{Tr}[\rho^2] = \frac{1+r^2}{2}$, with $r^2 = x^2 + z^2$. It turns out that a more convenient parametrization of this problem is given by the impurity, $L = 1 - P = \frac{1-r^2}{2}$, and the angle which the Bloch vector makes with the $z-$axis, θ, such that $x = r\sin\theta$ and $z = r\cos\theta$. This change of variables gives the following stochastic differential equations (SDEs)

$$dL = -4L\Big\{\Big[1 - (1 - 2L)u^2\Big]dt + \sqrt{1 - 2L}\, u\, dW\Big\}, \tag{7.4}$$

$$d\theta = \Big(\Omega_t + f(\theta, L)\Big)dt + g(\theta, L)dW, \tag{7.5}$$

where $u = \cos\theta$ and f and g are functions whose form we will not need. As in earlier work [47, 49, 50], we make the simplifying assumption that through Ω_t we are able to control u directly, thus making the determination of the forms of f and g unimportant in our context.

7.2.1 Stochastic purification

Given the measurement model in Sec. 7.2, one can now consider the problem of stochastic purification of a continuously measured qubit system. The objective of any feedback to the system would then be to purify the qubit. This aim of purification leads to two complementary control goals for a given measure of the purity (or impurity) of a system.

Control goal I For a given measure of purity (impurity), maximize (minimize) the average value of this measure, for a given running time of the control strategy

Control goal II For a given measure of purity (impurity), minimize the average time taken to achieve a particular value of the purity (impurity) measure.

These definition are natural considerations one might use to evaluate a particular control protocol. Although both control goals might seem equivalent, as we will show in the following sections, these are complementary goals but are not equivalent. For the particular case of L as the measure of impurity of the system, it was shown in Refs. [50] that Jacobs' protocol described in Ref. [47] is optimal for control goal I while the WR protocol in Ref. [49] is optimal for control goal II.

7.2.2 Proving optimality of a protocol

Before we begin the main matter, we will present a derivation of the Bellman equation using dynamical programming, which will be used to prove global optimality of a protocol in the following sections. This is based on material on in Ref. [95].

We first start with some definitions for Markov Processes. Let $\mathcal{T} = [t_0, t_1]$ be a finite time interval, and let Φ be a real-valued function on $\mathcal{T} \times \Sigma$, where Σ is the set of all possible state values. Then, define the backward evolution operator as the linear operator A *i.e.*

$$A\Phi(t,x) = \lim_{h\to 0^+} \frac{1}{h}\left\{E[\Phi(t+h, x(t+h))|t, x(t)] - \Phi(t,x)\right\}. \tag{7.6}$$

Let the space of functions $\mathcal{D}(A)$ be defined such that $A\Phi$ exists for each $\Phi \in \mathcal{D}(A)$, and the following properties hold:

- Φ, $\partial_t\Phi$ and $A\Phi$ are continuous on $\mathcal{T} \times \Sigma$.
- Both $E[\Phi(s, x(s))|t, x(t)]$ and $E\left[\int_t^s A\Phi(r, x(r))\, dr|t, x(t)\right]$ are bounded for $t < s$, $t, s \in \mathcal{T}$.
- Dynkin's formula:

$$E[\Phi(s, x(s))|t, x(t)] - \Phi(t,x) = E\left[\int_t^s A\Phi(r, x(r))\, dr|t, x(t)\right], \tag{7.7}$$

  holds for $t < s$.

In both control goals, it is always possible to specify the problem as finding the control function $u(t)$ to minimize a cost function defined as

$$J_u(t,x) = E\left[\int_t^T L(s, x(s), u(s))ds + \psi(x(T))|t, x(t)\right], \tag{7.8}$$

for some running interval $[t, T]$ where T is some terminal time. $L(s, x(s), u(s))$ is known as the running cost function and $\psi(x(T))$ is the terminal cost function.

The value function V is then defined as the infimum over all allowed control protocols of the cost function, $\mathcal{U}$, *i.e.*

$$V(t, x) = \inf_{u \in \mathcal{U}} J_u(t, x). \tag{7.9}$$

Bellman's principle of dynamic programming can now be derived by first noting that the value function can be defined recursively as

$$V(t, x) = \inf_{u \in \mathcal{U}} \left[\int_t^{t+h} L(s, x(s), u(s)) ds + V(t + h, x_u(t + h)) | t, x(t) \right], \tag{7.10}$$

where $x_u(t + h)$ is the state variable x evolving under the protocol u from t to $t + h$. Then, since Eq. (7.10) is defined as an infimum, we have

$$V(t, x) \leq E \left[\int_t^{t+h} L(s, x(s), u(s)) ds + V(t + h, x_u(t + h)) | t, x(t) \right]. \tag{7.11}$$

Then, dividing by h and taking the limit of $h \to 0^+$, we have

$$0 \leq \lim_{h \to 0^+} \frac{1}{h} E \left[\int_t^{t+h} L(s, x(s), u(s)) ds + V(t + h, x_u(t + h)) - V(t, x) | t, x(t) \right], \tag{7.12}$$

$$\leq L(t, x(t), u(t)) + \lim_{h \to 0^+} \frac{1}{h} E \left[\int_t^{t+h} A^u V(s, x(s)) ds | t, x(t) \right], \tag{7.13}$$

$$\leq L(t, x(t), u(t)) + A^u V(t, x(t)), \tag{7.14}$$

where we have assumed $V \in \mathcal{D}(A)$, and used Dynkin's formula Eq. (7.7) in the second line. Assuming that the infimum of Eq. (7.10) exists, then let $u^*(t)$ be the optimal control policy which obtains the infimum. Then, we must have

$$0 = L(t, x(t), u^*(t)) + A^{u^*} V(t, x(t)). \tag{7.15}$$

Thus, Eqs. (7.14) and (7.15) together make up the Bellman equation for which the optimal control policy must satisfy, and can be stated as

$$0 = \inf_{u \in \mathcal{U}} \{ L(t, x(t), u(t)) + A^u J_u(t, x(t)) \}, \tag{7.16}$$

with the terminal condition $V(T, x) = \psi(x(T))$.

We end this derivation by noting that for a stochastic process governed by the Itô stochastic differential equation

$$dx = a(t, x(t), u(t))dt + b(t, x(t), u(t))dW, \tag{7.17}$$

The evolution operator defined in Eq. (7.6) is

$$A^u\Phi(t,x) = \frac{\partial\Phi}{\partial t} + a(t, x(t), u(t))\frac{\partial\Phi}{\partial x} + \frac{1}{2}b^2(t, x(t), u(t))\frac{\partial^2\Phi}{\partial x^2}. \tag{7.18}$$

In the next section, we will present an intuitive proof of optimality due to Jacobs [47] which does not directly use the dynamical programming equations to prove optimality.

7.3 Jacobs' solution

Jacobs', motivated by previous work with Fuchs in [96], realized that to lead to the fastest increase in purity of a qubit in each measurement step, one needs to measure orthogonal to the current qubit direction in the bloch sphere. Then, given a measurement of the σ_z operator as in Sec. 7.2, implies that the feedback mechanism should always be such that the qubit is in the $x-y$ plane of the bloch sphere to achieve the largest increase in purity in each step. His protocol then sets the control $u(t) \equiv 0\ \forall\, t \in [t_0, t_1]$. We next show the proof of optimality of Jacobs' protocol as given in [47].

7.3.1 Intuitive N-step proof of optimality

The first observation we make of Jacobs' protocol ($u(t) = 0$) is that the stochastic differential equation for L, Eq. (7.4), becomes a deterministic control problem, *i.e.*

$$dL|_{u(t)=0} = -4Ldt. \tag{7.19}$$

Based on this property of the protocol, we restate Jacobs' solution as a theorem, and prove it. Before we restate his proof, we first define *rigorously* what it means to for a protocol to give the fastest increase in the purity of a qubit in each measurement step.

Definition 1 (Local optimality)**.** *Let $L_u(t) \in [0, \frac{1}{2}]$ be the impurity at time t under the protocol u. A protocol u^* is locally optimal at reducing the function $F[L_u(t)]$,*

if $\forall\, u \in [-1, 1]$, *the condition*

$$E(F[L_{u^*}(t+dt)]|L(t)) \leq E(F[L_u(t+dt)]|L(t)), \tag{7.20}$$

is satisfied, where $E[.]$ *denotes an expectation.*

Remark 1. The function $F[.]$ can, of course, be the identity function. For this case, $F[L_u(t)] = L_u(t)$, and Jacobs' protocol, $u(t) \equiv 0$, is locally optimal [96, 47].

Next, we define a function which increments the impurity by an infinitesimal amount under some protocol u.

Definition 2. *Let* $C_u : [0, \frac{1}{2}] \to [0, \frac{1}{2}]$ *denote the, in general stochastic, function that increments the impurity by an infinitesimal amount under the protocol* u*, such that*

$$C_u(L) = L + dL_u, \tag{7.21}$$

and let $\tilde{C} = C_{u=0}$ *be the increment under Jacobs' protocol.*

As previously noted, for $u = 0$, L evolves deterministically, with $dL_{u=0} = -\epsilon L$ where $\epsilon = 4dt$ is a constant. With these definitions, and the fact that $\tilde{C}$ is locally optimal at reducing the impurity L at each time step, Jacobs proves the following:

Theorem 2 (Jacobs [47])**.** *For the problem of minimizing the impurity* L *in some finite time interval* t*, the globally optimal protocol is the repeated application of the protocol* $u = 0$ *at each time step.*

Proof [47]: Since the equation for dL_u is, in general, stochastic, we will denote the possible values of $L_u(t+dt)$, given $L(t) = L$, by $\{{}_uL_i\}$, where value i occurs with probability p_i. Although the SDE (7.4) implies that the index i should be continuous, we will follow Jacobs in representing it by a discrete variable. Then, starting from the definition of local optimality, $\forall u \in [-1, 1]$,

$$\tilde{C}(L) = E[\tilde{C}(L)] \leq E[C_u(L)] = \sum_i p_i\, {}_uL_i, \tag{7.22}$$

where we have used the fact that $\tilde{C}$ is deterministic. Applying the optimal protocol $\tilde{C}$, this time to the left-most and right-most expressions, and using the fact that $\tilde{C}$ is a monotonic map, we have,

$$\tilde{C}^{(2)}(L) \leq \tilde{C}(\sum_i p_i\, {}_uL_i). \tag{7.23}$$

Jacobs then uses the linearity of the function $\tilde{C}$ to write the RHS as

$$\tilde{C}\Big(\sum_i p_{i\,u}L_i\Big) = \sum_i p_i \tilde{C}({}_uL_i). \tag{7.24}$$

Then, using local optimality, we have for all $u' \in [-1, 1]$,

$$\tilde{C}\Big(\sum_i p_{i\,u}L_i\Big) \leq \sum_i p_i E[C_{u'}({}_uL_i)], \tag{7.25}$$

$$= \sum_{i,j} p_i p_{j\ u',u}L_{i,j}. \tag{7.26}$$

This procedure can clearly be repeated to cover the entire running time of the protocol to prove that $\tilde{C}^{(N)}(L)$ is a lower bound on the expected impurity for any N-step control protocol.

Thus, it must be the case that $u(t) \equiv 0$ is a globally optimal protocol in reducing the impurity. □

As can be seen from the proof, Jacobs' protocol is optimal for control goal I, using the impurity L as the measure of impurity.

7.4 Wiseman-Ralph's variation on stochastic purification

In [49], Wiseman and Ralph considered stochastic purification from a different perspective. What was showed in Ref. [49] was that starting from a qubit in the maximally mixed state, the continuous measurement of the qubit in the z direction takes a shorter mean time to achieve a given purity compared to Jacobs' protocol, and in the limit of small impurity, can be shown to be twice as fast.

In this section, we show the derivation of the mean time solution, and its subsequent proof of optimality found in Ref. [50].

7.4.1 Solution through the Fokker-Planck equation

The WR protocol is as follows, first apply a unitary to the qubit such that it lies on the z-axis of the bloch sphere. No other controls are applied after this step. Since the qubit is continuously measured in the z basis, the qubit will remain on the z-axis for the rest of the evolution. We then can set $z = z_0$ and $x = 0$ at $t = t_0$. Then, the SDE for the z component of the bloch vector, Eq. (7.3) becomes

$$dz = 2(1 - z^2)dW. \tag{7.27}$$

The Fokker-Planck equation is a dynamical equation for the conditional probability density of z, $p(z,t|z_0,t_0)$, and is derived in Appendix C.1.

With this derivation, we can read off the Fokker-Planck equation for $p(z,t|z_0,t_0) = \varrho$ corresponding to the SDE (7.27),

$$\partial_t \varrho = 2\partial_z^2[(1-z^2)^2\varrho], \tag{7.28}$$

with initial condition $p(z,t_0|z_0,t_0) = \delta(z-z_0)$. We seek to solve for the mean time for which the impurity, $L = 1-z^2$ reaches $L \leq 1-Z^2$, given an initial value of z_0. This means specifying absorbing boundary conditions for the probability distribution at $|z| = Z$, or $p(z,t|z_0,t_0) = 0$ for $|z| = Z$. Let $G(t|z_0)$ be the probability that at time t the purity has not yet or just reached Z, given $z(t_0) = z_0$. Then we have

$$G(t|z_0,Z) = \int_{-Z}^{Z} dz\, p(z,t|z_0,t_0). \tag{7.29}$$

Let T be the random variable representing the time at which the impurity first reaches Z. This means that,

$$P(T \geq t) = G(t|z_0,Z), \tag{7.30}$$

$$\implies \int_t^\infty dt' p(T=t') = G(t|z_0,Z), \tag{7.31}$$

$$\implies p(T=t') = -\partial_t G(t|z_0,Z), \tag{7.32}$$

where we have let $p(T=t')$ be the probability of $T=t'$. With this, we can then write the mean T as

$$\langle T(z_0,Z)\rangle = \int_{t_0}^\infty dt\, t\, p(T=t) \tag{7.33}$$

$$= -\int_{t_0}^\infty dt\, t\, \partial_t G(t|z_0,Z) \tag{7.34}$$

$$= -tG(t|z_0,Z)\Big|_{t=0}^{t=\infty} + \int_{t_0}^\infty dt\, G(t|z_0,Z) \tag{7.35}$$

$$= \int_{t_0}^\infty dt\, G(t|z_0,Z). \tag{7.36}$$

Using the backward Fokker-Planck equation (see Appendix C.1 for details), we note that $G(t|z_0)$ satisfies the differential equation

$$\partial_t G(t|z_0,Z) = 2(1-z_0^2)^2\partial_{z_0}^2 G(t|z_0,Z). \tag{7.37}$$

Then, integrating this from $t \in [0, \infty)$ we get,

$$\int_{t_0}^{\infty} dt\, \partial_t G(t|z_0, Z) = 2(1 - z_0^2)^2 \partial_{z_0}^2 \langle T(z_0, Z)\rangle\,, \tag{7.38}$$

$$G(\infty|z_0, Z) - G(t_0|z_0, Z) = 2(1 - z_0^2)^2 \partial_{z_0}^2 \langle T(z_0, Z)\rangle\,, \tag{7.39}$$

$$-1 = 2(1 - z_0^2)^2 \partial_{z_0}^2 \langle T(z_0, Z)\rangle\,. \tag{7.40}$$

The solution to the above problem with boundary condition $T(\pm Z, Z) = 0$ is

$$\langle T(z_0, Z)\rangle = \frac{1}{4}(Z\text{arctanh}Z - z_0\text{arctanh}z_0). \tag{7.41}$$

With this solution in hand, we proceed to prove that this protocol is globally optimal at minimizing the mean time to achieve a given purity.

7.4.2 Proof of optimality

As in Ref. [50], we first derive the Bellman equation for this control problem, and then proceed to show that the WR protocol is optimal. The cost function of running the protocol u can be written as

$$J[u, t, L] = E[\int_t^{\tau^u} dt|L_t^u = L], \tag{7.42}$$

where τ^u is the mean time of reaching the threshold Z, under the protocol u, and the cost function has support $t \leq \tau^u$ and $L \geq 1 - Z^2$. This cost function can be simply interpreted as the time left for the protocol to achieve the desired threshold given some an impurity L at time t. The optimal control then satisfies

$$V(t, L) = \inf_u J[u, t, L]. \tag{7.43}$$

Using the general results of Sec. 7.2.2, this leads to the following Bellman equation,

$$-\frac{\partial V}{\partial t} = 1 - 4L\frac{\partial V}{\partial L} + \inf_u u^2 \mathcal{D}V, \tag{7.44}$$

$$\mathcal{D}V = 4L(1 - L)\left(2L\frac{\partial^2 V}{\partial L^2} + \frac{\partial V}{\partial L}\right). \tag{7.45}$$

Under the WR protocol, the mean time to achieve the target impurity Z^2 given some starting impurity z_0^2, is given by Eq. (7.41). This means that the cost function under this protocol is

$$W(t, L) = \left\langle T(L, Z^2)\right\rangle = \frac{1}{4}(\gamma(Z) - \gamma(\sqrt{1 - L})), \tag{7.46}$$

where $\gamma(s) = s\,\mathrm{arctanh}(s)$. Furthermore,

$$\partial_L \gamma(\sqrt{1-L}) = \frac{-1}{2L} - \frac{1}{2\sqrt{1-L}}\mathrm{arctanh}\sqrt{1-L}, \quad \text{and} \tag{7.47}$$

$$\partial_L^2 \gamma(\sqrt{1-L}) = \frac{1}{2L^2} + \frac{1}{4L(1-L)} - \frac{1}{4(1-L)^{3/2}}\mathrm{arctanh}\sqrt{1-L}. \tag{7.48}$$

With these, one can verify that,

$$\mathcal{D}W \leq 0, \tag{7.49}$$

for $L \in [0, \frac{1}{2}]$. It is then an algebraic exercise to show that

$$4L\frac{\partial W}{\partial L} - \mathcal{D}W = 1. \tag{7.50}$$

Since the constant control $u = 1$ is an admissible control, and $W(t, L)$ satisfies the equation

$$-\frac{\partial W}{\partial t} = 1 - 4L\frac{\partial W}{\partial L} + \mathcal{D}W, \tag{7.51}$$

since $\frac{\partial W}{\partial t} = 0$, $u = 1$ is the globally optimal protocol for this control problem.

7.5 Considering a family of purity measures

We now switch back to control goal I and reconsider Jacobs' problem of finding the shortest time to obtain a given cost function. We would like to consider a more general measure of purity, other than the forms considered in [47, 49, 50]. Further, instead of simply applying the full rigor of the Bellman equation, we first generalize the intuitive proof of optimality introduced in Sec. 7.3.1 to other cost functions, and analyze the results. We then go on to show that the conditions of this intuitive proof do not capture the entire parameter range for which Jacobs' protocol is globally optimal.

7.5.1 Rényi entropies

In the remainder of this section, we will be considering the problem of minimizing the Rényi entropies of order α

$$\mathcal{S}_\alpha(\rho) = \frac{1}{1-\alpha}\ln \mathrm{Tr}(\rho^\alpha), \tag{7.52}$$

given some initial impurity $L(t_0) = L_0$, and a terminal time $T = t - t_0$. The Rényi entropies are defined for $\alpha \geq 0$ with range $0 \leq S_\alpha(\rho) \leq \log \mathrm{rank}(\rho)$, and is zero only

for pure states. The consideration of Rényi entropies can be physically motivated by noticing that the Rényi entropy of order q, $\mathcal{S}_q$ is the q^{-1} derivative of the Gibbs Free energy of the system [97]. The von-Neumann entropy is a special case of the Rényi entropy when the order approaches 1, which is well-known to be negative the derivative of the Free energy with respect to temperature. When $\alpha = 2$ the Rényi entropy, often called the "Collision entropy", is minus the logarithm of the purity: $-\ln(P) = -\ln(1-L)$. In addition to being related to the free energy of a system, the Rényi entropies also bound the transformation complexity of quantum states [98].

7.5.2 Proving optimality intuitively

In this section, we prove the optimality of Jacobs' protocol using a suitable generalization of the proof given in Sec. 7.3.1. We notice that Jacobs' proof allows a generalization to convex increment functions, which was not required in Reference [47] as the functions considered were linear. To do this, we first generalize a few necessary functions:

Definition 3 (General cost function)**.** *Let $F[L]$ be a general cost function defined on $\mathcal{F} \subset \mathbb{R}$ with support $[0, \frac{1}{2}]$.*

Definition 4 (General increment)**.** *Let $C_u : \mathcal{F} \to \mathcal{F}$ be the general increment function such that it takes as argument a general cost function $F(L)$, and increments the value of L under the protocol u, i.e.*

$$C_u(F(L)) = F(L + dL_u). \tag{7.53}$$

And once again, let $\tilde{C} = C_{u=0}$ be the increment under Jacobs' protocol.

With these definitions, we now state and prove the following theorem.

Theorem 3. *The protocol $u = 0$ is the globally optimal control protocol for the minimization of a cost function $F(L)$, if $F(L)$ satisfies the following conditions:*

$$\mathcal{D}[F(L)] \geq 0, \tag{7.54}$$

where the operator $\mathcal{D}[]$ is defined as

$$\mathcal{D}[F(L)] \equiv 4L(1-2L)\Big(F'(L) + 2LF''(L)\Big), \tag{7.55}$$

with $F'(L) = \frac{\partial F}{\partial L}$, *and*

$$L\frac{F''(L)}{F'(L)}F''(L) - LF'''(L) - F''(L) \geq 0, \tag{7.56}$$

if the function $\tilde{C}[F]$ *is twice differentiable* ($\mathcal{C}^2$) *in* $\mathcal{F}$, *and the inverse of* $F(L)$ *exists.*

We prove Theorem 3 by first proving the following Lemma.

Lemma 2. *The protocol* $u = 0$ *is the globally optimal control protocol for the minimization of a cost function* $F(L)$, *if the increment function* $\tilde{C}[F]$ *satisfies local optimality*

$$E[\tilde{C}(F)] \leq E[C_u(F)], \tag{7.57}$$

and is a convex function of F, *i.e.*

$$\tilde{C}(\alpha F_1 + (1-\alpha)F_2) \leq \alpha\tilde{C}(F_1) + (1-\alpha)\tilde{C}(F_2), \tag{7.58}$$

for any admissible $F_1, F_2 \in \mathcal{F}$ *and* $\alpha \in [0,1]$, *such that* $\alpha F_1 + (1-\alpha)F_2 \in \mathcal{F}$.

Proof. The proof of this Lemma is almost identical to the proof of Theorem 2. Using the condition that $\tilde{C}$ satisfies local optimality for the cost function F, and the fact that the protocol $u = 0$ is deterministic, we have

$$\tilde{C}[F] \leq E[C_u(F)] = \sum_i p_{i\,u}F_i, \tag{7.59}$$

where once again we let F be a discrete variable (although our proof can be generalized to continuous variables). As before, we wish to apply $\tilde{C}$ to both the right-most and left expressions. Again, since $\tilde{C}$ is a deterministic protocol which locally minimizes F, it must also be a monotonic map. Then,

$$\tilde{C}^2[F] \leq \tilde{C}\left(\sum_i p_{i\,u}F_i\right). \tag{7.60}$$

Since $\tilde{C}$ is convex, by Jensen's inequality, we have

$$\tilde{C}\left(\sum_i p_{i\,u}F_i\right) \leq \sum_i p_i\,\tilde{C}({}_uF_i), \tag{7.61}$$

$$\leq \sum_i p_i E[C_u({}_uF_i)], \tag{7.62}$$

$$= \sum_{i,j} p_i p_{j\,u,u}F_{i,j}. \tag{7.63}$$

This can then be repeated to cover the running time of the protocol. Thus, $\tilde{C}^N[F]$ is the lower bound on the expected $F(L)$ for any N-step protocol. □

With Lemma 2 in hand, we now prove Theorem 3.

Proof of Theorem 3: The proof can be broken down into first showing that Eq. (7.54) implies local optimality of $\tilde{C}$, and then showing that Eq. (7.56) implies convexity of $\tilde{C}$. Local optimality of a protocol u^* according to Definition 1 implies also that

$$E[dF(L)|u^*, L] \leq E[dF(L)|u, L]. \tag{7.64}$$

For a function $F(L)$ which is $\mathcal{C}^2$ in L, it can be shown using Eq. (7.4) and Itô calculus that

$$E[dF] = E\Big[-4L\frac{dF}{dL}dt + u^2\mathcal{D}[F]dt\Big], \tag{7.65}$$

$$\mathcal{D}[F] \equiv 4L(1-2L)\Big(\frac{dF}{dL} + 2L\frac{d^2F}{dL^2}\Big). \tag{7.66}$$

Since the inequality in Eq. (7.64) becomes an equality for the locally optimal protocol, we need to solve the following minimization problem,

$$\min_u E[dF] = -4L\frac{dF}{dL} + \min_u\Big\{u^2\mathcal{D}[F]\Big\}, \tag{7.67}$$

$$= -4L\frac{dF}{dL} + \min\Big\{0, \mathcal{D}[F]\Big\}, \tag{7.68}$$

which evidently reduces to finding the sign of the function $\mathcal{D}[F]$, since $u \in [-1, 1]$. Then, $\mathcal{D}[F] \geq 0$ implies that Jacobs' protocol, $u = 0$, is the locally optimal protocol; $\mathcal{D}[F] \leq 0$ implies that the Wiseman-Ralph (WR) protocol [49], $u = 1$, is the locally optimal protocol. Thus, Eq. (7.54) implies local optimality of the protocol $u = 0$. Since we assume that the function $\tilde{C}$ is $\mathcal{C}^2$ in $\mathcal{F}$, convexity of $\tilde{C}$ also implies a positive second derivative, *i.e.*

$$\frac{d^2\tilde{C}[F]}{dF^2} \geq 0. \tag{7.69}$$

Now, the increment function $\tilde{C}$ can be written explicitly as

$$\tilde{C}(F(L)) = F(L + dL_{u=0}), \tag{7.70}$$

$$= F(qL), \tag{7.71}$$

where q a constant and in the second line we have used the fact that Jacobs' protocol is linear, *i.e.* $\tilde{C} = qL$. Letting $f = F(L)$, Eq. (7.71) can be written as

$$\tilde{C}(f) = F(qF^{-1}(f)). \tag{7.72}$$

With this, the second derivative becomes

$$\frac{d^2\tilde{C}(f)}{df^2} = \frac{q}{(F'(L))^2}\{qF''(qL) - F'(qL)\frac{F''(L)}{F'(L)}\}, \tag{7.73}$$

where we have used the abbreviations $L = F^{-1}(f)$. Since the increment function $\tilde{C}$ is defined only for infinitesimal time periods, we must have q less than, but very close to, unity. We thus let $q = 1 - \epsilon$ with $0 < \epsilon \ll 1$, and expand Eq. (7.73) to first order in ϵ, which gives

$$\frac{d^2\tilde{C}(f)}{df^2} \approx \frac{\epsilon}{(F'(L))^2}\left\{L\frac{F''(L)}{F'(L)}F''(L) - LF'''(L) - F''(L)\right\}. \tag{7.74}$$

Since the terms outside the curly braces are positive, we need only check for the positivity of the expression within the curly braces. The expression within the curly braces is precisely Eq. (7.56). Thus, Eq. (7.56) implies convexity of $\tilde{C}$.

Since, Eq. (7.54) and Eq. (7.56) imply local optimality and convexity of $\tilde{C}$ repectively, and Lemma 2 states that local optimality and convexity of $\tilde{C}$ implies global optimality, Equations (7.54) and (7.56) implies global optimality. □

Application to Rényi entropies

For our problem, the Rényi entropy can be parametrized by L and α

$$\mathcal{S}_\alpha(L) = \frac{1}{1-\alpha}\ln\left[\left(\frac{1+\sqrt{1-2L}}{2}\right)^\alpha + \left(\frac{1-\sqrt{1-2L}}{2}\right)^\alpha\right]. \tag{7.75}$$

Since the impurity $L \in [0, \frac{1}{2}]$, the above function has a well defined inverse and can be shown to be smooth in $L \in [0, \frac{1}{2}]$. Theorem 3 then states that Jacobs' protocol is globally optimal for the cost function $S_\alpha(L)$ if the conditions,

C1. Local optimality, *i.e.* $\mathcal{D}[\mathcal{S}_\alpha(L)] \geq 0$, and

C2. Convexity, *i.e.* $L\frac{\mathcal{S}''_\alpha(L)}{\mathcal{S}'_\alpha(L)}\mathcal{S}''_\alpha(L) - L\mathcal{S}'''_\alpha(L) - \mathcal{S}''_\alpha(L) \geq 0$,

are satisfied. We proceed to test both conditions numerically over the range $\alpha \in [0, 50]$, and find that for the range of α considered, convexity is satisfied for $\alpha < 1.103$ for $L = \frac{1}{2}$; local optimality is satisfied for $\alpha \in [0.823, 50]$ for $L = \frac{1}{2}$.

Furthermore, since the Rényi entropy is defined for all α, we analytically show that the min-entropy

$$\lim_{\alpha\to\infty} \mathcal{S}_\alpha \to -\ln\left(\frac{1+\sqrt{1-2L}}{2}\right), \tag{7.76}$$

also satisfies local optimality. Since it is not possible to numerically test all $\alpha > 50$, we conjecture that since $\mathcal{S}_\alpha$ for $\alpha \in [0.823, 50]\cup\{\infty\}$ satisfies local optimality, all $\mathcal{S}_\alpha$ for $\alpha \in [0.823, \infty)$ satisfies local optimality as well. These results are summarized in Fig. 7.1. The light red region is where convexity, *i.e.* condition C2 is satisfied; the light blue region is where local optimality, *i.e.* condition C1 is satisfied, and the dark blue region is when both conditions are simultaneously satisfied. It is

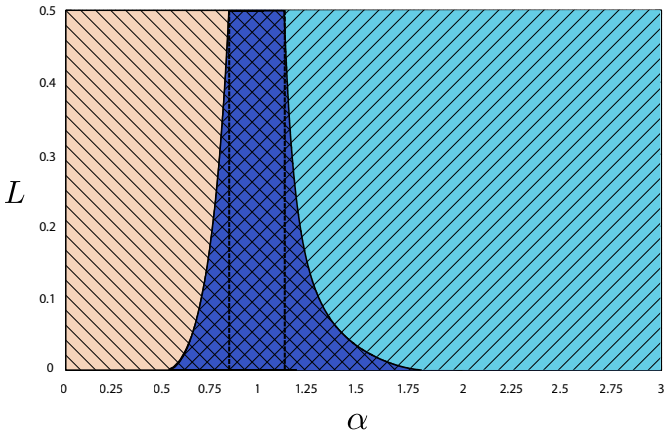

Figure 7.1: The dark blue shaded region is where we have both convexity and local optimality. The light red region is where only convexity is satisfied, and light blue is where only local optimality is satisfied. The x-axis of the graph is the order of the Rényi entropy, and the y-axis is the impurity L. Then, the region where Jacobs' proof of optimality holds is the region denoted by vertical dashed lines, $\alpha \in [0.823, 1.103]$, since the proof requires that local optimality and convexity be satisfied for all $L \in [0, \frac{1}{2}]$.

worth noting that Jacobs' proof only holds for $\alpha \in [0.823, 1.103]$, which is a subset of the dark blue region where both local optimality and convexity are satisfied. This can be seen in both Eqs. (7.24) and (7.25), where a non-optimal protocol u, may probabilistically increment the impurity L_i towards $L = \frac{1}{2}$. Thus, Jacobs' proof holds only when both conditions C1 and C2 hold for $L \in [0, \frac{1}{2}]$. In the next section, we will treat the problem of global optimality using Bellman's principle of dynamic programming.

7.5.3 Optimality via dynamic programming

In this section, we will derive the Bellman equation for this control problem, and show that for Jacobs' problem, local optimality is equivalent to global optimality.

Let

$$J_u(L,t) = E(F[L_u(T)]|L(t) = L) \tag{7.77}$$

be the expected cost function at a final time T, given an initial impurity L at time $t \leq T$, with evolution governed by protocol u. The globally optimal protocol u^* is then defined as the protocol which minimizes the above cost function, and satisfies

$$V(L,t) = \inf_u J_u(L,t). \tag{7.78}$$

Again using the results of Sec. 7.2.2, we arrive at the following Bellman equation,

$$\frac{\partial V(L,t)}{\partial t} - 4L\frac{\partial V(L,t)}{\partial L} + \min_u \Big(u^2 \tilde{\mathcal{D}}[V(L,t)]\Big) = 0, \tag{7.79}$$

$$\tilde{\mathcal{D}}[V] = 4L(1-L)\Big[\frac{\partial V}{\partial L} + 2L\frac{\partial^2 V}{\partial L^2}\Big], \tag{7.80}$$

where we have used the SDE Eq. (7.4). This minimization problem is equivalent to,

$$\frac{\partial V(L,t)}{\partial t} - 4L\frac{\partial V(L,t)}{\partial L} + \min\{0, \tilde{\mathcal{D}}[V(L,t)]\} = 0, \tag{7.81}$$

since $u \in [-1,1]$. In the above equation, we are again interested in finding the sign of a function that looks very similar to Eq. (7.54). However, it must be noted that in Eq. (7.81), the derivatives are with respect to the initial condition $L(t)$, and not the "local" parameters $L(t)$ as in Eq. (7.54). However, as we will show below, for Jacobs' protocol, local optimality everywhere is a necessary and sufficient condition for global optimality.

7.6 Global optimality iff local optimality in some cases

Let us consider a more general class of control problems with the following SDE for the controlled stochastic variable l:

$$dl = -k\,l\Big([1-\alpha(u,l,t)]\gamma(t)dt + \beta(u,l,t)\sqrt{\gamma(t)}dW\Big), \tag{7.82}$$

where u is the control parameter. We impose the following constraints on the functions $\gamma(t), \alpha(u,l,t)$, $\beta(u,l,t)$ and the constant k:

1. $k, \gamma, \alpha > 0$ for their respective domains.
2. $\alpha = \beta^2 \; \forall \, u, l, t$.
3. $\exists$ some $\tilde{u}$ such that $\beta(\tilde{u}, l, t) = 0 \; \forall \, l, t$.

With these, we now proceed by stating and proving the following theorem:

Theorem 4. *For the class of control problems satisfying the SDE (7.82), where k, γ, α and β satisfy the constraints (1-3), local optimality and global optimality are equivalent for the protocol $\tilde{u}$.*

Proof. From the SDE (7.82), it can be shown using Itô calculus that the function $F(l)$ obeys

$$E[dF_u] = k\, E\left[-\gamma l \frac{dF}{dl} + \gamma l \alpha \frac{dF}{dl} + \gamma l^2 \frac{\beta^2}{2} \frac{d^2F}{dl^2}\right] dt \tag{7.83}$$

$$= k\, E\left[-\gamma l \frac{dF}{dl} + \gamma l \alpha \left(\frac{dF}{dl} + \frac{l}{2} \frac{d^2F}{dl^2}\right)\right] dt, \tag{7.84}$$

where in the second line, we have used condition (2). Then, for a protocol u^* to be locally optimal, it must satisfy

$$E[dF_{u^*}] = \inf_u E[dF_u]. \tag{7.85}$$

In particular, for the protocol $\tilde{u}$ to be locally optimal, we must have

$$\frac{dF}{dl} + \frac{l}{2} \frac{d^2F}{dl^2} \geq 0, \tag{7.86}$$

which follows from applying the condition of positivity (condition (1)) in Eq. (7.84). We now let $\tilde{u}$ be a candidate optimal strategy and show the condition for $\tilde{u}$ to be the globally optimal strategy. Firstly, we note that the protocol $\tilde{u}$ is deterministic, since both $\beta(\tilde{u}, l, t)$ and $\alpha(\tilde{u}, l, t)$ vanish in Eq. (7.82). Then, the variable $l_{\tilde{u}}$ satisfies

$$dl_{\tilde{u}} = -k\gamma(t) l_{\tilde{u}} dt. \tag{7.87}$$

Solving the above equation using the initial conditions $l(t_0) = l_0$, we get

$$l_{\tilde{u}}(t) = l_0 e^{-k \int_{t_0}^{t} \gamma(t')dt'}. \tag{7.88}$$

Next, using the procedure outlined in the preceding section, we can write down the Bellman equation for global optimality in this problem;

$$\frac{\partial V}{\partial t_0} - \gamma_0 l_0 \frac{\partial V}{\partial l_0} + \inf_u \left(\gamma_0 l_0 \alpha_0 \left[\frac{\partial V}{\partial l_0} + \frac{l_0}{2} \frac{\partial^2 V}{\partial {l_0}^2} \right] \right) = 0, \tag{7.89}$$

where we have abbreviated $\alpha_0 = \alpha(u, l_0, t_0)$ and $\gamma_0 = \gamma(t_0)$, and have explicitly denoted the partial derivatives as with respect to the initial coordinates l_0 and t_0. Since $\tilde{u}$ is deterministic as previously noted, $V(l_0, t_0) = E[F(l)|l(t_0) = l_0] = F(l(t, l_0, t_0))$. We then have the relations

$$\frac{\partial V}{\partial t_0} = \frac{dF}{dl} \frac{\partial l}{\partial t_0}, \tag{7.90}$$

$$\frac{\partial V}{\partial l_0} = \frac{dF}{dl} \frac{\partial l}{\partial l_0}, \tag{7.91}$$

and so,

$$\frac{\partial V}{\partial t_0} - \gamma_0 l_0 \frac{\partial V}{\partial l_0} = \frac{dF}{dl} \left(\frac{\partial l}{\partial t_0} - \gamma_0 l_0 \frac{\partial l}{\partial l_0} \right), \tag{7.92}$$

which is evidently equal to 0, given Eq. (7.88). Then, the condition for $\tilde{u}$ to be the globally optimal protocol is

$$\frac{\partial V}{\partial l_0} + \frac{l_0}{2} \frac{\partial^2 V}{\partial {l_0}^2} \geq 0, \tag{7.93}$$

since if Eq. (7.93) were not satisfied, the infimum would not give $\alpha_0 = 0$. Using the relations (7.90) and (7.91), Eq. (7.93) becomes

$$e^{-k \int_{t_0}^{t} \gamma(t') dt'} \left(\frac{dF}{dl} + \frac{l}{2} \frac{d^2 F}{dl^2} \right) \geq 0, \tag{7.94}$$

$$\frac{dF}{dl} + \frac{l}{2} \frac{d^2 F}{dl^2} \geq 0, \tag{7.95}$$

which is evidently the same condition as Eq. (7.86). Thus, local optimality and global optimality are equivalent conditions for the protocol $\tilde{u}$. □

For our original problem, we have $k = 4$, $\gamma = 1$, $\alpha = u^2(1 - 2L)$ and $\beta = u\sqrt{1 - 2L}$, which can be easily verified to satisfy the constraints (1-3). Also, the protocol $\tilde{u}$ is $u = 0$, which is Jacobs' protocol. Thus, Jacobs' protocol is globally optimal at minimizing the Rényi entropy of order $\alpha > 0.823 \; \forall \, L, t$.

7.7 The curious case of the WR protocol

In this section, we now focus on the region where $\alpha < 0.5$. As evident from Fig. 7.1, the protocol $u^2 = 1$ is locally optimal $\forall\, L \in [0, \frac{1}{2}]$ and $\alpha < 0.5$. However, we were not able to show that it does not satisfy the Bellman equation.

7.7.1 Linear trajectory solution

For $u^2 = 1$, the protocol is no longer deterministic, and we require explicit solutions to Eq. (7.4). We treat this problem using linear quantum trajectory theory [99], which allow one to solve the generally non-linear stochastic differential equations in special cases.

Since the WR protocol is to first rotate the qubit to the z-axis on the bloch sphere, and then performing the continuous measurement on the qubit in the z direction, we have $x(t) = 0\ \forall\, t$. Furthermore, no further hamiltonian controls are applied to the system. With these considerations, the mean z component of the qubit bloch vector after some measurement time τ is

$$\tilde{z}(\tau, z_0) = \frac{z_0 \cosh(2w) + \sinh(2w)}{\cosh(2w) + z_0 \sinh(2w)}, \tag{7.96}$$

where z_0 is the initial value of the z component just after the initial rotation of the bloch vector to the z axis, and the random variable w has probability distribution

$$dp_w(\tau) = (\cosh(2w) + z_0 \sinh(2w)) \frac{1}{\sqrt{2\pi\tau}} e^{-\frac{w^2}{2\tau}} e^{-2\tau} dw. \tag{7.97}$$

Since the expectation of any function of the stochastic variable z can be expressed as

$$E(F(z(t))|z_0, t_0) = \int_{-\infty}^{\infty} F(\tilde{z}(t - t_0, z_0)) dp_w(t - t_0), \tag{7.98}$$

the expected Rényi entropy of order α, given $L(t_0) = L_0$ is

$$E(\mathcal{S}_\alpha(t)|L_0, t_0) = \int_{-\infty}^{\infty} \mathcal{S}_\alpha(L_0, w) \rho(w, L_0, t - t_0)\, dw, \tag{7.99}$$

where,

$$\mathcal{S}_\alpha(L_0, w) = \frac{1}{1-\alpha} \ln \left[\left(\frac{1 + z(w, L_0)}{2} \right)^\alpha + \left(\frac{1 - z(w, L_0)}{2} \right)^\alpha \right], \tag{7.100}$$

$$z(w, L_0) = \frac{\sqrt{1 - 2L_0} \cosh(2w) + \sinh(2w)}{\cosh(2w) + \sqrt{1 - 2L_0} \sinh(2w)}, \tag{7.101}$$

and the distribution ρ is,

$$\rho(w, L_0, \tau) = \Big(\cosh(2w) + \sqrt{1 - 2L_0}\sinh(2w)\Big)\frac{e^{-w^2/(2\tau)}}{\sqrt{2\pi\tau}}e^{-2\tau}. \tag{7.102}$$

7.7.2 Failure to prove optimality

Using the above equations with $W(L_0, t_0) = E(\mathcal{S}_\alpha(t)|L_0, t_0)$, we numerically showed that for $\alpha < 0.5$,

$$\tilde{\mathcal{D}}[W] < 0 \qquad \forall\, L \text{ and } t. \tag{7.103}$$

However, using $W(L_0, t_0)$ given by Eq. (7.99), we numerically verify that

$$\frac{\partial W(L_0, t_0)}{\partial t_0} - 4L_0\frac{\partial W(L_0, t_0)}{\partial L_0} + \tilde{\mathcal{D}}[W(L_0, t_0)] \neq 0, \qquad \forall\, L \text{ and } t. \tag{7.104}$$

This null result points to one of two scenarios: either the optimal control does not exist, or that the optimal control exists, and the WR protocol is not optimal.

Understanding the process of verification

In the previous section, we have shown numerically that the protocol $u(t) = 1$ $\forall t \in [t_0, T]$ does not satisfy the Bellman equation with this particular cost function.

This null result can be interpreted to be a statement that either the WR protocol is *not* the globally optimal protocol and another protocol is the globally optimal one, or that the control protocol $u^*(t)$, which satisfies the infimum over the set of admissible controls does not exist, and thus the pair of functions $(V(L, t), u^*(t))$ which satisfies the Bellman equation does not exist.

As we have set up the problem, the set of admissible control functions can be defined simply as

$$\mathcal{U} = \{u(t) : [t_0, T] \to [0, 1]\}, \tag{7.105}$$

which is the set of all functions which map the time interval $[t_0, T]$ to $[0, 1]$. This lack of additional constraints leads us to conjecture that this set of functions is not compact, and thus the infimum over the set of admissible controls might not exist. We are thus lead to the conjecture that the globally optimal protocol for minimization of the Rényi entropy of order $\alpha < 0.5$ does not exist.

CHAPTER 8

CONCLUSION AND OUTLOOK

This concluding chapter serves as a summary for the work performed in this thesis and hints at possible future analysis regarding each chapter.

In Chapter 2, we have presented an elegant formalism to treat open quantum systems. This formalism allows one to specify the statistics of the input bath fields accurately, and in principle allows one to solve for the output fields once the inputs are specified. Although solutions to general systems are usually not possible, for a linear system approximation as we have considered, we are able to solve completely the open system. Furthermore, it gives a systematic treatment of possible system losses and decoherence processes which is especially useful in the treatment of state preparation. We also note that in section Sec. 2.3, we have given an approach complimentary to the one found in Ref. [60]. The present approach allows one to determine the output pulse statistics given the input pulse statistics and is a very powerful approach, worthy of further investigation.

In Chapter 3, we detailed possible measurement scenarios for performing a Bell test. We presented the atom-light entangled state which is able to violate the CHSH inequality for the given measurement scenarios. We also presented our optimization methodology, which allowed us to state and prove Theorem 1, which says that the state 3.7, together with the one-photocounting measurement scenario of Sec. 3.5 implies that the violation of the CHSH inequality is always possible for perfect transmission, regardless of detector efficiency. What is interesting here is that in Ref. [58], a similar result was proven, but for a different state. However, it should be noted that in both the case of Ref. [58] and in theorem 1, we have the number of photons in the state tending to infinity to achieve a violation of the CHSH inequality. This seemingly points to the possibility that in the measurement scenario of Sec. 3.5, there are an infinite class of states which violate the CHSH

inequality for arbitrarily small photodetection efficiency.

Next, in Chapter 4, we present our proposed state production formalism. We showed a preliminary calculation explaining the need to displace the field in a particular measurement scenario. We then detail our methodology of the problem which builds on the work presented in Chapter 2, showing the steps to arrive at the final state production visibility, including the treatment of possible losses.

Then, in Chapter 5, we showed that the state production protocol we proposed in Chapter 4 can be integrated with *existing* optical setups to produce the desired state to a high fidelity. We next showed that the states produced can attain a CHSH violation in the measurement scenario of Sec. 3.5 even for a low photon counting efficiency of 25% with perfect transmission, or a line transmission of 64% with perfect detection efficiency. A somewhat problem of fast and efficient detection of the atomic state still remains, as the atom is inside the optical cavity with limited optical access. This problem however, might be surpassable with larger optical cavities as in Refs. [100] and [101]. This gives a very good outlook for optical cavity setups in eventually performing a loophole-free Bell test with such optical setups.

In principle, one may also consider circuit QED setups. The advantages of such setups are twofold. First, the very fast and efficient qubit state detection, on the order of 10 ns [30] potentially lowers the required propagation distances to laboratory scale distances (10 m or less). Second, in this system, large ratios of coupling constant to cavity decay, g/κ, can be achieved. The drawbacks with current technology are the limited efficiencies of both photodetection and homodyne detection [102] and the requirement to cool the propagation line down to cryogenic temperatures to avoid losses and blackbody radiation effects. The hope is that both these drawbacks, being of technological nature, can be eventually solved in near future experiments.

In Chapter 6, we presented work done in collaboration with the group of Christian Kurtsiefer at CQT. We showed how an effective description of the setup can be derived, and presented a conceptually simple method found in Ref. [90] to obtain observed statistics of the photon pair produced. In this treatment, one notes that it is not possible to derive efficiencies of the four-wave mixing process given the pulse shapes of the pumps, which might be interesting to experimentalists. Although conceptually simple, the full generality of the numerical treatment is, simply put, overwhelming. This then motivates us to try to strike some middle ground between the approximations used and the generality of the treatment, such that more interesting results can be derived. Appendix B is a documentation of ongoing work done by the author in this direction.

Finally, in Chapter 7, I have presented my brief survey of what it means for a protocol to be optimal. We showed the physical model we are considering, and presented results from Refs. [47, 49, 50]. We then generalized the optimality proof in Ref. [47] to be applicable to a larger class of cost functions. Then, using the family of Rényi entropies, we showed that this generalization of the proof does not capture the whole range of parameters for which the protocol of Ref. [47] is optimal. And finally, we showed the confounding case of a protocol being locally optimal for all infinitesimal time intervals throughout the running time of the protocol, but we could not show that it is the globally optimal protocol. These results clearly show that this problem is non-trivial in the sense that intuition might not always point in the right direction. We thus seek to show rigorously, that either the optimal control protocol exist in this problem, and a possible solution to this optimal control problem, or that the optimum does not exist, and then the WR protocol is a good approximation to the optimum protocol, since it is locally optimal everywhere.

APPENDIX A

BELL TESTS ON ENTANGLED COHERENT STATES

In this appendix, we detail the methodology for performing Bell tests on entangled coherent states. We first detail our methodology to compute the outcomes of homodyne measurements on coherent states. Using this methodology, we show how we approach the problem of performing fully homodyne measurements on entangle coherent states. Lastly, we test a particular type of Bell inequality suitable for continuous outcome measurements on a particular class of entangled coherent states, and the one and two photon NOON states.

A.1 Homodyne measurements on coherent state superpositions

We seek to make the measurement

$$\sigma_{\mathcal{X}} = 2\int dx\, |x\rangle\langle x| - \mathbb{1}, \tag{A.1}$$

on the subspace spanned by the vacuum and coherent states $|0\rangle$ and $|\alpha\rangle$ respectively, with the convention that $|x\rangle$ is the eigenstate of $(a+a^\dagger)/\sqrt{2}$. We first derive the wavefunction of the coherent state.

A.1.1 Basic derivations

We start by stating the wavefunction of the n^{th} fock state

$$\langle x|n\rangle = \frac{1}{\sqrt{2^n n!\sqrt{\pi}}} H_n(x) e^{-x^2/2}. \tag{A.2}$$

Then, using

$$|\alpha\rangle = e^{-|\alpha|^2/2} \sum_{n=0}^{\infty} \frac{\alpha^2}{\sqrt{n!}} |n\rangle, \tag{A.3}$$

and the Hermite polynomial generating function [103, 104]

$$e^{-t^2+2tx} = \sum_{n=0}^{\infty} H_n(x) \frac{t^n}{n!}, \tag{A.4}$$

we obtain

$$\langle x|\alpha = ae^{i\phi}\rangle = \psi_\alpha(x) = \frac{1}{\pi^{1/4}} e^{-\frac{1}{2}(x-\sqrt{2}a\cos\phi)^2} e^{i\sqrt{2}a\sin\phi(x-\frac{a\cos\phi}{\sqrt{2}})}, \tag{A.5}$$

where we have denoted $\alpha = ae^{i\phi}$, with $|\alpha| = a$ and $\arg\alpha = \phi$. As an example, we compute the c_1 function from Eq. (3.12). The c_1 function is

$$\begin{aligned} c_1 &= \frac{1}{2}\mathrm{Tr}[(|0\rangle\langle\alpha| + |\alpha\rangle\langle 0|)\sigma_{\mathcal{X}}], && \text{(A.6)} \\ &= \frac{1}{2}\Big[2\int_{-b}^{b} dx\,(\psi_0(x)\psi_\alpha^*(x) + \psi_0^*(x)\psi_\alpha(x)) - 2\langle 0|\alpha\rangle\Big], && \text{(A.7)} \\ &= \frac{2}{\sqrt{\pi}}\int_{-b}^{b} dx\, e^{-x^2}\cos(\sqrt{2}\alpha x) - e^{-\frac{|\alpha|^2}{2}}, && \text{(A.8)} \end{aligned}$$

where we have used the relation

$$\psi_0^*\psi_\alpha(\tilde{x} = x - \frac{a\cos\phi}{\sqrt{2}}) = \frac{1}{\sqrt{\pi}} e^{-\frac{1}{2}a^2\cos^2\phi} e^{-\tilde{x}^2} e^{i\sqrt{2}\tilde{x}a\sin\phi}, \tag{A.9}$$

and the fact that $\arg\alpha = \frac{\pi}{2}$. The above procedure is only for a X quadrature measurement. However, both $|0\rangle$ and $|\alpha\rangle$ are individually symmetric about their means, *i.e.* circularly symmetric in phase space, and a X quadrature measurement can be visualized as taking the projection of the phase space distribution onto the X quadrature; the above procedure allows one to find any homodyne measurement on this subspace, since any homodyne measurement with fixed relative phase with $|\alpha\rangle$ will give the same results up to a trivial sign. Thus, a $\sigma_{\mathcal{X}}$ quadrature measurement on the subspace spanned by $|0\rangle$ and $|ae^{i\phi}\rangle$ is equivalent to a $\sigma_{\mathcal{X}_{e^{i\theta}}}$ on the subspace spanned by $|0\rangle$ and $|ae^{i(\phi+\theta)}\rangle$. We use this observation extensively in this appendix.

A.1.2 A particular binning choice

The form of Eq. (A.9) shows that, other than the binning $[-b, b]$, another natural binning choice is $x \in [\frac{a\cos\phi}{\sqrt{2}}, \infty)$ or simply $\tilde{x} \in [0, \infty)$. This binning corresponds to choosing the mid-point of the two peaks of the projections of the distributions

of $|0\rangle$ and $|\alpha\rangle$, and intuitively would discriminate with equal probability, the $|0\rangle$ state from the $|\alpha\rangle$ state. Thus, it will probably act like the usual σ_z operator for 2 level systems. We show this point explicitly here.

Define

$$\sigma_{x_\phi} = 2\int_0^\infty d\tilde{x}_\phi |x_\phi\rangle\langle x_\phi| - \mathbb{1}, \tag{A.10}$$

as the measurement of the states onto the $x_\phi = (ae^{-i\phi} + a^\dagger e^{i\phi})/\sqrt{2}$ quadrature. Notice that we have used the natural binning $\tilde{x} \in [0, \infty)$. We want the form of the trace of this operator with the following 3 terms, $|0\rangle\langle 0|$, $|\alpha\rangle\langle\alpha|$ and $|\alpha\rangle\langle 0|$. The first 2 are simple, since,

$$\int_{\frac{a\cos\phi}{\sqrt{2}}}^\infty dx|\psi_0(x)|^2 = \frac{1}{\sqrt{\pi}}\int_{\frac{a\cos\phi}{\sqrt{2}}}^\infty dx e^{-x^2} = \frac{1}{2}[1 - \mathrm{erf}(\frac{a\cos\phi}{\sqrt{2}})] \tag{A.11}$$

and similarly,

$$\int_{\frac{a\cos\phi}{\sqrt{2}}}^\infty dx|\psi_\alpha(x)|^2 = \frac{1}{2}[1 - \mathrm{erf}(-\frac{a\cos\phi}{\sqrt{2}})] \tag{A.12}$$

So,

$$\mathrm{Tr}(|0\rangle\langle 0|\sigma_{x_\phi}) = -\mathrm{Tr}(|\alpha\rangle\langle\alpha|\sigma_{x_\phi}) = \mathrm{erf}(\frac{a\cos\phi}{\sqrt{2}}). \tag{A.13}$$

The cross term integral is not as simply, and gives

$$\int_{\frac{a\cos\phi}{\sqrt{2}}}^\infty dx\psi_0^*\psi_\alpha(x) = e^{-\frac{1}{2}a^2\cos^2\phi}\frac{1}{\sqrt{\pi}}\int_0^\infty dx e^{-x^2}e^{i\sqrt{2}xa\sin\phi}. \tag{A.14}$$

This integral can be simplified using the relations,

$$\int_0^\infty dx e^{-x^2}\cos(kx) = \frac{\sqrt{\pi}}{2}e^{-(\frac{k}{2})^2} \tag{A.15}$$

$$\int_0^\infty dx e^{-x^2}\sin(kx) = F(\frac{k}{2}) \tag{A.16}$$

where $F(x)$ is the dawson function defined as,

$$F(x) = e^{-x^2}\int_0^x e^{t^2}dt, \tag{A.17}$$

The integral (A.14) then becomes

$$\frac{1}{2}e^{-\frac{a^2}{2}} + i\frac{1}{\sqrt{\pi}}F(\frac{a\sin\phi}{\sqrt{2}})e^{-\frac{1}{2}a^2\cos^2\phi}. \tag{A.18}$$

With this in hand,

$$\mathrm{Tr}(|\alpha\rangle\langle 0|\,\sigma_{x_\phi}) = i\frac{2}{\sqrt{\pi}}F(\frac{a\sin\phi}{\sqrt{2}})e^{-\frac{1}{2}a^2\cos^2\phi} \tag{A.19}$$

Thus, in the subspace of $|0\rangle$ and $|\alpha\rangle$, the operator σ_{x_ϕ} acts as

$$\sigma_{x_\phi} \sim \mathrm{erf}(\frac{a\cos\phi}{\sqrt{2}})\sigma_z + \frac{2}{\sqrt{\pi}}F(\frac{a\sin\phi}{\sqrt{2}})e^{-\frac{1}{2}a^2\cos^2\phi}\sigma_y. \tag{A.20}$$

with the pauli operators

$$\sigma_z = |0\rangle\langle 0| - |\alpha\rangle\langle\alpha|, \tag{A.21}$$

$$\sigma_y = -i\,|0\rangle\langle\alpha| + i\,|\alpha\rangle\langle 0|\,. \tag{A.22}$$

Additionally, notice that the dawson function (A.17) is an odd function in x. This immediately implies that,

$$\sigma_{x_\phi} + \sigma_{x_{-\phi}} = 2\mathrm{erf}(\frac{a\cos\phi}{\sqrt{2}})\sigma_z, \quad \text{and} \tag{A.23}$$

$$\sigma_{x_\phi} - \sigma_{x_{-\phi}} = 2\frac{2}{\sqrt{\pi}}F(\frac{a\sin\phi}{\sqrt{2}})e^{-\frac{1}{2}a^2\cos^2\phi}\sigma_y. \tag{A.24}$$

Also, due to the rotational symmetry of the coherent states, the above can be rotated such that σ_{x_ϕ} applied to some $|\alpha\rangle$ is equivalent to σ_{p_ϕ} applied to $|\alpha = i\alpha\rangle$, where the angle ϕ is the (clockwise) angle the quadrature projection makes with the P quadrature.

We summarize these relations in Table A.1, where we have used the abbreviations $a_r = \frac{|\alpha|\cos\phi}{\sqrt{2}}$ and $a_i = \frac{|\alpha|\sin\phi}{\sqrt{2}}$.

	$\|0\rangle\langle 0\|$	$\|0\rangle\langle\alpha\|$	$\|\alpha\rangle\langle 0\|$	$\|\alpha\rangle\langle\alpha\|$
σ_ϕ	$\mathrm{erf}(a_r)$	$-i\frac{2}{\sqrt{\pi}}e^{-a_r^2}F(a_i)$	$i\frac{2}{\sqrt{\pi}}e^{-a_r^2}F(a_i)$	$-\mathrm{erf}(a_r)$
$\sigma_{-\phi}$	$\mathrm{erf}(a_r)$	$i\frac{2}{\sqrt{\pi}}e^{-a_r^2}F(a_i)$	$-i\frac{2}{\sqrt{\pi}}e^{-a_r^2}F(a_i)$	$-\mathrm{erf}(a_r)$
σ_p	$\mathrm{erf}(\frac{\lvert\alpha\rvert}{\sqrt{2}})$	0	0	$-\mathrm{erf}(\frac{\lvert\alpha\rvert}{\sqrt{2}})$
$\sigma_\phi + \sigma_{-\phi}$	$2\mathrm{erf}(a_r)$	0	0	$-2\mathrm{erf}(a_r)$
$\sigma_\phi - \sigma_{-\phi}$	0	$-i\frac{4}{\sqrt{\pi}}e^{-a_r^2}F(a_i)$	$i\frac{4}{\sqrt{\pi}}e^{-a_r^2}F(a_i)$	0

Table A.1: Summary of important results of Sec. A.1.2. Note that we have set $a_r = \frac{|\alpha|\cos\phi}{\sqrt{2}}$ and $a_i = \frac{|\alpha|\sin\phi}{\sqrt{2}}$.

A.2 Fully homodyne measurements on entangled coherent states

Armed with the derivations of the previous section, we are now ready to test states of the form Eq. (3.54) for violation of the CHSH inequality. The Bell operator can

be written,

$$\mathcal{B} = (A_0 + A_1)B_0 + (A_0 - A_1)B_1. \tag{A.25}$$

A.2.1 Choosing the binnings

We first make a simplification of the measurement operator of one party. This is not expected to give the best possible results, but is chosen to reduce the search space of possible measurements. Using the atomic measurements in Sec. 3.4 as a guide, we choose $A_0 = \sigma_\phi$ and $A_1 = \sigma_{-\phi}$. With this choice of A_0 and A_1, and given table A.1, it is obvious that the B_0 term will be big if it is some kind of σ_z like term, and B_1 term will be big if it is some kind of σ_y term, or if the state is conveniently chosen.

From intuition, a σ_z like term should maximally distinguish the $|0\rangle$ and $|\alpha\rangle$ states. From Sec. A.1.2, this must correspond to the quadrature measurement which has no relative phase between the quadrature measurement and α, and use a binning of the form $\tilde{x} \in [0, \infty)$. Thus, for $\arg\alpha = \frac{\pi}{2}$, if must correspond to the 3rd line of table A.1, *i.e.* we will use the operator σ_p as the B_0 term. Again intuitively, the σ_y term must maximize coherences, and must correspond to a relative phase between α and measurement of $\frac{\pi}{2}$. At this point, intuition does not help (at least for the author) anymore and we have to choose between using the binning $x \in [-b, b]$ or $\tilde{x} \in [0, \infty)$. We compare the magnitudes of the measurements on a state of the form

$$\frac{1}{2}\Big(|0\rangle\langle\alpha| + |\alpha\rangle\langle 0| \Big). \tag{A.26}$$

The first binning has already been computed in Sec. A.1 and gives the c_1 term, which is maximized by $b = \frac{\pi}{2\sqrt{2}\alpha}$. The second binning has also been calculated in Table A.1, but for a different state, which we assume to be $\frac{i}{2}(|0\rangle\langle\alpha| - |\alpha\rangle\langle 0|)$, and gives $2/\sqrt{\pi}F(\alpha)$. We then use mathematica to compute both functions for a range of α and plot the result in Fig. A.1. Fig. A.1 shows that c_1 always has a larger magnitude for $\alpha \in [0, 5]$. Thus, we will use the binning $x \in [-b, b]$.

A.2.2 Using a particular state

We first consider the state,

$$|\psi\rangle = \cos\nu|0,0\rangle - i\sin\nu|\alpha,\alpha\rangle. \tag{A.27}$$

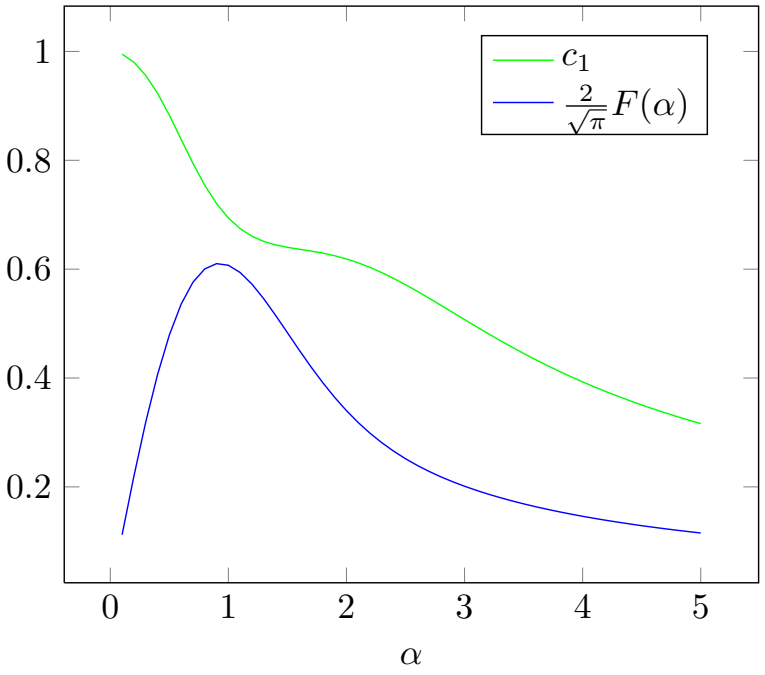

Figure A.1: Comparison of the magnitudes of the measurement using the binning $x \in [-b, b]$ and $\tilde{x} \in [0, \infty)$.

A quick check shows that the state is normalized, with ν independent of α, due to the factor of i. The density matrix is,

$$\begin{aligned}\rho &= |\psi\rangle\langle\psi| && \text{(A.28)}\\ &= \cos^2\nu|0,0\rangle\langle 0,0| - i\cos\nu\sin\nu\,|\alpha,\alpha\rangle\langle 0,0| \\ &+ i\cos\nu\sin\nu\,|0,0\rangle\langle\alpha,\alpha| + \sin^2\nu|\alpha,\alpha\rangle\langle\alpha,\alpha|. && \text{(A.29)}\end{aligned}$$

Taking the partial trace with $\sigma_{\{\pm\}} = \sigma_\phi \pm \sigma_{-\phi}$, we arrive at,

$$\mathrm{Tr_a}(\sigma_{\{+\}}\rho) = \varrho_+ = 2\Big(\cos^2\nu\,\mathrm{erf}(a_r)|0\rangle\langle 0| - \sin^2\nu\,\mathrm{erf}(a_r)|\alpha\rangle\langle\alpha|\Big), \quad \text{(A.30)}$$

$$\mathrm{Tr_a}(\sigma_{\{-\}}\rho) = \varrho_- = 2\frac{\sin 2\nu}{\sqrt{\pi}}F(a_i)e^{-a_r^2}(|0\rangle\langle\alpha| + |\alpha\rangle\langle 0|). \quad \text{(A.31)}$$

With this, $\langle\mathcal{B}\rangle$ evaluates to

$$\begin{aligned}\langle\mathcal{B}\rangle &= |\mathrm{Tr}\Big[\rho(\sigma_\phi + \sigma_{-\phi})\sigma_p + \rho(\sigma_\phi - \sigma_{-\phi})\sigma_x\Big]|, && \text{(A.32)}\\ &= |2\Big(\mathrm{erf}(a_r)\mathrm{erf}(\frac{|\alpha|}{\sqrt{2}}) + 2\frac{\sin 2\nu}{\sqrt{\pi}}e^{-a_r^2}F(a_i)c_1\Big)|, && \text{(A.33)}\end{aligned}$$

where we have used c_1 in Eq. (A.8) to simplify the expressions. To maximize over ν, first notice that $\mathrm{erf}(|\alpha|/\sqrt{2}) > 0$ and $c_1 > 0$. The positivity of c_1 can be shown numerically for $\alpha \in [0, 100]$, and then asymptotically for large α we showed in the

proof of Theorem 1 that $c_1 \sim \frac{1}{|\alpha|} > 0$. Thus, the maximization over ν depends on the signs of $\mathrm{erf}(a_r)$ and $F(a_i)$, and must yield

$$\langle \mathcal{B} \rangle_\nu = 2\Big(|\mathrm{erf}(a_r)|\, \mathrm{erf}(\frac{|\alpha|}{\sqrt{2}}) + \frac{2}{\sqrt{\pi}} e^{-a_r^2} |F(a_i)|\, c_1 \Big). \tag{A.34}$$

From this expression, we can also analytically maximize the angle ϕ. This is done by first reexpressing Dawson's function as $F(z) = \frac{\sqrt{\pi}}{2} e^{-z^2} \mathrm{erfi}(z)$, where $\mathrm{erfi}(x)$ is the imaginary error function. Then, we have

$$\langle \mathcal{B} \rangle_\nu = 2\Big(\mathrm{erf}(\frac{|\alpha| \cos\phi}{\sqrt{2}}) \mathrm{erf}(\frac{|\alpha|}{\sqrt{2}}) + \frac{1}{\sqrt{\pi}} e^{-a_r^2} F(a_i) K \Big), \tag{A.35}$$

$$= 2\mathrm{erf}(\alpha_h \cos\phi)\mathrm{erf}(\alpha_h) + 2c_1 e^{-\alpha_h^2} \mathrm{erfi}(\alpha_h \sin\phi), \tag{A.36}$$

where we have used the abbreviation $\alpha_h = |\alpha|/\sqrt{2}$. Using the relations

$$\partial_z \mathrm{erf}(z) = \frac{2}{\sqrt{\pi}} e^{-z^2}, \quad \text{and} \tag{A.37}$$

$$\partial_z \mathrm{erfi}(z) = \frac{2}{\sqrt{\pi}} e^{z^2}, \tag{A.38}$$

we obtain

$$\partial_\phi \langle \mathcal{B} \rangle = \frac{2}{\sqrt{\pi}} e^{-\alpha_h^2} e^{a_i^2} \alpha_h \Big[-2\mathrm{erf}(\alpha_h) \sin\phi + 2c_1 \cos\phi \Big]. \tag{A.39}$$

The stationary point of this is can be found to be

$$\tan\phi = \frac{c_1}{\mathrm{erf}(\alpha_h)}, \tag{A.40}$$

implying,

$$\cos\phi = \frac{\mathrm{erf}(\alpha_h)}{\sqrt{(\mathrm{erf}(\alpha_h))^2 + c_1^2}}, \quad \text{and} \tag{A.41}$$

$$\sin\phi = \frac{c_1}{\sqrt{(\mathrm{erf}(\alpha_h))^2 + c_1^2}}. \tag{A.42}$$

Thus,

$$\langle \mathcal{B} \rangle_{\nu,\phi} = 2\Big(\mathrm{erf}(\alpha_h) \mathrm{erf}\Big(\frac{\alpha_h \mathrm{erf}(\alpha_h)}{\sqrt{(\mathrm{erf}(\alpha_h))^2 + c_1^2}} \Big) + c_1 e^{-\alpha_h^2} \mathrm{erfi}\Big(\frac{\alpha_h c_1}{\sqrt{(\mathrm{erf}(\alpha_h))^2 + c_1^2}} \Big) \Big). \tag{A.43}$$

The last optimization over α is done numerically. This numerical optimization gives $\mathcal{B} = 2$ for some large α. Indeed, it can be shown that for α large, the

second term of the sum disappears due to the exponential decay of $e^{-\alpha_h^2}$, and $\cos\phi$, $\mathrm{erf}(\alpha_h) \approx 1$, giving $\mathcal{B} \to 2$. Thus, this state with these measurements does not violate the CHSH inequality.

A.3 Trying the Zohren-Gill inequalities

In this section, we test the inequality found in Ref. [81] using a state of the form

$$|\psi\rangle = N(|\alpha,\alpha\rangle + |-\alpha,-\alpha\rangle), \tag{A.44}$$

where $N^2 = \frac{1}{2(1+e^{-\alpha^2})}$, and given that fully homodyne measurements are used. From the experience with our previous treatment of homodyne measurements, given 2 homodyne measurements with angles ϕ_A and ϕ_B, we need the form of the wavefunction

$$\langle\psi|\Big(|x_A,x_B\rangle\langle x_A,x_B|\Big)|\psi\rangle. \tag{A.45}$$

To obtain this, we first note that

$$\psi^*_{-\alpha}(x)\psi_\alpha(x) = \frac{1}{\sqrt{\pi}}e^{-x^2}e^{-2\alpha^2\cos^2(\phi)}e^{i2\sqrt{2}\alpha x\sin(\phi)}, \tag{A.46}$$

where $\psi_\alpha(x) = \langle x_\phi|\alpha\rangle$. With this, the required wavefunction is then

$$\frac{\langle\psi|\Big(|x_A,x_B\rangle\langle x_A,x_B|\Big)|\psi\rangle}{|N|^2} = p(x_A,x_B|\phi_A,\phi_B), \tag{A.47}$$

$$\begin{aligned}
&= |\psi_\alpha(x_A)\psi_\alpha(x_B)|^2 + |\psi_{-\alpha}(x_A)\psi_{-\alpha}(x_B)|^2 \\
&+ \psi^*_{-\alpha}(x_A)\psi_\alpha(x_A)\psi^*_{-\alpha}(x_B)\psi_\alpha(x_B) + \text{h.c}, \qquad \text{(A.48)}\\
&= \frac{1}{\pi}\Big\{e^{-(x_A-\alpha_r\cos\phi_A)^2-(x_B-\alpha_r\cos\phi_B)^2} \\
&+ e^{-(x_A+\alpha_r\cos\phi_A)^2-(x_B+\alpha_r\cos\phi_B)^2} \\
&+ 2e^{-x_A^2-x_B^2}e^{-\alpha_r^2(\cos^2(\phi_A)+\cos^2(\phi_B))} \\
&\times\cos\{2\alpha_r(x_A\sin(\phi_A)+x_B\sin(\phi_B))\}\Big\}, \qquad \text{(A.49)}
\end{aligned}$$

where we have denoted $\alpha_r = \sqrt{2}\alpha$. The inequality requires the computation of probabilities of the form $P(A<B)$. This implies that the integrals required are of the form

$$\int_{-\infty}^{\infty}\int_{x_A}^{\infty} p(x_A,x_B|\phi_A,\phi_B)dx_B\,dx_A. \tag{A.50}$$

For the Gaussian functions in the first two lines of Eq. (A.49), this integral can be written in the analytical form

$$\frac{1}{\pi}\int_{-\infty}^{\infty}\int_{x_A}^{\infty} e^{-(x_A-a)^2-(x_B-b)^2}dx_B\,dx_A = \frac{1}{2\sqrt{\pi}}\int_{-\infty}^{\infty} e^{-y^2}\mathrm{erfc}(y+a-b)dy. \quad (A.51)$$

To derive the form of the integral of the last term of Eq. (A.49), it is helpful to change to polar coordinates. In this case, we have $x_A = r\cos\theta$ and $x_B = r\sin\theta$ and

$$\int_{-\infty}^{\infty}\int_{x_A}^{\infty} dx_B\,dx_A = \int_{\frac{\pi}{4}}^{\frac{5\pi}{4}}\int_0^{\infty} r\,dr\,d\theta. \quad (A.52)$$

The cross term integral then becomes

$$\begin{aligned}
&\frac{1}{\pi}\int_{-\infty}^{\infty}\int_{x_A}^{\infty} e^{-x_A^2-x_B^2}\cos\{2\alpha_r(x_A\sin(\phi_A)+x_B\sin(\phi_B))\}dx_B\,dx_A && (A.53)\\
&= \frac{1}{\pi}\int_{\frac{\pi}{4}}^{\frac{5\pi}{4}}\int_0^{\infty} re^{-r^2}\cos\{2\alpha_r r(\cos\theta\sin(\phi_A)+\sin\theta\sin(\phi_B))\}\,dr\,d\theta, && (A.54)\\
&= \frac{1}{\pi}\frac{1}{2}\int_{\frac{\pi}{4}}^{\frac{5\pi}{4}} 1-\kappa(\theta)F(\frac{\kappa(\theta)}{2})\,d\theta, && (A.55)\\
&= \frac{1}{2}\Big(1-\frac{1}{\pi}\int_{\frac{\pi}{4}}^{\frac{5\pi}{4}}\kappa(\theta)F(\frac{\kappa(\theta)}{2}\,d\theta)\Big), && (A.56)
\end{aligned}$$

where $\kappa(\theta) = 2\alpha_r(\cos\theta\sin(\phi_A)+\sin\theta\sin(\phi_B))$, and $F(x)$ is Dawson's integral given in Eq. (A.17). With these, we have

$$\begin{aligned}
\frac{p(A<B)}{N^2} = \frac{1}{2\sqrt{\pi}}\int_{-\infty}^{\infty} e^{-y^2}\{&\mathrm{erfc}[y+\alpha_r(\cos\phi_A-\cos\phi_B)]\\
&+\mathrm{erfc}[y-\alpha_r(\cos\phi_A-\cos\phi_B)]\}\,dy\\
&+\Big(1-\frac{1}{\pi}\int_{\frac{\pi}{4}}^{\frac{5\pi}{4}}\kappa(\theta)F(\frac{\kappa(\theta)}{2})\,d\theta\Big)e^{-\alpha_r^2(\cos^2\phi_A+\cos^2\phi_B)}. \quad (A.57)
\end{aligned}$$

Expecting some analytical optimization, we will want to find the derivative of the above with respect to ϕ_A or ϕ_B. We note the following useful relations:

$$\begin{aligned}
\frac{d}{dz}\mathrm{erfc}(z) &= -\frac{2}{\sqrt{\pi}}e^{-z^2} && (A.58)\\
\frac{d}{dz}F(z) &= 1-2zF(z) && (A.59)\\
\partial_{\phi_A}\kappa(\theta) &= 2\alpha_r\cos\theta\cos\phi_A && (A.60)\\
\partial_\kappa\kappa F(\frac{\kappa}{2}) &= \kappa(\frac{1}{2}-\frac{\kappa}{2}F(\frac{\kappa}{2}))+F(\frac{\kappa}{2}) && (A.61)\\
&= \frac{\kappa}{2}+(1-\frac{\kappa^2}{2})F(\frac{\kappa}{2}) && (A.62)
\end{aligned}$$

with this, the first two terms of the first partial derivative of Eq. (A.57) w.r.t ϕ_A (the erfc terms) equate to 0. However, the derivatives of the Dawson function seem daunting. Thus, we first check numerically if a violation can be achieved and around what values to limit our analytical optimization. Before we proceed, we first write down the inequality that we test:

$$P(A_2 < B_2) + P(B_2 < A_1) + P(A_1 < B_1) + P(B_1 \leq A_2) \geq 1. \tag{A.63}$$

A numerical study of the optimization space shows that the above sum of probabilities is very weakly dependent on the measurement angles, and has a minimum value of 1.408, around some $\alpha < 1$. Since the numerical search gives a null violation, we do not continue the analytical search. In the next subsection, we test a two different states to check if they violate the inequality.

A.3.1 Testing different states

In this subsection, we try the following states instead,

$$|0,1\rangle + |1,0\rangle, \quad \text{and,} \tag{A.64}$$

$$|0,2\rangle + |2,0\rangle, \tag{A.65}$$

which are the $N = 1, 2$ versions of the NOON state. Recall the wavefunction

$$\langle x|n\rangle = \psi_N(x) = \frac{1}{\sqrt{2^n n!\sqrt{\pi}}} H_n(x) e^{-\frac{x^2}{2}}. \tag{A.66}$$

With this, the wavefunction of the NOON state can be written as

$$|\psi_0(x_A)|^2|\psi_N(x_B)|^2 + |\psi_N(x_A)|^2|\psi_0(x_B)|^2 + 2\psi_0\psi_N(x_A)\psi_0\psi_N(x_B). \tag{A.67}$$

The first term gives an integral of the form

$$\int_{-\infty}^{\infty}\int_{x_A}^{\infty} \frac{1}{\pi} e^{-x_A^2} \frac{1}{2^n n!} H_n^2(x_B) e^{-x_B^2}\, dx_B dx_A, \tag{A.68}$$

$$\int_{\frac{\pi}{4}}^{\frac{5\pi}{4}}\int_0^{\infty} \frac{H_n^2(r\sin\theta)}{2^n n!\pi} r e^{-r^2}\, dr\, d\theta. \tag{A.69}$$

The integral over r can be solved by using the identity given in page 166 of [104], which gives

$$\int_0^{\infty} x e^{-x^2} \sum_{n=0}^{\infty} \frac{H_n^2(kx)}{2^n n!} t^n\, dx = \frac{1}{2}\frac{1}{1 - t(2k^2 - 1)}\sqrt{\frac{1+t}{1-t}}, \tag{A.70}$$

the required integral can then be found by finding the coefficient of the required term in the series expansion of the RHS. For the case of $N = 1$, the coefficient is k^2, and for $N = 2$, it is $2k^4 - k^2 + \frac{1}{4}$. I have not been able to find a closed form expression of the coefficients of the series expansion for $\sqrt{\frac{1+t}{1-t}}$, and so will leave it as this. With this, Eq. (A.69) evaluates to $\frac{1}{2}$ for $N = 1$, and 0 for $N = 2$. The second term of Eq. (A.67) is just with sin $\rightarrow$ cos, and also gives $\frac{1}{2}$ for $N = 1$, and 0 for $N = 2$.

The cross term gives the integral

$$2\int_{-\infty}^{\infty}\int_{x_A}^{\infty}\frac{1}{\pi}e^{-x_A^2-x_B^2}\frac{1}{2^n n!}H_n(x_A)H_n(x_B)\,dx_B\,dx_A, \tag{A.71}$$

$$=\frac{2}{\pi}\int_{\frac{\pi}{4}}^{\frac{5\pi}{4}}\int_0^{\infty}\frac{H_n(r\cos\theta)H_n(r\sin\theta)}{2^n n!}re^{-r^2}\,dr\,d\theta. \tag{A.72}$$

The r integral can again be evaluated using the identity on page 166 of Ref. [104], which similarly gives

$$\int_0^{\infty}\sum_{n=0}^{\infty}\frac{H_n(r\cos\theta)H_n(r\sin\theta)}{2^n n!}re^{-r^2}t^n dr=\frac{1}{2}\frac{\sqrt{1-t^2}}{1-t\sin 2\theta}. \tag{A.73}$$

Again, the general expansion eludes me. For $N = 1$, this gives $\frac{1}{2}\sin 2\theta$ and for $N = 2$, gives $\frac{-1}{4}\cos 4\theta$. Both functions give 0 after the θ integral.

We can then input these values into the inequality. For the state $\frac{1}{\sqrt{2}}(|0,2\rangle + |2,0\rangle)$, $P(A < B) = 0$. And thus the sum of probabilities is 2. For $\cos\nu|1,0\rangle + \sin\nu|0,1\rangle$ gives $P(A < B) = \frac{1}{2}$, and so the sum or probabilities is also 2. Thus, both states do not violate the inequality. Note that although we have not done it, our methodology can easily be generalized to any NOON state due to the ease at which the r integrals can be evaluated.

APPENDIX B

ONGOING FOUR-WAVE MIXING CALCULATIONS

In this appendix, we present an ongoing calculation for the four-wave mixing experiment.

This appendix is structured as follows. We first present the derivation of the generalization Einstein relations for the correlation functions of the Langevin forces for a two-level atom. This technique can be similarly generalized to multi-level atoms as we are dealing with. Next, we go straight to the Maxwell-Bloch equations for the system including all decay processes and Langevin forces. Next, we derive input-output relations and some useful commutators and show how these can be used to compute the required $G^{(2)}$ function. Lastly, we list down a set of approximations which we think will be sufficient to reproduce the results of Ref. [89].

B.1 Generalized Einstein relations

In this section, we first write down the outline of the derivations of the Generalized Einstein relations following [105], then we try to find these relations for our problem. These relations express the correlation functions of Langevin forces to the dissipation rates of the atom, and can be viewed from a fluctuation-dissipation theorem lens. The latter concept says that in the case of Brownian motion, the origins of the random forces that kicks the pollen molecules in water and the frictional forces which damp out motion of the pollen molecules is the same. This is conceptually very nice, and much work on this has been done by Kubo and others[1], however, I have not been able to find a clear and concise derivation of the

[1]See Ref. [106] for a nice review of the fluctuation dissipation theorem.

quantities I require, which is the multi time correlation functions of the Langevin forces.

B.1.1 Derivation in the case of a two-level atom

In this subsection, we show the derivation of the correlation functions for a two-level atom driven by a classical field, and coupled to a quantum field (which acts as the spontaneous emission reservoir). The idea of the derivation is not difficult.

Consider the optical bloch equations of this case, and including the spontaneous emission rates we can write for the set of $S_q = \{\sigma^\dagger, \sigma, \sigma_z\}$,

$$\frac{d}{dt}S_q = \sum_{q''} \mathcal{B}_{q,q''} S_{q''} + \lambda_q + F_q(t) \tag{B.1}$$

where $F_q(t)$ is the Langevin force term, which has zero average value *i.e.*

$$\langle F_q \rangle = 0. \tag{B.2}$$

The correlation functions that we wish to derive are,

$$\left\langle F_q^\dagger(t) F_{q'}(t') \right\rangle = 2D_{q\,q'} g(t-t'), \tag{B.3}$$

where $D_{q\,q'}$ is a diffusion constant on the order of the atomic decay rate Γ, and $g(t-t')$ is a function of $t-t'$ of width $\tau_c = 1/ck_M$, and having an integral equal to 1. These relations come due to the existence of 2 very different time scales, Γ^{-1} and τ_c, with the correlation time much shorter than the decay time *i.e.* $\tau_c \ll \Gamma^{-1}$. We first note that

$$\langle F_q(t) S_{q'}(t') \rangle = 0 \qquad \text{if } t - t' \gg \tau_c. \tag{B.4}$$

This can be seen by first formally integrating Eq. (B.1), and then, since $S_{q'}$ depends linearly on $F_{q''}$, and using the properties of $g(t-t')$. Thus, $S_{q'}$ cannot be correlated with the Langevin force for t sufficiently distant in the future of t'. We next define the drift velocity of S_q as,

$$\mathcal{D}(S_q) = \sum_{q''} \mathcal{B}_{q,q''} S_{q''} + \lambda_q, \tag{B.5}$$

which governs the evolution of the means in the usual Bloch equations. Then,

$$\frac{d}{dt}S_q = \mathcal{D}(S_q) + F_q(t). \tag{B.6}$$

Now, consider the atomic operator $S_q^\dagger S_{q'}$. The pauli algebra allows us to reexpress this in terms of the pauli operators again, and we can write

$$\frac{d}{dt}\left\langle S_q^\dagger(t)S_{q'}(t)\right\rangle = \left\langle \mathcal{D}(S_q^\dagger(t)S_{q'}(t))\right\rangle \tag{B.7}$$

$$\left\langle \dot{S}_q^\dagger(t)S_{q'}(t)\right\rangle + \left\langle S_q^\dagger(t)\dot{S}_{q'}(t)\right\rangle = \left\langle \mathcal{D}(S_q^\dagger(t)S_{q'}(t))\right\rangle \tag{B.8}$$

$$\begin{aligned}\left\langle \mathcal{D}(S_q^\dagger(t)S_{q'}(t))\right\rangle &= \left\langle \mathcal{D}(S_q^\dagger(t))S_{q'}(t)\right\rangle + \left\langle S_q(t)^\dagger\mathcal{D}(S_{q'}(t))\right\rangle \\ &\quad + \left\langle F_q^\dagger(t)S_{q'}(t)\right\rangle + \left\langle S_q^\dagger(t)F_{q'}(t)\right\rangle .\end{aligned} \tag{B.9}$$

To calculate the last 2 terms of the above expression, we note that the Langevin forces $F_q(t)$ are not correlated with the operators $S_{q'}(t-\Delta t)$ if $\Delta t \gg \tau_c$. Thus, we integrate Eq. (B.1) between $t-\Delta t$ and t, so that we can express $S_{q'}(t)$ as a function of $S_{q'}(t-\Delta t)$. We choose Δt to be relatively small compared to Γ^{-1} (but still satisfying $\Delta t \gg \tau_c$, which is possible due to the large separation in time scales). This small Δt allows us to approximate the evolution of $S_q(t)$ to first order in Δt, which from Eq. (B.1) is

$$S_{q'}(t) = S_{q'}(t-\Delta t) + \Delta t(D)(S_{q'}(t-\Delta t) + \int_{t-\Delta t}^{t} F_{q'}(t')\,dt'. \tag{B.10}$$

Now, $\mathcal{D}(S_{q'}(t-\Delta t)$ is linear in $S_{q'}$ and thus, $\left\langle F_q^\dagger(t)\mathcal{D}(S_{q'}(t-\Delta t)\right\rangle = 0$. Then, the last 2 terms of Eq. (B.9) become

$$\left\langle F_q^\dagger(t)S_{q'}(t) + S_q^\dagger(t)F_{q'}(t)\right\rangle = \int_{t-\Delta t}^{t}\left\langle F_q^\dagger(t)F_{q'}(t') + F_q^\dagger(t')F_{q'}(t)\right\rangle\,dt' \tag{B.11}$$

$$= 2D_{q\,q'}\int_{t-\Delta t}^{t}[g(t-t') + g(t'-t)]\,dt' \tag{B.12}$$

$$= 2D_{q\,q'}\int_{-\Delta t}^{\Delta t} g(\tau)\,d\tau = 2D_{q\,q'} \tag{B.13}$$

where in the last line we notice that $\int_{t-\Delta t}^{t} g(t-t')\,dt'$ "sums" $g(t')$ in $t' \in [0,\Delta t]$ and $\int_{t-\Delta t}^{t} g(t'-t)\,dt'$ "sums" it from $t' \in [-\Delta t, 0]$, and since $\Delta t \gg \tau_c$, this integral is 1. Thus, the generalized Einstein relation is

$$2D_{q\,q'} = \left\langle \mathcal{D}(S_q^\dagger(t)S_{q'}(t))\right\rangle - \left[\left\langle \mathcal{D}(S_q^\dagger(t))S_{q'}(t)\right\rangle + \left\langle S_q(t)^\dagger\mathcal{D}(S_{q'}(t))\right\rangle\right] \tag{B.14}$$

B.2 Attacking the problem

With the previous derivation in hand, we can attack the problem proper. The equations of motions for the 4-wave mixing situation are: For the fields

$$(c\partial_z + \partial_t)S(z,t) = ig_s Ln(z)\tilde{\sigma}_{32}(z,t), \tag{B.15}$$

$$(c\partial_z + \partial_t)D(z,t) = ig_d Ln(z)\tilde{\sigma}_{03}(z,t), \tag{B.16}$$

and for the atomic operators,

$$\begin{aligned}\partial_t\tilde{\sigma}_{01}(z,t) = &-\left(\frac{\Gamma_1}{2} + i\delta_{p1}\right)\tilde{\sigma}_{01} \\ &+ i\Omega_{p1}[\tilde{\sigma}_{11} - \tilde{\sigma}_{00}] - i\Omega^*_{p2}(t - z/c)\tilde{\sigma}02 + ig_d D\tilde{\sigma}^\dagger_{13} + \hat{F}_{01},\end{aligned} \tag{B.17}$$

$$\begin{aligned}\partial_t\tilde{\sigma}_{12}(z,t) = &-\left(\frac{\Gamma_{21}}{2} + i\delta_{p2}\right)\tilde{\sigma}_{12} \\ &+ i\Omega^*_{p2}[\tilde{\sigma}_{22} - \tilde{\sigma}_{11}] + i\Omega^*_{p1}\tilde{\sigma}02 - ig_s S\tilde{\sigma}^\dagger_{13} + \hat{F}_{12},\end{aligned} \tag{B.18}$$

$$\begin{aligned}\partial_t\tilde{\sigma}_{32}(z,t) = &-\left(\frac{\Gamma_{23}}{2} + i\delta_s\right)\tilde{\sigma}_{32} \\ &+ ig_s S[\tilde{\sigma}_{22} - \tilde{\sigma}_{33}] - i\Omega_{p2}\tilde{\sigma}13^\dagger + ig^*_d D^\dagger\tilde{\sigma}_{02} + \hat{F}_{32},\end{aligned} \tag{B.19}$$

$$\begin{aligned}\partial_t\tilde{\sigma}_{03}(z,t) = &-\left(\frac{\Gamma_3}{2} + i\delta_d\right)\tilde{\sigma}_{03} \\ &+ ig_d D[\tilde{\sigma}_{33} - \tilde{\sigma}_{00}] + i\Omega_{p1}\tilde{\sigma}13 - ig^*_s S^\dagger\tilde{\sigma}_{02} + \hat{F}_{03},\end{aligned} \tag{B.20}$$

$$\begin{aligned}\partial_t\tilde{\sigma}_{02}(z,t) = &-\left(\frac{\gamma_{02}}{2} + i\Delta_{2p}\right)\tilde{\sigma}_{02} \\ &+ i\Omega_{p1}\tilde{\sigma}_{12} - i\Omega_{p2}\tilde{\sigma}_{01} - ig_s S\tilde{\sigma}03 + ig_d D\tilde{\sigma}_{32} + \hat{F}_{02},\end{aligned} \tag{B.21}$$

$$\begin{aligned}\partial_t\tilde{\sigma}_{13}(z,t) = &-\left(\frac{\gamma_{13}}{2} + i\Delta_w\right)\tilde{\sigma}_{13} \\ &+ i\Omega^*_{p1}\tilde{\sigma}_{03} + i\Omega_{p2}\tilde{\sigma}^\dagger_{32} - ig_s S^\dagger\tilde{\sigma}12 - ig_d D\tilde{\sigma}^\dagger_{01} + \hat{F}_{13},\end{aligned} \tag{B.22}$$

where all Rabi frequencies are taken at the retarded time, *i.e.* $\Omega_i = \Omega_i(t - z/c)$. The field propagation equations can be simplified by noting that for some function

$$g(z,\tau) = f(z, t = \tau + z/c) \tag{B.23}$$

then,

$$c\partial_z g(z,\tau) = (c\partial_z + \partial_t)f(z, t = \tau + z/c). \tag{B.24}$$

This is relation that used in many references, but is hardly explained anywhere. The above "explanation" can be found in [107], however, the more mathematically inclined reader will be delighted to know that this relation can also be derived by

using the definitions of derivatives as limits and some taylor expansions. Then, following Gorshkov in [91] we define the dimensionless $\tilde{z}$ as

$$\tilde{z} = \frac{1}{N}\int_0^z dz'\, n(z'), \tag{B.25}$$

and using the retarded time $\tau = t - z/c$, we can rewrite the equations of motion as:

$$\partial_{\tilde{z}} S(\tilde{z},\tau) = i\frac{g_s L N}{c}\tilde{\sigma}_{32}(\tilde{z},\tau) \tag{B.26}$$

$$\partial_{\tilde{z}} D(\tilde{z},\tau) = i\frac{g_d L N}{c}\tilde{\sigma}_{03}(\tilde{z},\tau) \tag{B.27}$$

$$\begin{aligned}\partial_\tau \tilde{\sigma}_{01}(\tilde{z},\tau) = &-\left(\frac{\Gamma_1}{2} + i\delta_{p1}\right)\tilde{\sigma}_{01} \\ &+ i\Omega_{p1}(\tau)[\tilde{\sigma}_{11} - \tilde{\sigma}_{00}] - i\Omega^*_{p2}(\tau)\tilde{\sigma}_{02} + ig_d D\tilde{\sigma}^\dagger_{13} + \hat{F}_{01}\end{aligned} \tag{B.28}$$

$$\begin{aligned}\partial_\tau \tilde{\sigma}_{12}(\tilde{z},\tau) = &-\left(\frac{\Gamma_{21}}{2} + i\delta_{p2}\right)\tilde{\sigma}_{12} \\ &+ i\Omega^*_{p2}(\tau)[\tilde{\sigma}_{22} - \tilde{\sigma}_{11}] + i\Omega^*_{p1}(\tau)\tilde{\sigma}_{02} - ig_s S\tilde{\sigma}^\dagger_{13} + \hat{F}_{12}\end{aligned} \tag{B.29}$$

$$\begin{aligned}\partial_\tau \tilde{\sigma}_{32}(\tilde{z},\tau) = &-\left(\frac{\Gamma_{23}}{2} + i\delta_s\right)\tilde{\sigma}_{32} \\ &+ ig_s S[\tilde{\sigma}_{22} - \tilde{\sigma}_{33}] - i\Omega_{p2}(\tau)\tilde{\sigma}^\dagger_{13} + ig^*_d D^\dagger\tilde{\sigma}_{02} + \hat{F}_{32}\end{aligned} \tag{B.30}$$

$$\begin{aligned}\partial_\tau \tilde{\sigma}_{03}(\tilde{z},\tau) = &-\left(\frac{\Gamma_3}{2} + i\delta_d\right)\tilde{\sigma}_{03} \\ &+ ig_d D[\tilde{\sigma}_{33} - \tilde{\sigma}_{00}] + i\Omega_{p1}(\tau)\tilde{\sigma}_{13} - ig^*_s S^\dagger\tilde{\sigma}_{02} + \hat{F}_{03}\end{aligned} \tag{B.31}$$

$$\begin{aligned}\partial_\tau \tilde{\sigma}_{02}(\tilde{z},\tau) = &-\left(\frac{\gamma_{02}}{2} + i\Delta_{2p}\right)\tilde{\sigma}_{02} \\ &+ i\Omega_{p1}\tilde{\sigma}_{12} - i\Omega_{p2}\tilde{\sigma}_{01} - ig_s S\tilde{\sigma}_{03} + ig_d D\tilde{\sigma}_{32} + \hat{F}_{02}\end{aligned} \tag{B.32}$$

$$\begin{aligned}\partial_\tau \tilde{\sigma}_{13}(\tilde{z},\tau) = &-\left(\frac{\gamma_{13}}{2} + i\Delta_w\right)\tilde{\sigma}_{13} \\ &+ i\Omega^*_{p1}\tilde{\sigma}_{03} + i\Omega_{p2}\tilde{\sigma}^\dagger_{32} - ig_s S^\dagger\tilde{\sigma}_{12} - ig_d D\tilde{\sigma}^\dagger_{01} + \hat{F}_{13}\end{aligned} \tag{B.33}$$

B.3 Relevant quantities

The set of Eqs. (B.26-B.33) represents the starting point from which we attack the problem. These equations will completely describe the physical situation we wish to model. However, before we proceed further, it is prudent to first look at the goal of the calculation lest we get lost in the jungle of symbols.

Since are seeking the detection probability of one photon triggered on the other entangled photon, we are in essence measuring the two-time correlation function

$$G^{(2)}_{FG}(t,t') = \left\langle G^{\dagger}_{\text{out}}(t)F^{\dagger}_{\text{out}}(t')F_{\text{out}}(t')G_{\text{out}}(t)\right\rangle, \tag{B.34}$$

where F_{out} and G_{out} represent the annihilation operators of the output field modes which would correspond to either the signaller or idler modes. Inspired by Sec. 2.3, let us first ignore the position dependences and first assume that the output modes are related to the input modes and system operators by

$$F_{\text{out}}(t) = F_{\text{in}}(t) + \Sigma_F(t), \tag{B.35}$$
$$G_{\text{out}}(t) = G_{\text{in}}(t) + \Sigma_G(t), \tag{B.36}$$

where Σ_i is the system operator coupled to the bath mode i. Then, define the commutator

$$C = [F_{\text{in}}(t'), \Sigma_G(t)]. \tag{B.37}$$

Now, if both input modes are in the vacuum state, we have

$$\begin{aligned} G^{(2)}_{FG}(t,t') &= \left\langle G^{\dagger}_{\text{out}}(t)F^{\dagger}_{\text{out}}(t')F_{\text{out}}(t')G_{\text{out}}(t)\right\rangle, && \text{(B.38)}\\ &= \left\langle \Sigma^{\dagger}_G(t)(F_{\text{in}}(t') + \Sigma_F(t'))^{\dagger}(F_{\text{in}}(t') + \Sigma_F(t'))\Sigma_G(t)\right\rangle, && \text{(B.39)}\\ &= \langle \Sigma^{\dagger}_G(t)\Big[F^{\dagger}_{\text{in}}(t')\Sigma_F(t') + F^{\dagger}_{\text{in}}(t')F_{\text{in}}(t') + \Sigma^{\dagger}_F(t')F_{\text{in}}(t')\\ &+ \Sigma^{\dagger}_F(t')\Sigma_F(t')\Big]\Sigma_G(t)\rangle, && \text{(B.40)}\\ &= \left\langle C^{\dagger}\Sigma_F(t')\Sigma_G(t) + C^{\dagger}C + \Sigma^{\dagger}_G(t)\Sigma^{\dagger}_F(t')C + \Sigma^{\dagger}_G(t)\Sigma^{\dagger}_F(t')\Sigma_F(t')\Sigma_G(t)\right\rangle. && \text{(B.41)} \end{aligned}$$

Thus, we need to derive the form of the commutator C, and require the computation of certain correlation functions of system operators.

B.4 Deriving input-output relations and commutators

We have the field propagation equations

$$\partial_{\tilde{z}} S(\tilde{z},\tau) = i\frac{g_s LN}{c}\tilde{\sigma}_{32}(\tilde{z},\tau), \quad \text{and,} \tag{B.42}$$
$$\partial_{\tilde{z}} D(\tilde{z},\tau) = i\frac{g_d LN}{c}\tilde{\sigma}_{03}(\tilde{z},\tau). \tag{B.43}$$

The input fields are defined as $O_{\text{in}}(t) = O(0,t)$, and the output fields are $O_{\text{out}}(t) = O(L,t)$, where O is either S or D. In terms of the functions with dimensionless coordinates, the input field is $\tilde{O}(0,\tau) = O_{\text{in}}(\tau)$ and the output field is $\tilde{O}(1,\tau) = O_{\text{out}}(\tau + L/c)$. Then, letting $p_\alpha = \frac{g_\alpha LN}{c}$, we can write

$$S(\tilde{z},\tau) - S_{\text{in}}(\tau) = ip_s \int_0^{\tilde{z}} d\tilde{z}'\, \tilde{\sigma}_{32}(\tilde{z}',\tau), \quad \text{and,} \tag{B.44}$$

$$S_{\text{out}}(\tau + L/c) - S_{\text{in}}(\tau) = ip_s \int_0^{1} d\tilde{z}\, \tilde{\sigma}_{32}(\tilde{z},\tau), \tag{B.45}$$

and the corresponding equations for the idler field. Using the same arguments as in Sec. 2.2.4, we deduce that

$$[S_{\text{in}}(t), P(z,t')] = 0 \qquad \text{for,} t > t' + z/c, \tag{B.46}$$

where $P(z,t')$ is some system operator. This must be true, since a system operator should not depend on the input operator at later times, and conversely,

$$[S_{\text{out}}(t), P(z,t')] = 0 \qquad \text{for,} t + (L-z)/c < t'. \tag{B.47}$$

In terms of the retarded time functions, these are

$$[S_{\text{in}}(t), \tilde{P}(z,\tau)] = 0 \qquad \text{for,} t > \tau, \tag{B.48}$$

$$[S_{\text{out}}(t + L/c), \tilde{P}(z,\tau)] = 0 \qquad \text{for,} t + L/c < \tau. \tag{B.49}$$

With these relations, we need to combine them with Eqs. (B.45) and (B.44) to derive the Input Output relations for the system.

B.5 Approximations

In this section, we list down the two approximations which vastly simplify the set of equations (B.26-B.33).

1. During the interaction, the atomic ensemble is almost always in the ground state *i.e.*

$$\sigma_{ii} \approx \delta_{i,0}. \tag{B.50}$$

2. Second order quantum effects are weak, compared to the corresponding effects due to the pump fields. Second order quantum terms are terms which involve the absorption or emission of a photon in the signaller or idler modes, accompanied by an atomic raising or lower operator.

These approximations allow us to write the equations as,

$$\partial_{\tilde{z}} S(\tilde{z},\tau) = i\frac{g_s LN}{c}\tilde{\sigma}_{32}(\tilde{z},\tau), \tag{B.51}$$

$$\partial_{\tilde{z}} D(\tilde{z},\tau) = i\frac{g_d LN}{c}\tilde{\sigma}_{03}(\tilde{z},\tau), \tag{B.52}$$

$$\partial_\tau \tilde{\sigma}_{01}(\tilde{z},\tau) \approx -\left(\frac{\Gamma_1}{2} + i\delta_{p1}\right)\tilde{\sigma}_{01} - i\Omega_{p1}(\tau) - i\Omega^*_{p2}(\tau)\tilde{\sigma}_{02} + \hat{F}_{01}, \tag{B.53}$$

$$\partial_\tau \tilde{\sigma}_{12}(\tilde{z},\tau) \approx -\left(\frac{\Gamma_{21}}{2} + i\delta_{p2}\right)\tilde{\sigma}_{12} + i\Omega^*_{p1}(\tau)\tilde{\sigma}_{02} + \hat{F}_{12}, \tag{B.54}$$

$$\partial_\tau \tilde{\sigma}_{32}(\tilde{z},\tau) \approx -\left(\frac{\Gamma_{23}}{2} + i\delta_s\right)\tilde{\sigma}_{32} - i\Omega_{p2}(\tau)\tilde{\sigma}^\dagger_{13} + \hat{F}_{32}, \tag{B.55}$$

$$\partial_\tau \tilde{\sigma}_{03}(\tilde{z},\tau) \approx -\left(\frac{\Gamma_3}{2} + i\delta_d\right)\tilde{\sigma}_{03} - ig_d D + i\Omega_{p1}(\tau)\tilde{\sigma}_{13} + \hat{F}_{03}, \tag{B.56}$$

$$\partial_\tau \tilde{\sigma}_{02}(\tilde{z},\tau) \approx -\left(\frac{\gamma_{02}}{2} + i\Delta_{2p}\right)\tilde{\sigma}_{02} + i\Omega_{p1}\tilde{\sigma}_{12} - i\Omega_{p2}\tilde{\sigma}_{01} + \hat{F}_{02,} \tag{B.57}$$

$$\partial_\tau \tilde{\sigma}_{13}(\tilde{z},\tau) \approx -\left(\frac{\gamma_{13}}{2} + i\Delta_w\right)\tilde{\sigma}_{13} + i\Omega^*_{p1}\tilde{\sigma}_{03} + i\Omega_{p2}\tilde{\sigma}^\dagger_{32} + \hat{F}_{13}. \tag{B.58}$$

These reduced equations can now be solved in smaller chunks by noting that the set of equations involving $\{\tilde{\sigma}^\dagger_{32}, \tilde{\sigma}_{03}, \tilde{\sigma}_{13}\}$ are strangely decoupled from the other atomic operators.

B.6 Outlook

In this Appendix, I have presented our ongoing calculation with the four-wave mixing setup. The material presented is necessary (and almost sufficient) to complete the calculation, however, due to various constraints, the calculation is currently unfinished, as can be seen in Sec. B.4 and the previous section. It is believed however, that the calculation will reproduce the measured results of Ref. [89]. Hopefully, this method can also give previously inaccessible results, like the optimal pulse shape for entangled photon pair production *etc.*.

APPENDIX C

THE FOKKER-PLANCK EQUATION

In this appendix, we give some background derivations for Chapter 7 for completeness of this work. We first present a derivation of the Fokker-Planck equation from the Chapman-Kolmogorov equations. We next show the connection between the usual Itô stochastic differential equation (SDE) and the Fokker-Planck equation.

C.1 Derivation from the Chapman-Kolmogorov equation

In this section, we derive the forward and backward Fokker-Planck equations from the Chapman-Kolmogorov equations. This section is heavily based on Ref. [108] and the reader should refer to this reference for more details.

The basic tenet of this derivation is the Chapman-Kolmogorov equation for Markovian processes. The Markovian process $X(t)$ is assumed to be a time-dependent random variable such that we can sample values x_1, x_2 etc. of $X(t)$ at different times, and a joint probability density $p(x,t)$ exists which describes the system completely. Then, the Chapman-Kolmogorov equation can be stated as

$$p(x_1,t_1|x_3,t_3) = \int dx_2\, p(x_1,t_1|x_2,t_2)p(x_2,t_2|x_3,t_3), \tag{C.1}$$

which is a very intuitive statement of probabilities (at least to this author).

C.1.1 Forward evolution

The derivation requires three conditions for all $\epsilon > 0$:

1. The limit
$$\lim_{\Delta t\to 0}\frac{1}{\Delta t}p(x,t+\Delta t|z,t)=W(x|z,t), \tag{C.2}$$
exists uniformly in x,z and $t\ \forall\ |x-z|\geq\epsilon$.

2. $\lim_{\Delta t\to 0}\frac{1}{\Delta t}\int_{|x-z|<\epsilon}dx\,(x-z)p(x,t+\Delta t|z,t)=A(z,t)+O(\epsilon)$,

3. $\lim_{\Delta t\to 0}\frac{1}{\Delta t}\int_{|x-z|<\epsilon}dx\,(x-z)^2p(x,t+\Delta t|z,t)=B(z,t)+O(\epsilon)$,

where the last 2 conditions have the limits existing uniformly in z,ϵ and t. Let $f(z)$ an arbitrary function which is twice continuously differentiable in some region $\mathcal{R}\subset\mathbb{C}$. Consider the time evolution of the expectation of $f(x)$,

$$\partial_t\int dx\,f(x)p(x,t|y,t')=\int dx\,f(x)\lim_{\Delta t\to 0}\frac{1}{\Delta t}[p(x,t+\Delta t|y,t')-p(x,t|y,t')], \tag{C.3}$$

$$=\lim_{\Delta t\to 0}\frac{1}{\Delta t}\Big\{\int dx\int dz\,f(x)p(x,t+\Delta t|z,t)p(z,t|y,t')$$
$$-\int dz\,f(z)p(z,t|y,t')\Big\}. \tag{C.4}$$

Since $f(z)$ is twice continuously differentiable

$$f(z)=f(x)+(x-z)\partial_z f(z)+\frac{1}{2}(x-z)^2\partial_z^2 f(z), \tag{C.5}$$

for $|x-z|<\epsilon$. Then, inserting this into Eq. (C.4) and breaking up the integration region into $|x-z|<\epsilon$ and $|x-z|\geq\epsilon$, we obtain

$$\lim_{\Delta t\to 0}\frac{1}{\Delta t}\Big\{\int dx\int dz\,f(x)p(x,t+\Delta t|z,t)p(z,t|y,t')-\int dz\,f(z)p(z,t|y,t')\Big\} \tag{C.6}$$

$$=\lim_{\Delta t\to 0}\frac{1}{\Delta t}\Big\{\int_{|x-z|<\epsilon}dx\,dz\,\Big[(x-z)\partial_z f(z)+\frac{1}{2}(x-z)^2\partial_z^2 f(z)\Big]$$
$$\times\,p(x,t+\Delta t|z,t)p(z,t|y,t')$$
$$+\int_{|x-z|\geq\epsilon}dx\,dz\,f(x)p(x,t+\Delta t|z,t)p(z,t|y,t')$$
$$+\int_{|x-z|<\epsilon}dx\,dz\,f(z)p(x,t+\Delta t|z,t)p(z,t|y,t')$$
$$-\int dz\,f(z)\Big[\int dx\,p(x,t+\Delta t|z,t)\Big]p(z,t|y,t')\Big\}, \tag{C.7}$$

where in the last line of Eq. (C.7), we have used that fact that the probability distribution is normalized. Combing the last two lines of Eq. (C.7) and using the

conditions (1-3), we arrive at

$$\int dz\, f(z)\partial_t p(z,t|y,t') = \int dz \left[A(z,t)\partial_z f(z) + \frac{1}{2}B(z,t)\partial_z^2 f(z)\right]p(z,t|y,t') + f(z)\{\int dx\, W(x|z,t)p(x,t|y,t') - W(x|z,t)p(z,t|y,t')\}. \tag{C.8}$$

The first line of the above can be rewritten by first writing out the integration region explicitly and integrating by parts, such that we obtain

$$\int_{\mathcal{R}} dz \left[A(z,t)\partial_z f(z) + \frac{1}{2}B(z,t)\partial_z^2 f(z)\right]p(z,t|y,t') \tag{C.9}$$

$$= \int_{\mathcal{R}} dz\, f(z)\Big[- \partial_z A(z,t)p(z,t|y,t') + \frac{1}{2}\partial_z^2 B(z,t)p(z,t|y,t')\Big] + \Big(A\, p(z,t|y,t')f(z) + \frac{1}{2}B\, p(z,t|y,t')\partial_z f(z) - \frac{f(z)}{2}\partial_z B\, p(z,t|y,t')\Big)\Big|_{\partial\mathcal{R}}, \tag{C.10}$$

where $\partial\mathcal{R}$ represents the surface of the region $\mathcal{R}$. Next, we define the support of function $f(z)$ to be $\mathcal{R}' \subset R$[1]. With this additional constraint on $f(z)$, the surface terms vanish, and we finally obtain:

$$\frac{\partial}{\partial t}p(z,t|y,t') = -\frac{\partial}{\partial z}[A(z,t)p(z,t|y,t')] + \frac{1}{2}\frac{\partial^2}{\partial z^2}[B(z,t)p(z,t|y,t')] + \int dx\, [W(z|x,t)p(x,t|y,t') - W(x|z,t)p(z,t|y,t')]. \tag{C.11}$$

This equation is referred to in Ref. [108] as the differential Chapman-Kolmogorov equation, but I was unable to find any reference to this name. The Fokker-Planck equation is then obtained by setting $W(z|x,t) = 0$, *i.e.*

$$\frac{\partial}{\partial t}p(x,t|y,t') = -\frac{\partial}{\partial x}[A(x,t)p(x,t|y,t')] + \frac{1}{2}\frac{\partial^2}{\partial x^2}[B(x,t)p(x,t|y,t')]. \tag{C.12}$$

Since $W(z|x,t)$ is related to the continuity of the probability distribution by Eq. (1), setting $W(z|x,t) = 0$ implies that the resulting solution of the Fokker-Planck equation is continuous.

C.1.2 Backward evolution

In this subsection, we present the derivation of the backward Fokker-Planck equation from the Chapman-Kolmogorov equation. This equation differs from the forward equation only by the variables which are kept constant. The derivation

[1] The interested reader is referred to Ref. [108] pp 50 for further discussion on this point.

starts by immediately considering

$$\partial_{t'} p(x,t|y,t') = \lim_{\Delta t' \to 0} \frac{1}{\Delta t'} [p(x,t|y,t'+\Delta t') - p(x,t|y,t')] \tag{C.13}$$

$$= \lim_{\Delta t' \to 0} \frac{1}{\Delta t'} \int dz\, p(z,t'+\Delta t'|y,t')[p(x,t|y,t'+\Delta t') - p(x,t|z,t'+\Delta t')], \tag{C.14}$$

where we have used the Chapman-Kolmogorov equation in the second term, and used completeness of the distribution in the first term. Assuming that the probability distribution $p(x,t|y,t')$ is continuous and bounded for some $t - t' > \delta > 0$, we can further write

$$\lim_{\Delta t' \to 0} \frac{1}{\Delta t'} \int dz\, p(z,t'+\Delta t'|y,t')[p(x,t|y,t'+\Delta t') - p(x,t|z,t'+\Delta t')] \tag{C.15}$$

$$= \lim_{\Delta t' \to 0} \frac{1}{\Delta t'} \int dz\, p(z,t'+\Delta t'|y,t')[p(x,t|y,t') - p(x,t|z,t')]. \tag{C.16}$$

Now we use a similar trick as in Sec. C.1.1, by breaking the integral into $|z-y| < \epsilon$ and $|z-y| \geq \epsilon$. Then, by performing the taylor expansion

$$p(x,t|z,t') = p(x,t|y,t') + (z-y)\partial_y p(x,t|y,t') + \frac{1}{2}(z-y)^2 \partial_y^2 p(x,t|y,t') \tag{C.17}$$

for $|z-y| < \epsilon$, and inserting the conditions (1-3), we arrive at

$$\frac{\partial}{\partial t'} p(x,t|y,t') = -A(y,t')\frac{\partial}{\partial y} p(x,t|y,t') - \frac{1}{2} B(y,t')\frac{\partial^2}{\partial y^2} p(x,t|y,t') + \int dz\, W(z|y,t')[p(x,t|y,t') - p(x,t|z,t')]. \tag{C.18}$$

Upon setting $W(z|y,t') = 0$, we have the backward Fokker-Planck equation

$$\frac{\partial}{\partial t'} p(x,t|y,t') = -A(y,t')\frac{\partial}{\partial y} p(x,t|y,t') - \frac{1}{2} B(y,t')\frac{\partial^2}{\partial y^2} p(x,t|y,t'). \tag{C.19}$$

C.2 Obtaining the Fokker-Planck equation from stochastic differential equations

In this section, we present a simple derivation of the relation between the Fokker-Planck equation and stochastic differential equations. Given some stochastic variable $x(t)$ with SDE

$$dx = a(x,t)dt + b(x,t)dW, \tag{C.20}$$

we can find the evolution of $\langle f(x(t))\rangle$ for some function $f(x)$ which is twice continuously differentiable ($\mathcal{C}^2$) in x, using Itô 's rule. This is

$$\frac{\partial\langle f(x(t))\rangle}{\partial t} = \left\langle a(x,t)\frac{df}{dx} + \frac{1}{2}b^2(x,t)\frac{d^2f}{dx^2}\right\rangle. \tag{C.21}$$

Since the expectation is taken with respect to the conditional probability $p(x,t|x_0,t_0) = \varrho$, we can expand the above as

$$\frac{\partial}{\partial t}\int_{\mathcal{R}} dx\, \varrho f(x) = \int_{\mathcal{R}} dx\, \left(a(x,t)\frac{df}{dx} + \frac{1}{2}b^2(x,t)\frac{d^2f}{dx^2}\right)\varrho, \tag{C.22}$$

$$\begin{aligned}\int_{\mathcal{R}} dx\, f(x)\partial_t\varrho = &\int_{\mathcal{R}} dx\, f(x)\left(-\partial_x a(x,t)\varrho + \frac{1}{2}\partial_x^2 b^2(x,t)\varrho\right)\\ &+ \left(a(x,t)\varrho f(x) + \frac{1}{2}b^2\varrho\frac{\partial f}{\partial x} - \frac{f(x)}{2}\frac{\partial b^2\varrho}{\partial x}\right)\Big|_{\partial\mathcal{R}},\end{aligned} \tag{C.23}$$

where we have assumed the stochastic variable has allowed evolution within the region $\mathcal{R}$ with surface $\partial\mathcal{R}$. Using a similar argument as Sec. C.1.1, we defining the function $f(x)$ to have support only in a region $\mathcal{R}' \subset \mathcal{R}$. This definition forces the surface terms to vanish, and we obtain the forward Fokker-Planck equation,

$$\partial_t p(x,t|x_0,t_0) = -\partial_x[a(x,t)p(x,t|x_0,t_0)] + \frac{1}{2}\partial_x^2[b^2(x,t)p(x,t|x_0,t_0)]. \tag{C.24}$$

With this derivation, we can identify the drift and diffusion terms in Eqs. (2) and (3) with the terms of the SDE, which are

$$A(x,t) = a(x,t), \quad \text{and,} \tag{C.25}$$

$$B(x,t) = b^2(x,t). \tag{C.26}$$

APPENDIX D

NUMERICAL ALGORITHMS

In this Appendix, we present a set of numerical integration routines. These routines are used extensively in this thesis to tackle ALL numerical integrations required in this work. The flexibility of these routines lies in the fact that the required pre-computation step can be done once, and the results saved for use in any quadrature routine. In this work, we seek to provide an intuitive understanding of the algorithms, and give theorems only when they are fully understood by the author[1].

D.1 Gaussian quadrature

The goal of Gaussian quadrature is to be able to accurately approximate the value of the integral

$$\int_a^b w(x) f(x)\, dx, \tag{D.1}$$

where $w(x)$ is called the weight function, and $f(x)$ is an arbitrary function. We first define an infinite set of orthogonal polynomials p_n on the interval $[a, b]$, such that the following holds:

$$\langle p_i | p_j \rangle = \int_a^b w(x) p_i(x) p_j(x)\, dx = \delta_{ij}, \tag{D.2}$$

and $p_0 = 1$, and the subscript denotes the order of the polynomial. Note that with this definition, these orthogonal polynomials form a basis over the interval $[a, b]$ with weight function $w(x)$, any function can be expanded as a linear combination of these polynomials. Then, the theorem of Gauss/Jacobi is

[1] Which unfortunately is not always.

Theorem 5. *The approximation,*

$$\int_a^b w(x)f(x)\,dx \approx \sum_{k=1}^{N} w_k\, f(x_k), \tag{D.3}$$

is exact for all polynomial $f(x)$ of order $\leq 2N-1$, with x_k and w_k defined as

$$\sum_{j=1}^{N} w_j\, p_k(x_j) = \delta_{k0} \quad \forall\, k \leq N-1, \tag{D.4}$$

where the x_j's are the roots of $p_N(x)$.

Proof. Let $f(x)$ be a polynomial of order $\leq 2N-1$. Then, $f(x)$ can be expressed as

$$f(x) = p_N(x)q(x) + r(x), \tag{D.5}$$

where $q(x), r(x)$ are both polynomials of order $\leq N-1$. Substituting this into the integral, we have

$$\begin{aligned}
\int_a^b w(x)f(x)\,dx &= \int_a^b w(x)(p_N(x)q(x)+r(x))\,dx, && \text{(D.6)}\\
&= \int_a^b w(x)\left(p_N(x)\sum_{i=0}^{N-1} c_i p_i(x) + p_0 \sum_{i=0}^{N-1} d_i p_i(x)\right)dx, && \text{(D.7)}\\
&= d_0, && \text{(D.8)}
\end{aligned}$$

where we have used the orthogonality relations of the polynomials, and the fact that $p_0 = 1$. Now, the approximation is

$$\begin{aligned}
\sum_{k=1}^{N} w_k\, f(x_k) &= \sum_{k=1}^{N} w_k\left(p_N(x_k)q(x_k)+r(x_k)\right), && \text{(D.9)}\\
&= \sum_{k=1}^{N} w_k\left(p_N(x_k)\sum_{i=0}^{N-1} c_i p_i(x_k) + \sum_{i=0}^{N-1} d_i p_i(x_k)\right), && \text{(D.10)}\\
&= d_0, && \text{(D.11)}
\end{aligned}$$

where we used Eq. (D.4) and the fact that x_j are roots of $p_N(x)$. □

D.2 Highly oscillatory quadrature

In this section, we present one method for performing numerical integrations on highly oscillatory functions found in Refs. [109, 110, 111]. Contrary to what one might expect, this techniquee seem to be fairly recent additions to the literature of numerical integration, which came as a big surprise for the author. The main

question is the numerical evaluation of the integral

$$\int_a^b f(x)e^{-ikg(x)}dx. \tag{D.12}$$

This integral on first sight seems very similar to usual integrals. However, one quickly realizes that for $k \gg g(x)$, the integrand widly oscillates. A simple Gauss-type integration over the range $[a, b]$ must surely fail, since the integrand is no longer well approximated with a polynomial. Note that this method is not the definitive algorithm to approach the problem, and other methods indeed exist, see for instance Ref. [112] for one elegant example.

D.2.1 Filon-type quadrature

In this section, we present a generalized Filon-type quadrature from Ref. [111]. This idea was first proposed in Ref. [109], and generalized in Ref. [110]. However it was only proved in [111] to increase in accuracy for increased oscillation strengths k.

The idea of this method is not too hard to explain, and can be interpreted simply as a polynomial approximation of the function $f(x)$, *i.e.*

$$f(x) \approx \sum_j c_j x^j. \tag{D.13}$$

Then, the integration proceeds as follows:

$$\int_a^b f(x)e^{-ikg(x)}dx \approx \int_a^b \sum_j c_j x^j e^{-ikg(x)}dx, \tag{D.14}$$

$$= \sum_j c_j \int_a^b x^j e^{-ikg(x)}dx, \tag{D.15}$$

$$= \sum_j c_j m_j. \tag{D.16}$$

where we denoted the moments $m_j = \int_a^b x^j e^{-ikg(x)}dx$. So, if the moments of the function $e^{-ikg(x)}$ are known, and not too complex to compute, this technique becomes a viable way to numerically evaluate the integral Eq. (D.12). However, if these moments are unknown, this method is almost useless, since it breaks up an oscillatory integral into a sum of oscillatory integrals without any change in the oscillation strength, which defeats the purpose.

Further, this method leaves open the choice of the coefficients of the interpolating polynomial c_j, and evidently requires a good polynomial approximation to

the function $f(x)$ to be useful as well. We next show an example in which we compute a fourier transform type integral by using this method.

Example: Fourier transforms

In this simple example, we consider an integral of the form:

$$\int_a^b f(x)e^{ikx}dx. \tag{D.17}$$

This is the well known fourier transform with a bounded domain. It is the simplest example where the moments m_j are known analytically, and are not too computationally expensive to compute. Also, in optical system, $k \sim \frac{1}{\lambda} \sim 10^7$ which is really huge, so a brute force attack on this integration is expensive, although still doable in practice.

The moments have closed-form solutions which can be seen from

$$\begin{aligned} m_j &= \int_{-a}^{b} x^j e^{ikx}dx, && \text{(D.18)}\\ &= \int_{-ika}^{-ikb} (-ik)^{-j-1} t^j e^{-t}dt, && \text{(D.19)}\\ &= \gamma(j+1,-ikb) - \gamma(j+1,-ika), && \text{(D.20)} \end{aligned}$$

where we have used the definition for the lower incomplete gamma function given by

$$\gamma(n,x) = \int_0^x t^{n-1}e^{-t}dt. \tag{D.21}$$

Unfortunately, Matlab 7.10 does *not* implement an incomplete gamma function which accepts complex numbers, and so this is not a good method for direct implementation in matlab. These moments can however, be defined recursively by performing an integration by parts:

$$\begin{aligned} m_j &= \int_{-a}^{b} x^j e^{ikx}dx, && \text{(D.22)}\\ &= \frac{1}{ik}\left(b^j e^{ikb} - a^j e^{ika}\right) - \frac{j}{ik}\int_a^b x^{j-1}e^{ikx}dx, && \text{(D.23)}\\ &= D_j + i\frac{j}{k}m_{j-1}, && \text{(D.24)} \end{aligned}$$

with

$$m_0 = D_0. \tag{D.25}$$

An implementation would then be to loop up from m_0 to the required number of moments, which is pretty cheap computationally to implement as well. Next, to

approximate $f(x)$, we choose the Chebyshev nodes to approximate the function. These nodes are well known in numerical analysis to give a small interpolation error in the interpolating polynomial, and are given by

$$x_k = \cos\left(\frac{2k-1}{2N}\pi\right), \quad k = 1, 1, ...N. \tag{D.26}$$

To approximate $f(x)$, we solve the Vandermonde system,

$$\sum_{ij} v_{ij} c_j = f(x_i), \tag{D.27}$$

with the elements of $N \times N$ Vandermonde matrix defined by

$$v_{ij} = x_i^{j-1}, \tag{D.28}$$

where the x_i's are the Chebyshev nodes given in Eq. (D.26). Thus, we "simply" solve the N linear equations to arrive at the coefficients c_j. However, it must be noted that the Vandermonde matrix is in general very ill-conditioned, such that its determinant is very small, making inverting unstable numerically. An example with the Chebyshev nodes is for $N = 50$, the determinant of V is $\sim 10^{-318}$, which is as good as a singular matrix for a computer. There are ways to invert this matrix in the literature, exploiting the structure of the matrix [113, 114]. However, preliminary testing showed that they were not ideal. Instead, we picked a small value of $N = 20$ such that Matlab is able to find a satisfactory inverse.

BIBLIOGRAPHY

[1] R. H. Brown and R. Twiss. "Correlation between photons in two coherent beams of light". *Nature* 177.4497 (1956), pp. 27–29.

[2] L. Mandel and E. Wolf. *Optical coherence and quantum optics*. Cambridge university press, 1995.

[3] R. J. Glauber. "Nobel Lecture: One hundred years of light quanta". *Rev. Mod. Phys.* 78.4 (2006), pp. 1267–1278.

[4] R. J. Glauber. "The quantum theory of optical coherence". *Phys. Rev.* 130.6 (1963), p. 2529.

[5] L. Mandel and E. Wolf. "Coherence properties of optical fields". *Rev. Mod. Phys.* 37.2 (1965), p. 231.

[6] M. O. Scully and M. S. Zubairy. *Quantum Optics*. Cambridge University Press, 1997.

[7] C. Chou, D. Hume, T Rosenband, and D. Wineland. "Optical clocks and relativity". *Science* 329.5999 (2010), pp. 1630–1633.

[8] L. K. Grover. "A fast quantum mechanical algorithm for database search". In: *Proceedings of the twenty-eighth annual ACM symposium on Theory of computing*. ACM. 1996, pp. 212–219.

[9] P. W. Shor. "Polynomial-time algorithms for prime factorization and discrete logarithms on a quantum computer". *SIAM journal on computing* 26.5 (1997), pp. 1484–1509.

[10] D. R. Simon. "On the power of quantum computation". *SIAM Journal on Computing* 26.5 (1997), pp. 1474–1483.

[11] M. A. Nielsen and I. L. Chuang. *Quantum computation and quantum information*. Cambridge university press, 2010.

[12] N. Brunner, D. Cavalcanti, S. Pironio, V. Scarani, and S. Wehner. "Bell nonlocality". *arXiv:1303.2849* (2013).

[13] H. J. Kimble. "The quantum internet". *Nature* 453.7198 (2008), pp. 1023–1030.

[14] C. H. Bennett, G. Brassard, et al. "Quantum cryptography: Public key distribution and coin tossing". In: *Proceedings of IEEE International Conference on Computers, Systems and Signal Processing*. Vol. 175. 0. New York. 1984.

[15] A. K. Ekert. "Quantum cryptography based on Bell's theorem". *Phys. Rev. Lett.* 67.6 (1991), pp. 661–663.

[16] N. Gisin, G. Ribordy, W. Tittel, and H. Zbinden. "Quantum cryptography". *Rev. Mod. Phys.* 74.1 (2002), pp. 145–195.

[17] R. P. Feynman. "Simulating physics with computers". *Int. Jour. Theor. Phys.* 21.6 (1982), pp. 467–488.

[18] A. Ekert and R. Jozsa. "Quantum computation and Shor's factoring algorithm". *Rev. Mod. Phys.* 68.3 (1996), p. 733.

[19] D. Bouwmeester, A. K. Ekert, A. Zeilinger, et al. *The physics of quantum information*. Vol. 38. Springer Berlin, 2000.

[20] A. Acín, N. Brunner, N. Gisin, S. Massar, S. Pironio, and V. Scarani. "Device-independent security of quantum cryptography against collective attacks". *Phys. Rev. Lett.* 98.23 (2007), p. 230501.

[21] S. Pironio, A. Acín, S. Massar, A. B. de La Giroday, D. N. Matsukevich, P. Maunz, S. Olmschenk, D. Hayes, L. Luo, T. A. Manning, et al. "Random numbers certified by Bell's theorem". *Nature* 464.7291 (2010), pp. 1021–1024.

[22] C.-E. Bardyn, T. C. Liew, S. Massar, M. McKague, and V. Scarani. "Device-independent state estimation based on Bell's inequalities". *Phys. Rev. A* 80.6 (2009), p. 062327.

[23] R. Rabelo, M. Ho, D. Cavalcanti, N. Brunner, and V. Scarani. "Device-independent certification of entangled measurements". *Phys. Rev. Lett.* 107.5 (2011), p. 050502.

[24] A. Aspect, J. Dalibard, and G. Roger. "Experimental test of Bell's inequalities using time-varying analyzers". *Phys. Rev. Lett.* 49.25 (1982), p. 1804.

[25] G. Weihs, T. Jennewein, C. Simon, H. Weinfurter, and A. Zeilinger. "Violation of Bell's inequality under strict Einstein locality conditions". *Physical Review Letters* 81.23 (1998), p. 5039.

[26] T. Scheidl, R. Ursin, J. Kofler, S. Ramelow, X.-S. Ma, T. Herbst, L. Ratschbacher, A. Fedrizzi, N. K. Langford, T. Jennewein, et al. "Violation of local realism with freedom of choice". *Proc. Natl. Acad. Sci.* 107.46 (2010), pp. 19708–19713.

[27] M. Giustina, A. Mech, S. Ramelow, B. Wittmann, J. Kofler, J. Beyer, A. Lita, B. Calkins, T. Gerrits, S. W. Nam, et al. "Bell violation using entangled photons without the fair-sampling assumption". *Nature* (2013).

[28] D. N. Matsukevich, P. Maunz, D. L. Moehring, S. Olmschenk, and C. Monroe. "Bell Inequality Violation with Two Remote Atomic Qubits". *Phys. Rev. Lett.* 100 (2008), p. 150404.

[29] M. A. Rowe, D. Kielpinski, V Meyer, C. A. Sackett, W. M. Itano, C. Monroe, and D. J. Wineland. "Experimental violation of a Bell's inequality with efficient detection". *Nature* 409.6822 (2001), pp. 791–794.

[30] M. Ansmann, H Wang, R. C. Bialczak, M. Hofheinz, E. Lucero, M Neeley, A. O'Connell, D Sank, M Weides, J Wenner, et al. "Violation of Bell's inequality in Josephson phase qubits". *Nature* 461.7263 (2009), pp. 504–506.

[31] H. M. Wiseman and G. J. Milburn. "All-optical versus electro-optical quantum-limited feedback". *Phys. Rev. A* 49.5 (1994), p. 4110.

[32] S. Lloyd. "Coherent quantum feedback". *Phys. Rev. A* 62.2 (2000), p. 022108.

[33] M. Yanagisawa and H. Kimura. "Transfer function approach to quantum control-part I: Dynamics of quantum feedback systems". *IEEE Trans. Autom. Control* 48.12 (2003), pp. 2107–2120.

[34] M. Yanagisawa and H. Kimura. "Transfer function approach to quantum control-part II: Control concepts and applications". *IEEE Trans. Autom. Control* 48.12 (2003), pp. 2121–2132.

[35] M. R. James, H. I. Nurdin, and I. R. Petersen. "H^∞ control of linear quantum stochastic systems". *IEEE Trans. Autom. Control* 53.8 (2008), pp. 1787–1803.

[36] H. M. Wiseman, S. Mancini, and J. Wang. "Bayesian feedback versus Markovian feedback in a two-level atom". *Phys. Rev. A* 66.1 (2002), p. 013807.

[37] V. P. Belavkin. "Nondemolition measurements, nonlinear filtering and dynamic programming of quantum stochastic processes". In: *Modeling and Control of Systems*. Springer, 1989, pp. 245–265.

[38] A. C. Doherty and K. Jacobs. "Feedback control of quantum systems using continuous state estimation". *Phys. Rev. A* 60.4 (1999), p. 2700.

[39] A. C. Doherty, S. Habib, K. Jacobs, H. Mabuchi, and S. M. Tan. "Quantum feedback control and classical control theory". *Phys. Rev. A* 62 (2000), p. 012105.

[40] C. M. Caves and G. Milburn. "Quantum-mechanical model for continuous position measurements". *Phys. Rev. A* 36.12 (1987), p. 5543.

[41] H. Wiseman and G. Milburn. "Quantum theory of optical feedback via homodyne detection". *Phys. Rev. Lett.* 70.5 (1993), p. 548.

[42] H. Wiseman. "Quantum theory of continuous feedback". *Phys. Rev. A* 49.3 (1994), p. 2133.

[43] H. M. Wiseman and A. Doherty. "Optimal unravellings for feedback control in linear quantum systems". *Phys. Rev. Lett.* 94.7 (2005), p. 070405.

[44] H. M. Wiseman and G. J. Milburn. *Quantum measurement and control*. Cambridge University Press, 2010.

[45] L. Bouten, S. Edwards, and V. Belavkin. "Bellman equations for optimal feedback control of qubit states". *J. Phys. B: At. Mol. Phys.* 38.3 (2005), p. 151.

[46] J Gough, V. Belavkin, and O. Smolyanov. "Hamilton–Jacobi–Bellman equations for quantum optimal feedback control". *Jour. Opt. B: Quant. Semi. Opt.* 7.10 (2005), S237.

[47] K. Jacobs. "How to project qubits faster using quantum feedback". *Phys. Rev. A* 67.3 (2003), p. 030301.

[48] J. Combes and K. Jacobs. "Rapid state reduction of quantum systems using feedback control". *Phys. Rev. Lett.* 96.1 (2006), p. 010504.

[49] H. M. Wiseman and J. Ralph. "Reconsidering rapid qubit purification by feedback". *New J. Phys.* 8.6 (2006), p. 90.

[50] H. M. Wiseman and L. Bouten. "Optimality of feedback control strategies for qubit purification". *Quantum Inf. Process.* 7.2-3 (2008), pp. 71–83.

[51] C. W. Gardiner and M. J. Collett. "Input and output in damped quantum systems: Quantum stochastic differential equations and the master equation". *Phys. Rev. A* 31.6 (1985), pp. 3761–3774.

[52] H. Carmichael. *Statistical methods in quantum optics, vol. 1: Master equations and Fokker-Planck equations*. Springer, Berlin, 1999.

[53] C. Gardiner and P. Zoller. *Quantum noise: a handbook of Markovian and non-Markovian quantum stochastic methods with applications to quantum optics*. Vol. 56. Springer, 2004.

[54] C. Ciuti and I. Carusotto. "Input-output theory of cavities in the ultrastrong coupling regime: The case of time-independent cavity parameters". *Phys. Rev. A* 74.3 (2006), p. 033811.

[55] D. F. Walls and G. G. J. Milburn. *Quantum optics*. Springer, 2008.

[56] J. F. Clauser, M. A. Horne, A. Shimony, and R. A. Holt. "Proposed Experiment to Test Local Hidden-Variable Theories". *Phys. Rev. Lett.* 23 (1969), pp. 880–884.

[57] C. Teo, J. Minář, D. Cavalcanti, and V. Scarani. "Improved analysis of a proposal for a realistic loophole-free Bell test with atom-light entanglement". *arXiv:1308.5031* (2013).

[58] M. Araújo, M. T. Quintino, D. Cavalcanti, M. F. Santos, A. Cabello, and M. T. Cunha. "Tests of Bell inequality with arbitrarily low photodetection efficiency and homodyne measurements". *Phys. Rev. A* 86 (2012), p. 030101.

[59] N Sangouard, J.-D. Bancal, N. Gisin, W Rosenfeld, P. Sekatski, M Weber, and H Weinfurter. "Loophole-free Bell test with one atom and less than one photon on average". *Phys. Rev. A* 84.5 (2011), p. 052122.

[60] Y. Wang, J. Minář, L. Sheridan, and V. Scarani. "Efficient excitation of a two-level atom by a single photon in a propagating mode". *Phys. Rev. A* 83.6 (2011), p. 063842.

[61] M. Boissonneault, J. M. Gambetta, and A. Blais. "Dispersive regime of circuit QED: Photon-dependent qubit dephasing and relaxation rates". *Phys. Rev. A* 79.1 (2009), p. 013819.

[62] M. Brune, E. Hagley, J. Dreyer, X. Maître, A. Maali, C. Wunderlich, J. M. Raimond, and S. Haroche. "Observing the Progressive Decoherence of the "Meter" in a Quantum Measurement". *Phys. Rev. Lett.* 77 (1996), pp. 4887–4890.

[63] A. Rauschenbeutel, G. Nogues, S. Osnaghi, P. Bertet, M. Brune, J.-M. Raimond, and S. Haroche. "Step-by-step engineered multiparticle entanglement". *Science* 288.5473 (2000), pp. 2024–2028.

[64] S. Haroche and J.-M. Raimond. *Exploring the quantum: Atoms, cavities, and photons*. Oxford Univ. Press, 2006.

[65] D. Cavalcanti, N. Brunner, P. Skrzypczyk, A. Salles, and V. Scarani. "Large violation of Bell inequalities using both particle andwave measurements". *Phys. Rev. A* 84 (2011), p. 022105.

[66] A. Gilchrist, P. Deuar, and M. D. Reid. "Contradiction of Quantum Mechanics with Local Hidden Variables for Quadrature Phase Amplitude Measurements". *Phys. Rev. Lett.* 80 (1998), pp. 3169–3172.

[67] A. E. Lita, A. J. Miller, and S. W. Nam. "Counting near-infrared single-photons with 95% efficiency". *Opt. Express* 16.5 (2008), pp. 3032–3040.

[68] R. H. Hadfield. "Single-photon detectors for optical quantum information applications". *Nature Photon.* 3.12 (2009), pp. 696–705.

[69] M. T. Quintino, M. Araújo, D. Cavalcanti, M. F. Santos, and M. T. Cunha. "Maximal violations and efficiency requirements for Bell tests with photodetection and homodyne measurements". en. *J. Phys. A: Math. Theor.* 45.21 (2012), p. 215308.

[70] F. Henkel, M. Krug, J. Hofmann, W. Rosenfeld, M. Weber, and H. Weinfurter. "Highly efficient state-selective submicrosecond photoionization detection of single atoms". *Phys. Rev. Lett.* 105.25 (2010), p. 253001.

[71] P. H. Eberhard. "Background level and counter efficiencies required for a loophole-free Einstein-Podolsky-Rosen experiment". *Phys. Rev. A* 47 (1993), R747–R750.

[72] B. C. Sanders. "Review of entangled coherent states". *J. Phys. A: Math. Theor.* 45.24 (2012), p. 244002.

[73] B. C. Sanders. "Entangled coherent states". *Phys. Rev. A* 45 (1992), pp. 6811–6815.

[74] M. Stobinska, H. Jeong, and T. C. Ralph. "Violation of Bell's inequality using classical measurements and nonlinear local operations". *Phys. Rev. A* 75.5 (2007), p. 52105.

[75] A. Ourjoumtsev, H. Jeong, R. Tualle-Brouri, and P. Grangier. "Generation of optical 'Schrödinger cats' from photon number states". *Nature* 448.7155 (2007), pp. 784–786.

[76] A. Ourjoumtsev, F. Ferreyrol, R. Tualle-Brouri, and P. Grangier. "Preparation of non-local superpositions of quasi-classical light states". *Nature Phys.* 5.3 (2009), pp. 189–192.

[77] K. Wakui, H. Takahashi, A. Furusawa, and M. Sasaki. "Photon subtracted squeezed states generated with periodically poled $KTiOPO_4$". *Opt. Express* 15.6 (2007), pp. 3568–3574.

[78] M. Takeoka, H. Takahashi, and M. Sasaki. "Large-amplitude coherent-state superposition generated by a time-separated two-photon subtraction from a continuous-wave squeezed vacuum". *Phys. Rev. A* 77.6 (2008), p. 062315.

[79] S. Van Enk and O Hirota. "Entangled coherent states: Teleportation and decoherence". *Phys. Rev. A* 64.2 (2001), p. 022313.

[80] B Wang and L.-M. Duan. "Engineering superpositions of coherent states in coherent optical pulses through cavity-assisted interaction". *Phys. Rev. A* 72.2 (2005), p. 022320.

[81] S. Zohren and R. D. Gill. "Maximal Violation of the Collins-Gisin-Linden-Massar-Popescu Inequality for Infinite Dimensional States". *Phys. Rev. Lett.* 100 (2008), p. 120406.

[82] A. Blais, R.-S. Huang, A. Wallraff, S. M. Girvin, and R. J. Schoelkopf. "Cavity quantum electrodynamics for superconducting electrical circuits: An architecture for quantum computation". *Phys. Rev. A* 69 (2004), p. 062320.

[83] A. Wallraff, D. I. Schuster, A. Blais, L. Frunzio, J. Majer, M. H. Devoret, S. M. Girvin, and R. J. Schoelkopf. "Approaching Unit Visibility for Control of a Superconducting Qubit with Dispersive Readout". *Phys. Rev. Lett.* 95 (2005), p. 060501.

[84] S. Ritter, C. Nölleke, C. Hahn, A. Reiserer, A. Neuzner, M. Uphoff, M. Mücke, E. Figueroa, J. Bochmann, and G. Rempe. "An elementary quantum network of single atoms in optical cavities". *Nature* 484.7393 (2012), pp. 195–200.

[85] K. M. Birnbaum, A. Boca, R. Miller, A. D. Boozer, T. E. Northup, and H. J. Kimble. "Photon blockade in an optical cavity with one trapped atom". *Nature* 436.7047 (2005), pp. 87–90.

[86] M. G. Paris. "Displacement operator by beam splitter". *Phys. Lett. A* 217.2 (1996), pp. 78–80.

[87] S. Ritter. private communication. 2012.

[88] C. J. Hood. "Real-time measurement and trapping of single atoms by single photons". PhD thesis. California Institute of Technology, 2000.

[89] B. Srivathsan, G. K. Gulati, B. Chng, G. Maslennikov, D. Matsukevich, and C. Kurtsiefer. "Narrow Band Source of Transform-Limited Photon Pairs via Four-Wave Mixing in a Cold Atomic Ensemble". *Phys. Rev. Lett.* 111.12 (2013), p. 123602.

[90] H.-H. Jen. "Theory of light-matter interactions in cascade and diamond type atomic ensembles". PhD thesis. Georgia Institute of Technology, 2010.

[91] A. V. Gorshkov. "Novel Systems and Methods for Quantum Communication, Quantum Computation, and Quantum Simulation". PhD thesis. Harvard University Cambridge, Massachusetts, 2009.

[92] G. W. Drake. *Springer handbook of atomic, molecular, and optical physics*. Springer, 2006.

[93] P. N. Butcher and D. Cotter. *The elements of nonlinear optics*. Vol. 9. Cambridge University Press, 1991.

[94] B. Srivathsan, G. K. Gulati, B. Chng, G. Maslennikov, D. Matsukevich, and C. Kurtsiefer. In Preparation. 2013.

[95] W. H. Fleming and H. M. Soner. *Controlled Markov processes and viscosity solutions*. Vol. 25. Springer New York, 2006.

[96] C. A. Fuchs and K. Jacobs. "Information-tradeoff relations for finite-strength quantum measurements". *Physical Review A* 63.6 (2001), p. 062305.

[97] J. C. Baez. "Rényi entropy and free energy". *arXiv:1102.2098* (2011).

[98] W. van Dam and P. Hayden. "Renyi-entropic bounds on quantum communication". *arXiv:quant-ph/0204093* (2002).

[99] K. Jacobs and P. L. Knight. "Linear quantum trajectories: Applications to continuous projection measurements". *Phys. Rev. A* 57 (1998), pp. 2301–2310.

[100] S. E. Morin, C. C. Yu, and T. W. Mossberg. "Strong Atom-Cavity Coupling over Large Volumes and the Observation of Subnatural Intracavity Atomic Linewidths". *Phys. Rev. Lett.* 73 (1994), pp. 1489–1492.

[101] S. A. Aljunid, B. Chng, J. Lee, M. Paesold, G. Maslennikov, and C. Kurtsiefer. "Interaction of light with a single atom in the strong focusing regime". *J. Mod. Opt.* 58.3-4 (2011), pp. 299–305.

[102] S. Girvin. private communication. 2012.

[103] M. Abramowitz and I. A. Stegun. *Handbook of Mathematical Functions: With Formulars, Graphs, and Mathematical Tables*. Vol. 55. DoverPublications. com, 1964.

[104] W. W. Bell. *Special functions for scientists and engineers*. Courier Dover Publications, 2004.

[105] C. Cohen-Tannoudji, J. Dupont-Roc, G. Grynberg, and P. Meystre. "Atom-Photon Interactions: Basic Processes and Applications". *Physics Today* 45 (1992), p. 115.

[106] R. Kubo. "The fluctuation-dissipation theorem". *Rep. Prog. Phys.* 29.1 (1966), p. 255.

[107] K. Hammerer, A. S. Sørensen, and E. S. Polzik. "Quantum interface between light and atomic ensembles". *Reviews of Modern Physics* 82.2 (2010), p. 1041.

[108] C. W. Gardiner et al. *Handbook of stochastic methods*. Vol. 3. Springer Berlin, 1985.

[109] L. N. G. Filon. "On a quadrature formula for trigonometric integrals". In: *Proc. Roy. Soc.* Vol. 49. 1. 1928, pp. 38–47.

[110] E. Flinn. "A modification of Filon's method of numerical integration". *J. ACM* 7.2 (1960), pp. 181–184.

[111] A. Iserles and S. P. Nørsett. "Efficient quadrature of highly oscillatory integrals using derivatives". *Proc. R. Soc. A* 461.2057 (2005), pp. 1383–1399.

[112] D. Huybrechs and S. Vandewalle. "On the evaluation of highly oscillatory integrals by analytic continuation". *SIAM J. Numer. Anal.* 44.3 (2006), pp. 1026–1048.

[113] A. Björck and V. Pereyra. "Solution of Vandermonde systems of equations". *Math. Comput.* 24.112 (1970), pp. 893–903.

[114] A Eisinberg and G Fedele. "On the inversion of the Vandermonde matrix". *Appl. Math. Comput.* 174.2 (2006), pp. 1384–1397.